Controlling and measuring quantum transport of heat in trapped-ion crystals

A. Bermudez, M. Bruderer, and M. B. Plenio
Institut für Theoretische Physik, Albert-Einstein-Allee 11, Universität Ulm, 89069 Ulm, Germany
Center for Integrated Quantum Science and Technology, Albert-Einstein-Allee 11, Universität Ulm, 89069 Ulm

Measuring heat flow through nanoscale systems poses formidable practical difficulties as there is no 'ampere meter' for heat. We propose to overcome this problem by realizing heat transport through a chain of trapped ions. Laser cooling the chain edges to different temperatures induces a current of local vibrations (vibrons). We show how to efficiently control and measure this current, including fluctuations, by coupling vibrons to internal ion states. This demonstrates that ion crystals provide a suitable platform for studying quantum transport, e.g., through thermal analogues of quantum wires and quantum dots. Notably, ion crystals may give access to measurements of the elusive large fluctuations of bosonic currents and the onset of Fourier's law. These results are supported by numerical simulations for a realistic implementation with specific ions and system parameters.

In view of the rapid development of nanoscale technologies [1], understanding charge and heat transport at the microscopic level has become a central topic of current research. As already shown for fermions [2], charge transport at the nanoscale is typically governed by quantum effects. For bosons, the transport of heat by phonons has been predicted to have analogous properties [3]. However, experiments are considerably more challenging in this case, as there is no device capable of measuring local heat currents [3]. Moreover, the heat reservoirs and temperature probes required to study heat transport, usually entail spurious interface effects. Within these restrictions, most experimental efforts have focused on detecting temperature profiles [4] in different devices [1, 5, 6].

In this Letter, we show that trapped-ion crystals are a promising platform to overcome these limitations. By exploiting laser-induced couplings between transverse quantized vibrations (vibrons) and internal degrees of freedom (spins) of the ions, we show how to control and measure the heat current across an ion chain [Fig. 1**(a)**]. We introduce a *quantum transport toolbox* containing all functionalities required for treating heat currents on the same footing as electrical currents. To be more precise, ions at the edges of the crystal are Doppler-cooled to different temperatures, and act as reservoirs that sustain a non-equilibrium heat flow through the bulk of the crystal [Fig. 1**(b)**]. To probe this transport, we propose to map the information of the vibron number or heat current (including their fluctuations) onto the spins, which can be measured via spin-dependent fluorescence [7]. For conventional materials, the quest for such a probing device is formidable, as it would require measuring the heat flow through a single atom.

We demonstrate the versatility of our toolbox with two examples: a *thermal quantum wire* (TQW), and a *thermal quantum dot* (TQD). In the TQW, we study the onset of Fourier's law [8] in a mesoscopic system, which predicts a temperature gradient across a heat conductor. This law requires the transition from ballistic to diffusive transport, which can be induced by either *i)* dephasing through noisy modulations of the trap frequencies [9], or *ii)* disorder due to an engineered spin-vibron coupling [10]. The TQD highlights the differences of bosonic and fermionic transport [11], captured by the statistics of the fluctuations [12]. Building on the idea of laser-assisted tunneling [13, 14], we show how to measure current fluctuations. Moreover, the TQD can be operated as a switch for the heat current, a first step towards a single-spin heat transistor.

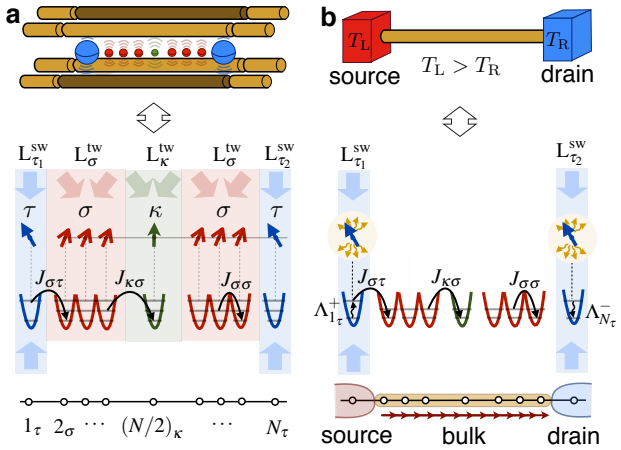

Figure 1. **Heat transport toolbox: (a)** (upper panel) Mixed-species (blue$=\tau$, red$=\sigma$, green$=\kappa$) ion crystal in a linear Paul trap. Our ideas also apply to surface trap arrays. (lower panel) The spin and vibrational degrees of freedom of the ions are indicated with arrows and wells, respectively. We show the laser arrangements L^{sw}_{τ} (L^{tw}_{σ},L^{tw}_{κ}) to control the incoherent (coherent) vibrational dynamics of the ions, where $J_{\alpha\beta}$ represents the vibron tunneling. **(b)** (upper panel) Scheme for a thermal quantum wire (TQW) connected to two reservoirs held at different temperatures. (lower panel) A sufficiently strong laser cooling with strengths $\Lambda^-_{\ell_\tau} > \Lambda^+_{\ell_\tau}$, allows to treat the edge τ-ions as heat reservoirs, whereas the bulk σ, κ ions act as the TQW.

We note that the control of heat in trapped ions is a topic of increasing interest. In Ref. [15], the propagation of vibrational excitations along an ion chain has been assessed theoretically. The use of single trapped ions as heat engines has been proposed in [16]. Finally, and more relevant to the present topic, the thermalization of a sympathetically-cooled ion chain has been studied in [17] by Langevin dynamics [18]. We believe that the toolbox hereby introduced, which is based on a thorough first-principle derivation, will be genuinely useful for the development of heat transport experiments with trapped ions.

Model.– We consider a linear Coulomb crystal with three types of ions [Fig. 1**(a)**]. The quanta of the collective crystal vibrations (i.e. the phonons) are customary used as a data bus for quantum information processing [19]. In this work, however, we are interested in the individual transverse oscillations

of the ions, whose quanta will be called *vibrons*, and are responsible for a local electric dipole. As demonstrated in recent experiments [20], the interaction between these dipoles leads to a tight-binding model for the transverse vibrations ($\hbar = 1$)

$$H_{\rm tb} = \sum_{\alpha,i_\alpha} \omega_{i_\alpha} a^\dagger_{i_\alpha} a_{i_\alpha} + \sum_{\alpha,\beta} \sum_{i_\alpha \neq j_\beta} \left(J_{i_\alpha j_\beta} a^\dagger_{i_\alpha} a_{j_\beta} + \text{H.c.} \right), \quad (1)$$

where the bosonic operators $a^\dagger_{i_\alpha}(a_{i_\alpha})$ create (annihilate) the local vibrons, and we have used latin indices to label the lattice sites $i,j \in \{1 \cdots N\}$, and greek sub-indices to label the species $\alpha,\beta \in \{\sigma,\tau,\kappa\}$ [Fig. 1**(a)**]. According to Eq. (1), the ion crystal is a natural playground for bosonic lattice models [21], where the bosonic particles correspond to the vibrons, the lattice is determined by the underlying crystal structure, and the trapping and dipole-dipole couplings are responsible for the on-site energies ω_{i_α}, and the long-range tunnelings $J_{i_\alpha j_\beta}$ [22].

In addition to the vibrations, we exploit two selected atomic levels of each ion, hereafter referred to as spins $|s_{i_\alpha}\rangle \in \{|\uparrow_{i_\alpha}\rangle, |\downarrow_{i_\alpha}\rangle\}$. The spin Hamiltonian is $H^\alpha_{\rm s} = \frac{1}{2}\sum_{i_\alpha} \omega^\alpha_0 \sigma^z_{i_\alpha}$, where $\sigma^z_{i_\alpha} = |\uparrow_{i_\alpha}\rangle\langle\uparrow_{i_\alpha}| - |\downarrow_{i_\alpha}\rangle\langle\downarrow_{i_\alpha}|$, and the atomic transition is characterized by the frequency ω^α_0 and the linewidth Γ_α.

Let us now augment the vibron and spin dynamics given by $H_{\rm tb} + H_{\rm s}$ with additional incoherent and coherent contributions to obtain the tools for studying quantum transport:

(i) For the *incoherent* dynamics, we employ a laser $\mathrm{L}^{\rm sw}_\alpha$ forming a standing wave along the direction of the vibrons. This drives a dipole-allowed transition of the α-spins, simultaneously modifying the number of vibrational excitations. For a fast decay of the α-spins [22], the interplay of these two processes yields an effective dissipation of the vibrons

$$\mathscr{D}^{i_\alpha}_{\rm v}(\mu) = \mathscr{D}[\Lambda^+_{i_\alpha}, a^\dagger_{i_\alpha}, a_{i_\alpha}](\mu) + \mathscr{D}[\Lambda^-_{i_\alpha}, a_{i_\alpha}, a^\dagger_{i_\alpha}](\mu), \quad (2)$$

where $\mathscr{D}[\Lambda, O_1, O_2](\bullet) = \Lambda(O_1 \bullet O_2 - O_2 O_1 \bullet) + \text{H.c.}$ is a generic super-operator throughout this work. The local heating (cooling) strengths $\Lambda^+_{i_\alpha}$ ($\Lambda^-_{i_\alpha}$), which depend on the spectral functions of the couplings [23], can be tuned by controlling the laser parameters in the Doppler regime [22, 26].

(ii) For the *coherent* dynamics, we apply a spin-dependent traveling wave $\mathrm{L}^{\rm tw}_\alpha$, which consists of a pair of non-copropagating laser beams. The wave originates from two-photon processes, whereby the spin state is virtually excited by absorbing a photon from a laser beam, and subsequently de-excited by photon emission into the remaining laser beam [22]. This results in a spin-vibron interaction

$$H^{i_\alpha}_{\rm sv}(t) = \tfrac{1}{2}(\Delta\omega^+_\alpha + \Delta\omega^-_\alpha \sigma^z_{i_\alpha}) \cos(\nu_\alpha t - \varphi_\alpha) a^\dagger_{i_\alpha} a_{i_\alpha}, \quad (3)$$

where the parameters $\Delta\omega^\pm_\alpha, \nu_\alpha, \varphi_\alpha$ are fully controllable [29].

The Hamiltonian and Lindblad terms in Eqs. (1) to (3) form our Liouvillian toolbox for studying quantum transport in ion crystals: the *driven dissipative spin-vibron model*

$$\mathscr{L}_{\rm ddsv}(\mu) = -\mathrm{i}\left[H_{\rm tb} + \sum_{\alpha,i_\alpha \in \mathfrak{C}} H^{i_\alpha}_{\rm sv}(t), \mu \right] + \sum_{\alpha,i_\alpha \in \mathfrak{I}} \mathscr{D}^{i_\alpha}_{\rm v}(\mu). \quad (4)$$

Here, the sums over $\mathfrak{C}$ and $\mathfrak{I}$ comprise ions subjected to either additional coherent or incoherent effects, respectively. Let us remark that our toolbox avoids using single-ion laser addressing by exploiting different species α for each functionality.

A key function of our toolbox is the possibility of designing reservoirs. Ideally, a reservoir in quantum transport theory is a system capable of supplying and absorbing carriers without changing its state. In our case, this can be achieved by using a red-detuned laser $\mathrm{L}^{\rm sw}_\alpha$ such that the dissipation in Eq. (2) implements a cooling process at the rate $\gamma_{i_\alpha} = \mathrm{Re}\{(\Lambda^-_{i_\alpha})^* - \Lambda^+_{i_\alpha}\}$. For sufficiently strong laser intensities, the cooling dominates over the tunneling $\gamma_{i_\alpha} \gg J_{i_\alpha, j_\beta}$ [22]. Thus, the ion does not have enough time to exchange vibrons with the rest of the chain before thermalizing. More importantly, the constantly cooled ions remain in a thermal state $\mu^{\rm th}_{i_\alpha}$ with average vibron number (equivalently temperature), $\bar{n}_{i_\alpha} = \mathrm{Re}\{\Lambda^+_{i_\alpha}\}/\gamma_{i_\alpha}$, and thus provide an accurate realization of a vibronic reservoir.

Thermal quantum wire.– We now consider how to design a thermal quantum wire (TQW) with our toolbox. We choose certain ion species [22], such that dissipation only occurs for the τ-ions $\Gamma_\tau \gg \Gamma_\sigma, \Gamma_\kappa$ (i.e. $\sigma,\kappa \in \mathfrak{C}$ and $\tau \in \mathfrak{I}$). By placing the τ-ions at the edges of the chain, the dissipator (2) realizes the starting point of different transport studies [31]. Considering the strong-cooling regime with $\bar{n}_{1_\tau} > \bar{n}_{N_\tau}$, the τ-ions resemble a vibronic battery. The left reservoir constantly supplies vibrons in the attempt to equilibrate with the TQW by increasing its vibrational excitations. Conversely, the right reservoir keeps absorbing vibrons in its effort to lower the vibrational excitations in the TQW. When combined, the reservoirs sustain a flow of heat along the TQW [Fig. 1**(b)**].

To start with, we assess how the TQW thermalizes due to the contact with the reservoirs on a time-scale much longer than $\gamma^{-1}_{i_\tau}$. Since the vibron tunnelings are much smaller than the edge cooling rates, the edge vibrons are "integrated out" by projecting onto the state $\mu \to \mu^{\rm th}_{1_\tau} \otimes \mu_{\rm bulk} \otimes \mu^{\rm th}_{N_\tau}$. We obtain a dissipative spin-vibron model for the reduced density matrix of the bulk of the wire, namely $\partial_t \mu_{\rm bulk} = \mathscr{L}^{\rm bulk}_{\rm ddsv}(\mu_{\rm bulk})$, where

$$\mathscr{L}^{\rm bulk}_{\rm ddsv}(\bullet) = -\mathrm{i}\left[H_{\rm rtb} + \sum_{\alpha,i_\alpha \in \mathfrak{C}} H^{i_\alpha}_{\rm sv}(t), \bullet \right] + \sum_{\alpha i_\alpha, \beta j_\beta \in \mathfrak{C}} \mathscr{D}_{i_\alpha j_\beta}(\bullet). \quad (5)$$

Here, $H_{\rm rtb}$ is identical to the tight-binding model (1) with renormalized tunnelings and on-site energies [22]. The more relevant part for the thermalization of the bulk ions is the dissipation due to tunneling exchange with the reservoirs. This is similar to Eq. (2) but extended to all possible pairs of ions

$$\mathscr{D}_{i_\alpha j_\beta} = \mathscr{D}[\tilde{\Lambda}^+_{i_\alpha, j_\beta}, a^\dagger_{i_\alpha}, a_{j_\beta}] + \mathscr{D}[\tilde{\Lambda}^-_{i_\alpha, j_\beta}, a_{i_\alpha}, a^\dagger_{j_\beta}],$$

where we introduced non-local cooling and heating strengths $\tilde{\Lambda}^-_{i_\alpha, j_\beta} = \sum_{\ell_\tau} \frac{1}{2}\Gamma^{\ell_\tau}_{i_\alpha, j_\beta}(\bar{n}_{\ell_\tau} + 1)$, and $\tilde{\Lambda}^+_{i_\alpha, j_\beta} = \sum_{\ell_\tau} \frac{1}{2}\Gamma^{\ell_\tau}_{i_\alpha, j_\beta}\bar{n}_{\ell_\tau}$, respectively. These parameters depend on the sequential bulk-edge-bulk tunneling processes via the coupling matrix $\Gamma^{\ell_\tau}_{i_\alpha, j_\beta} = 2\pi J_{i_\alpha, \ell_\tau} \rho_{\ell_\tau}(\omega_{i_\alpha}) J_{\ell_\tau, j_\beta}$, where we have introduced a Lorentzian density of states for the laser-cooled τ-ions

$$\rho_{\ell_\tau}(\varepsilon) = \frac{1}{\pi} \frac{\gamma_{\ell_\tau}}{[(\varepsilon - \delta_{\ell_\tau}) - \omega_{\ell_\tau}]^2 + \gamma^2_{\ell_\tau}}, \quad \delta_{\ell_\tau} = \mathrm{Im}\{\Lambda^+_{\ell_\tau} - (\Lambda^-_{\ell_\tau})^*\}.$$

The process of thermalization of the TQW becomes clear from this derivation: Tunneling of vibrons from the bulk of

the wire into the reservoirs, and back, introduces an effective dissipation responsible for its thermalization. The cubic decay of the dipole-dipole tunnelings with distance suggests that the thermalization mainly occurs by exchange of vibrons between the reservoirs and the neighboring bulk ions. Moreover, since $\gamma_{\ell_\tau} \gg J_{i_\alpha j_\beta}$ the broad density of states $\rho_{\ell_\tau}(\varepsilon)$ does not allow to resolve the different vibrational levels of the TQW. We can thus predict a homogeneous steady-state vibron occupation

$$\langle n_{i_\alpha}\rangle_{\rm ss} = \frac{\Gamma_{\rm L}\bar{n}_{\rm L}+\Gamma_{\rm R}\bar{n}_{\rm R}}{\Gamma_{\rm L}+\Gamma_{\rm R}}, \qquad \alpha, i_\alpha \in \mathfrak{C}, \tag{6}$$

where we have defined the system-reservoir couplings as $\Gamma_{\rm L} = \Gamma^{1_\tau}_{2_\sigma,2_\sigma}$ and $\Gamma_{\rm R} = \Gamma^{N_\tau}_{(N-1)_\sigma,(N-1)_\sigma}$, and the reservoir mean vibron numbers $\bar{n}_{\rm L} = \bar{n}_{1_\tau}, \bar{n}_{\rm R} = \bar{n}_{N_\tau}$. Similar arguments apply to the vibron current, defined through $\partial_t n_{i_\alpha} = I^{\rm vib}_{\to i_\alpha} - I^{\rm vib}_{i_\alpha \to}$, which turns out to be independent of the length of the TQW

$$\langle I^{\rm vib}_{i_\alpha\to}\rangle_{\rm ss} = \langle I^{\rm vib}_{\to i_\alpha}\rangle_{\rm ss} = \frac{\Gamma_{\rm L}\Gamma_{\rm R}}{\Gamma_{\rm L}+\Gamma_{\rm R}}(\bar{n}_{\rm L}-\bar{n}_{\rm R}), \quad \alpha, i_\alpha \in \mathfrak{C}. \tag{7}$$

Numerical solutions of the full dissipative dynamics in Eq. (5) confirms our predictions [22]. These results violate *Fourier's law* of thermal conduction [8], which predicts: *(i)* A linear temperature gradient, which is equivalent to $\langle n_{i_\alpha}\rangle_{\rm FL} = \bar{n}_{\rm L} + (\bar{n}_{\rm R}-\bar{n}_{\rm L})i_\alpha/N$. *(ii)* A heat current that is inversely proportional to the length of the wire $\langle I^{\rm vib}_{i_\alpha\to}\rangle_{\rm FL} \propto (\bar{n}_{\rm L}-\bar{n}_{\rm R})/N$. The violation of these predictions is not a surprise, since Fourier's law only applies to diffusive processes. In our case, however, Eqs. (6)-(7) describe the ballistic transport of vibrons through the TQW, and are completely analogous to the equivalent expressions for electronic transport [32].

We consider two phase-breaking processes for a ballistic-diffusive crossover: *dephasing* [33] and *disorder* [34]. One should not expect a perfect recovery of Fourier's law for the small crystals realized in trapped-ion laboratories. However, we show that diffusion leads to clear signatures in the vibron occupation measurable in state-of-the-art experiments.

To engineer dephasing, a possibility is to modulate the trap frequencies with a noisy voltage [9]. We model such noise as a dynamic fluctuation of the on-site energies in Eq. (1), $\omega_{i_\alpha} \to \omega_{i_\alpha} + \delta\omega_{i_\alpha}(t)$, where $\delta\omega_{i_\alpha}(t)$ is a random process [22]. In a Born-Markov approximation, this leads to an additional term in Eq. (4), $\mathscr{L}_{\rm ddsv} \to \mathscr{L}_{\rm ddsv} + \mathscr{D}_{\rm d}$, where we have introduced

$$\mathscr{D}_{\rm d}(\bullet) = \sum_{\alpha,\beta}\sum_{i_\alpha,j_\beta} \Gamma_{\rm d} e^{-\frac{|\mathbf{r}^0_{i_\alpha}-\mathbf{r}^0_{j_\beta}|}{\xi_{\rm c}}}(n_{i_\alpha}\bullet n_{j_\beta} - n_{j_\beta}n_{i_\alpha}\bullet) + {\rm H.c.},$$

such that $\Gamma_{\rm d}$ is the dephasing rate, and $\xi_{\rm c}$ accounts for a noise correlation length [35]. In Fig. 2**(a)**, we show the homogeneous distribution of vibrons along the TQW in the absence of dephasing. When dephasing with $\xi_{\rm c} \ll L$ is switched on, we observe the onset of a linear gradient along the microtrap array [upper panel of Fig. 2**(b)**], which pinpoints the presence of diffusive transport. For the linear Paul trap, the inhomogeneity of the crystal modifies the linear gradient leading to an anomalous Fourier's law [lower panel of Fig. 2**(b)**].

Let us now turn to the problem of disorder. The scattering of vibrons by impurities can be modeled by modifying the on-site energies of Eq. (1), $\omega_{i_\alpha} \to \omega_{i_\alpha} + \Delta\omega_\alpha$, where $\Delta\omega_\alpha$ is a static random variable. To obtain such disorder, we apply a strong static spin-vibron coupling (3) with parameters $\nu_\alpha = 0, \varphi_\alpha = 0, \Delta\omega^+_\alpha = 0$, and $\Delta\omega^-_\alpha \neq 0$, such that the vibrons crossing the TQW experience an inhomogeneous landscape of on-site energies depending on the spin configuration [10]. When each bulk spin is initialized in $|+_{i_\alpha}\rangle = (|\uparrow_{i_\alpha}\rangle + |\downarrow_{i_\alpha}\rangle)/\sqrt{2}$, the tight-binding model (1) becomes stochastic [22], $H_{\rm tb} \to H_{\rm stb}$

$$H_{\rm stb} = \sum_{\alpha,i_\alpha}\varepsilon_{i_\alpha}a^\dagger_{i_\alpha}a_{i_\alpha} + \sum_{\alpha,\beta}\sum_{i_\alpha\neq j_\beta}\left(J_{i_\alpha j_\beta}a^\dagger_{i_\alpha}a_{j_\beta} + {\rm H.c.}\right).$$

Here, the on-site energies for the ions $\alpha, i_\alpha \in \mathfrak{C}$ are binary random variables sampling $\varepsilon_{i_\alpha} \in \{\omega_\alpha - \frac{1}{2}\Delta\omega^-_\alpha, \omega_\alpha + \frac{1}{2}\Delta\omega^-_\alpha\}$ with a flat probability distribution $p(\varepsilon_{i_\alpha}) = \frac{1}{2}$ inherited from the quantum parallelism. This randomness leads to Anderson localization, whereby normal modes display a finite localization length $\xi_{\rm loc}$ [36]. For the small ion crystals of length L here considered, the modes with $\xi_{\rm loc} \gg L$ contribute ballistically, those with $\xi_{\rm loc} \lesssim L$ introduce diffusion, and $\xi_{\rm loc} \ll L$ do not contribute to the transport. Hence, one can expect that the heat transport will be much richer in the disordered case. In the upper (lower) panel of Fig. 2**(c)**, we display the disorder-averaged distribution of vibrons along the TQW of a microtrap array (linear Paul trap). Far away from the edges, we recognize again the linear gradient representative of Fourier's law.

To distinguish between ballistic and diffusive transport we require a measuring tool for the vibron occupations. We suggest a general scheme for mapping the mean value of any vibron operator $\langle O_{i_\alpha}\rangle_{\rm ss}$, and its fluctuation spectrum

$$S_{O_{i_\alpha}O_{i_\alpha}}(\omega) = \int_0^\infty {\rm d}t \langle \tilde{O}_{i_\alpha}(t)\tilde{O}_{i_\alpha}(0)\rangle_{\rm ss} e^{-{\rm i}\omega t}, \quad \tilde{O}_{i_\alpha} = O_{i_\alpha} - \langle \tilde{O}_{i_\alpha}\rangle_{\rm ss},$$

onto the spin coherences, while disturbing the vibron states minimally. This idea goes along the lines of exploiting a qubit to measure phase fluctuations in a Bose-Einstein condensate [37] or full counting statistics of charge transport [38].

By engineering a spin-vibron coupling of the form $\tilde{H}^O_{\rm sv} = \sum_{i_\kappa}\frac{1}{2}\lambda_O O_{i_\kappa}\sigma^z_{i_\kappa}$, where λ_O is a weak coupling constant, the mean value and the fluctuations of the vibronic operator O_{i_κ} can be measured by Ramsey-type interferometry [22]. If the probe consists of a single κ-ion [39] initialized by a $\pi/2$-pulse in the spin state $|+_{i_\kappa}\rangle$, the κ-spin acquires phase information about the steady-state vibron observable. In order to recover this information, we perform another $\pi/2$-pulse, and measure the probability of observing the κ-ion in the spin-down state. This is equivalent to the measurement of the spin coherences

$$\langle \tilde{\sigma}^x_{i_\kappa}(t)\rangle = \cos(\lambda_O\langle O_{i_\kappa}\rangle_{\rm ss}t)e^{-\lambda_O^2 {\rm Re}\{S_{O_{i_\kappa}O_{i_\kappa}}(0)\}t}. \tag{8}$$

Therefore, the period (decay) of these spin oscillations yields the mean value (zero-frequency fluctuations) of the vibron operator $\langle O_{i_\kappa}\rangle_{\rm ss}$ ($S_{O_{i_\kappa}O_{i_\kappa}}(0)$). Due to the excellent accuracies of projective spin measurements with ion traps, which exceed 99% with millisecond detection times [19], probing the steady-state vibrons with this method promises to be very efficient. Specifically, the scheme allows us to measure the mean vibron number $O_{i_\kappa} = n_{i_\kappa}$. The required Ramsey-type coupling

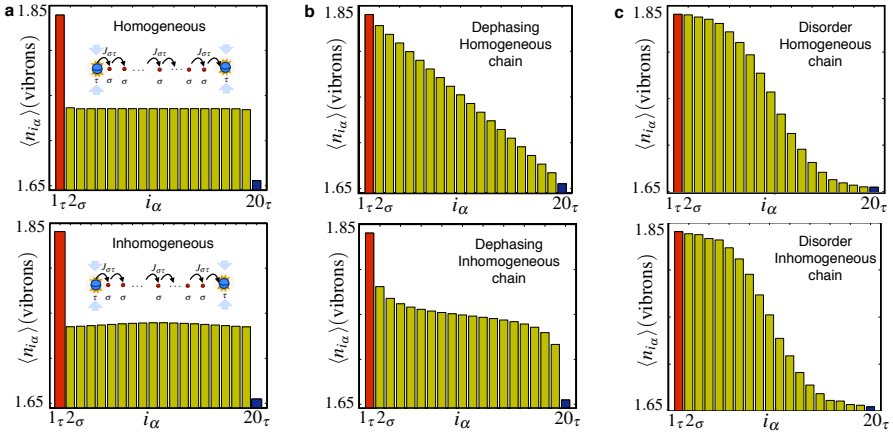

Figure 2. **Fourier's law:** Steady-state of a chain with $N = 20$ ions (upper panels: microtrap array, lower panels: linear Paul trap). We display the vibron distribution in **(a)** the ballistic regime, which is in agreement with the numerical results of [17], **(b)** the dephasing-induced diffusive regime, and **(c)** the disorder-induced diffusive regime.

is obtained directly by switching on a weak static spin-vibron coupling (3) with parameters $\nu_\kappa = 0, \varphi_\kappa = 0, \Delta\omega_\sigma^+ = 0$, and $\Delta\omega_\kappa^- \neq 0$. Then, the dynamics of the probe spin gives directly the mean vibron number $\langle n_{i_\kappa}\rangle_{\rm sss}$ and its fluctuations $S_{n_{i_\kappa}n_{i_\kappa}}(0)$. Let us note that, if the probe consists of several κ-ions, we get information about density-density correlators.

Thermal quantum dot and single-spin heat switch.– For realizing a thermal quantum dot (TQD), we consider a single κ-ion at position p_κ in the bulk of the crystal. We use the remaining σ-ions as thermal contacts by employing a strong static spin-phonon coupling (3) with parameters $\nu_\sigma = 0, \varphi_\sigma = 0, \Delta\omega_\sigma^+ = 0$, and $\Delta\omega_\sigma^- \neq 0$. When preparing the spins in $|\psi_0\rangle = |\downarrow_\sigma \cdots \downarrow_\sigma\rangle|\phi_\kappa\rangle|\uparrow_\sigma \cdots \uparrow_\sigma\rangle$, there is a large shift of the on-site energies at p_κ, inhibiting tunneling across the junction. Hence, the two halves of the chain thermalize independently $\langle n_{i_\sigma}\rangle_{\rm ss} = \bar{n}_{\rm L}$ for $i_\sigma < p_\kappa$, and $\langle n_{i_\sigma}\rangle_{\rm ss} = \bar{n}_{\rm R}$, for $i_\sigma > p_\kappa$, leading to an analogue of a quantum dot between two leads. The Liouvillian is $\mathscr{L}_{\rm ddtb}^{\rm bulk} = \mathscr{L}_{\rm L} + \mathscr{L}_{\rm L\kappa R} + \mathscr{L}_{\rm R}$, where $\mathscr{L}_{\rm L/R}$ describe the uncoupled halves (5), and $\mathscr{L}_{\rm L\kappa R}$ describes the TQD.

So far, the transport through the TQD is blocked by the large mismatch of on-site energies. The main idea is to switch it on by the remaining gadget in our toolbox, a dynamical spin-vibron coupling (3) for the κ-ion. For spin-independent drivings $\Delta\omega_\kappa^- = 0$, the periodic modulation of the on-site energies assists the tunnelings by absorbing energy from the driving to overcome the on-site gradient [14]. In this work, we propose to exploit the genuine spin-dependence of the drivings to build a *single-spin heat switch* and a *current probe*.

For the single-spin heat switch, the parameters of the spin-vibron coupling (3) are $\nu_\kappa = \frac{1}{2}\Delta\omega_\sigma^-$, $\varphi_\kappa = 0$, $\Delta\omega_\kappa^- = \Delta\omega_\kappa^+$, which lead to $\mathscr{L}_{\rm L\kappa R}(\bullet) = -{\rm i}[H_{\rm L\kappa R}^{\rm PAT}, \bullet] + \mathscr{D}_{p_\kappa p_\kappa}(\bullet)$, where

$$H_{\rm L\kappa R}^{\rm PAT} = -\sum_{i_\sigma < p_\kappa} J_{p_\kappa i_\sigma}^{\rm PAT}(\sigma_{p_\kappa}^z) a_{p_\kappa}^\dagger a_{i_\sigma} + \sum_{i_\sigma > p_\kappa} J_{p_\kappa i_\sigma}^{\rm PAT}(\sigma_{p_\kappa}^z) a_{p_\kappa}^\dagger a_{i_\sigma} + {\rm H.c.}.$$

Here, the tunneling becomes a spin operator through the argument of the first Bessel's function $J_{p_\kappa i_\sigma}^{\rm PAT}(\sigma_{p_\kappa}^z) = \tilde{J}_{p_\kappa i_\sigma}\mathfrak{J}_1\big(\zeta_\kappa(1+\sigma_{p_\kappa}^z)\big)$, where $\zeta_\kappa = \Delta\omega_\kappa^+/2\nu_\kappa$ [22]. We note that $J_{p_\kappa i_\sigma}^{\rm PAT}(\sigma_{p_\kappa}^z)|\downarrow_{p_\kappa}\rangle = 0$, while $J_{p_\kappa i_\sigma}^{\rm PAT}(\sigma_{p_\kappa}^z)|\uparrow_{p_\kappa}\rangle \neq 0$. Therefore, by controlling the κ-spin state via microwave π-pulses, it is possible to switch on/off the heat current through the TQD. Note that different switches have also been exploited in [41] to control the entanglement dynamics in harmonic chains.

For a Ramsey probe of the vibron current, we need a minimally-perturbing mapping of the current onto the κ-spin. This requires a bichromatic spin-vibron coupling (3) with specific parameters [42]. The first frequency assists the heat flow

$$H_{\rm L\kappa R}^{\rm PAT} = \sum_{i_\sigma}(\tilde{J}_{i_\sigma,p_\kappa}^{\rm PAT} a_{i_\sigma}^\dagger a_{p_\kappa} + {\rm H.c.}), \quad \tilde{J}_{i_\sigma,p_\kappa}^{\rm PAT} = -{\rm i}2\tilde{J}_{i_\sigma p_\kappa}\mathfrak{J}_1(\pi),$$

such that the dressed tunneling becomes purely imaginary. This is crucial to devise the probe, since the second frequency leads to $H_{\rm sv}^I = \frac{1}{2}\tilde{\lambda}_I I_{p_\kappa}^{\rm vib}\sigma_{p_\kappa}^z$, where $I_{p_\kappa} = \frac{1}{2}(I_{p_\kappa\to}^{\rm vib} + I_{\to p_\kappa}^{\rm vib})$. In the limit $\zeta_{\kappa,2} \to 0$, $\tilde{\lambda}_I \approx 4\zeta_{\kappa,2}/\pi$, we get a Ramsey probe (8) for the current mean value $\langle I_{p_\kappa}^{\rm vib}\rangle$ and fluctuations $S_{I_{p_\kappa}^{\rm vib} I_{p_\kappa}^{\rm vib}}(0)$.

The ability to measure these fluctuations is essential for the comparison between fermionic and bosonic currents through the so-called Fano factor $\mathscr{F} = S_{I_{p_\kappa}^{\rm vib} I_{p_\kappa}^{\rm vib}}(0)/2\langle I_{p_\kappa}^{\rm vib}\rangle$. For the heat current trough the TQD, we expect strong super-Poissonian fluctuations, which are most pronounced for symmetric coupling to the thermal leads and increase linearly with $\bar{n}_L$ in the regime $\bar{n}_L \gg \bar{n}_R$ [12, 43]. Unlike the sub-Poissonian fluctuations in electrical currents, the super-Poissonian fluctuations in heat currents have not been observed yet.

Conclusions.– In summary, we have outlined the implementation of an ion-trap toolbox for quantum heat transport, which provides *(i)* analogues of thermal reservoirs, quantum dots and wires; *(ii)* a way of engineering on-site disorder and dephasing, and *(iii)* noninvasive probes for both vibron occupations and currents. We emphasize that the incorporation of these functionalities significantly extends the possible range of experiments on heat transport. Laser-cooling the edge ions to either coherent or squeezed vibron states [44], may constitute other valuable supplements to our toolbox. We expect, in addition, interesting effects in the presence of non-linearities, such as the interplay with Mott insulators [21], thermal rectification [45], and structural phase transitions [46]. In a

non-equilibrium transport version of the spin-Peierls instability [47], it will also be interesting to explore if a finite heat current can be correlated to the structural change.

We are supported by PICC and by the Alexander von Humboldt Foundation. A.B. thanks FIS2009-10061, QUITEMAD.

[1] D. G. Cahill, W. K. Ford, K. E. Goodson, G. D. Mahan, A. Majumdar, H. J. Maris, R. Merli, and S. R. Phillpot, J. Appl. Phys. **93,** 793 (2003); E. Pop, Nano Res. **3,** 147 (2010).

[2] S. Gustavsson, R. Leturcq, M. Studer, I. Shorubalko, T. Ihn, K. Ensslin, D.C. Driscoll and A.C. Gossard, Surf. Sci. Rep. **64,** 191 (2009); N. A. Zimbovskaya and M. R. Pederson, Phys. Rep. **509,** 1 (2011).

[3] Y. Dubi and M. Di Ventra, Rev. Mod. Phys. **83,** 131 (2011).

[4] A. Majumdar, Annu. Rev. Mater. Sci. **29,** 505 (1999).

[5] P. Kim, L. Shi, A. Majumdar, and P. L. McEuen, Phys. Rev. Lett. **87,** 215502 (2001); R. Chen, A.I. Hochbaum, P. Murphy, J. Moore, P. Yang, and A. Majumdar, Phys. Rev. Lett. **101,** 105501 (2008); J. H. Seol, I. Jo, A. L. Moore, L. Lindsay, Z. H. Aitken, M. T. Pettes, X. Li, Z. Yao, R. Huang, D. Broido, N. Mingo, R. S. Ruoff, and L. Shi, Science **328,** 213 (2010).

[6] K. Schwab, E. A. Henriksen, J. M. Worlock, and M. L. Roukes, Nature, **404**, 974 (2000).

[7] D. J. Wineland, C. Monroe, W. M. Itano, D. Leibfried, B. E. King, and D. M. Meekhof, J. Res. Natl. I. St. Tech. **103,** 259 (1998).

[8] *See* S. Lepri, R. Livi, and A. Politi, Phys. Rep. **377,** 1(2003), *and references therein*.

[9] C. J. Myatt, B. E. King, Q. A. Turchette, C. A. Sackett, D. Kielpinski, W. M. Itano, C. Monroe, and D. J. Wineland, Nature **403,** 269 (2000).

[10] A. Bermudez, M. A. Martin-Delgado, and D. Porras, New J. Phys. **12,** 123016 (2010).

[11] M. Esposito, U. Harbola, and S. Mukamel, Rev. Mod. Phys. **81,** 1665 (2009).

[12] U. Harbola, M. Esposito, and S. Mukamel, Phys. Rev. B, **76,** 085408 (2007).

[13] D. H. Dunlap and V. M. Kenkre, Phys. Rev. B **34,** 3625 (1986); F. Grossman, T. Dittrich, P. Jung, and P. Hänggi, Phys. Rev. Lett. **67,** 516 (1991); M. Holthaus, Phys. Rev. Lett. **69,** 351 (1992).

[14] A. Bermudez, T. Schaetz, and D. Porras, Phys. Rev. Lett. **107,** 150501 (2011); *ibid.* New J. Phys. **14,** 053049 (2012).

[15] T. Pruttivarasin, M. Ramm, I. Talukdar, A. Kreuter, and H. Häffner, New J. Phys. **13,** 075012 (2011).

[16] O. Abah, J. Rossnagel, G. Jacob, S. Deffner, F. Schmidt-Kaler, K. Singer, and E. Lutz, Phys. Rev. Lett. **109,** 203006 (2012).

[17] G-D Lin and L-M Duan, New J. Phys. **13,** 075015 (2011).

[18] U. Zürcher and P. Talkner, Phys. Rev. A **42,** 3267 (1990); *ibid.* **42,** 3278 (1990).

[19] T. D. Ladd, F. Jelezko, R. Laflamme, Y. Nakamura, C. Monroe, and J. L. OBrien, Nature **464,** 45 (2010).

[20] K. R. Brown, C. Ospelkaus, Y. Colombe, A. C. Wilson, D. Leibfried, and D. J. Wineland, Nature **471,** 196 (2011); M. Harlander, R. Lechner, M. Brownnutt, R. Blatt, and W. Hänsel, Nature **471,** 200 (2011); S. Haze, Y. Tateishi, A. Noguchi, K. Toyoda, and S. Urabe, Phys. Rev A **85,** 031401(R) (2012).

[21] D. Porras and J.I. Cirac, Phys. Rev. Lett. **93,** 263602 (2004).

[22] See the Supplemental Material.

[23] J. I. Cirac, R. Blatt, P. Zoller, and W. D. Phillips, Phys. Rev. A **46,** 2668 (1992).

[24] M. D. Barrett, B. DeMarco, T. Schaetz, V. Meyer, D. Leibfried, J. Britton, J. Chiaverini, W. M. Itano, B. Jelenkovic, J. D. Jost, C. Langer, T. Rosenband, and D. J. Wineland, Phys. Rev. A **68,** 042302 (2003); J. P. Home, M. J. McDonnell, D. J. Szwer, B. C. Keitch, D. M. Lucas, D. N. Stacey, and A. M. Steane, Phys. Rev. A **79,** 050305(R) (2009); J. P. Home, D. Hanneke, J. D. Jost, J. M. Amini, D. Leibfried, and D. J. Wineland, Science **325,** 1227 (2009).

[25] A. Walther, U. Poschinger, K. Singer, and F. Schmidt-Kahler, Appl. Phys. B **107,** 1061 (2012).

[26] Note that laser cooling of mixed crystals has been shown for traveling waves [24], and standing-wave cooling may be achieved along the lines of Ref. [25]. A possible alternative to obtain the required strong cooling are the schemes based on the dynamical Stark-shift [27] or pulsed sequences [28].

[27] A. Retzker and M. B. Plenio, New J. Phys. **9,** 279 (2007).

[28] S. Machnes, M. B. Plenio, B. Reznik, A. M. Steane, and A. Retzker, Phys. Rev. Lett. **104,** 183001 (2010).

[29] Note that similar couplings, but linear in the vibron operators, have been demonstrated experimentally [30].

[30] D. Leibfried, B. DeMarco, V. Meyer, D. Lucas, M. Barrett, J. Britton, W. M. Itano, B. Jelenkovic, C. Langer, T. Rosenband, and D. J. Wineland, Nature **422,** 412 (2003); A. Friedenauer, H. Schmitz, J. T. Glueckert, D. Porras, and T. Schaetz, Nat. Phys. **4,** 757 (2008).

[31] K. Saito, Europhys. Lett. **61,** 34 (2003); M. Michel, M. Hartmann, J. Gemmer, G. T. Mahler, Eur. Phys. J. B **34**, 325 (2003); T. Prosen, New J. Phys. **10,** 043026 (2008).

[32] J.C. Cuevas and E. Scheer, Molecular Electronics: An Introduction to Theory and Experiment (World Scientific, London, 2010).

[33] Y. Dubi, Y. and M. Di Ventra, Phys. Rev. E **79,** 042101 (2009); A. Asadian, D. Manzano, M. Tiersch, and H. J. Briegel, Phys. Rev. E **87,** 012109 (2013).

[34] R. J. Rubin and W. L. Greer, J. Math. Phys. **12,** 1686 (1971); A. Casher and J. L. Lebowitz, J. Math. Phys. **12,** 1701 (1971).

[35] The parameter ξ_c may be controlled accurately in microtrap arrays, and to some extent in the more standard linear Paul traps.

[36] P. W. Anderson, Phys. Rev. **109,** 1492 (1958).

[37] M. Bruderer and D. Jaksch, New J. Phys. **8,** 87 (2006).

[38] G. B. Lesovik, F. Hassler and G. Blatter, Phys. Rev. Lett. **96,** 106801 (2006).

[39] Since the coherence of the spins used to introduce disorder is lost due to the strong spin-vibron couplings, we modify the configuration in Fig. 1**(a)** by introducing a small number of κ-ions for measuring, while reserving the σ-spins for disorder.

[40] H. Haeffner, C. F. Roos, and R. Blatt, Phys. Rep. **469,** 155 (2008).

[41] M.B. Plenio, J. Hartley, and J. Eisert, New J. Phys. **6,** 36 (2004).

[42] The parameters of the bi-chromatic spin-vibron coupling are $\varphi_{\kappa,1}=\frac{\pi}{2}$, $\varphi_{\kappa,2}=0$, $\nu_{\kappa,1}=\nu_{\kappa,2}=\frac{1}{2}\Delta\omega_{\sigma}^{-}$, and $\Delta\omega_{\kappa,1}^{-}=\Delta\omega_{\kappa,2}^{-}=0$. $\zeta_{\kappa,1}=\Delta\omega_{\kappa,1}^{+}/2\nu_{\kappa,1}=\pi$, $\zeta_{\kappa,2}=\Delta\omega_{\kappa,2}^{+}/2\nu_{\kappa,2}\ll 1$.

[43] M. Kindermann, Yu. V. Nazarov, and C. W. J. Beenakker, Phys. Rev. Lett. **88,** 063601 (2002).

[44] J. F. Poyatos, J.I. Cirac, and P. Zoller, Phys. Rev. Lett. **77**, 4728 (1996).

[45] D. Segal and A. Nitzan, Phys. Rev. Lett. **94,** 034301 (2005).

[46] S. Fishman, G. De Chiara, T. Calarco, and G. Morigi, Phys. Rev. B **77,** 064111 (2008); A. Retzker, R.C. Thompson, D.M.

Segal and M.B. Plenio, Phys. Rev. Lett. **101,** 260504 (2008).
[47] A. Bermudez and M.B. Plenio, Phys. Rev. Lett. **109,** 010501 (2012).

I. SUPPLEMENTAL MATERIAL: CONTROLLING AND MEASURING THE QUANTUM TRANSPORT OF HEAT IN TRAPPED-ION CRYSTALS

In this supplemental material (SM), we present a detailed derivation of the expressions used in the main text. Besides, we test its validity by comparing the analytical expressions to numerical results for ion-trap setups with realistic parameters. Therefore, this SM will also be useful to guide an experimental realization of the ideas discussed in our work. The contents of this SM are organized as follows:

CONTENTS

Appendix A: Trapped-ion toolbox for quantum transport

The objective of this section is to present a detailed derivation, supported by numerical simulations, of the three gadgets in our toolbox: the vibronic tight-binding model (1), the controlled dissipation (2), and the spin-vibron coupling (3).

1. Tight-binding model for the vibrons

Let us start by describing how the Hamiltonian (1) for the transverse vibrons in a linear ion chain is derived. The dynamics of an ensemble of $N=N_\sigma+N_\tau+N_\kappa$ ions of three different species/isotopes is described by the following Hamiltonian

$$H=\sum_{\nu}\sum_{\alpha,i_\alpha}\left(\frac{p_{i_\alpha,\nu}^2}{2m_\alpha}+\frac{1}{2}m_\alpha\omega_{\alpha,\nu}^2 r_{i_\alpha,\nu}^2\right)+\frac{e_0^2}{2}\sum_{\alpha,\beta}\sum_{i_\alpha\neq j_\beta}\frac{1}{|\mathbf{r}_{i_\alpha}-\mathbf{r}_{j_\beta}|}, \tag{A1}$$

where $\nu\in\{x,y,z\}$ labels the different directions of motion, the latin indexes $i,j\in\{1\cdots N\}$ label the ions, and the greek sub-indexes $\alpha,\beta\in\{\sigma,\tau,\kappa\}$ specify the particular type of ion. Here, $\omega_{\alpha,\nu}$ are the trap frequencies for each ion species along the different axes, and $e_0^2=e^2/4\pi\varepsilon_0$ is expressed in terms of the electron charge and the vacuum permittivity.

When the trap frequencies fulfill $\omega_{\alpha,z}\ll\omega_{\alpha,x},\omega_{\alpha,y}$, the equilibrium of the trapping and Coulomb forces leads to a Wigner-type crystal at low temperatures, the so-called Coulomb crystal. The crystalline equilibrium positions lie along the z-axis $\mathbf{r}_{i_\alpha}^0=z_{i_\alpha}^0\mathbf{e}_z$, and are given by the solution of the following system of algebraic equations

$$\mu_\alpha\kappa_\alpha\tilde{z}_{i_\alpha}^0-\sum_{\beta}\sum_{j_\beta\neq i_\alpha}\frac{\tilde{z}_{i_\alpha}^0-\tilde{z}_{j_\beta}^0}{|\tilde{z}_{i_\alpha}^0-\tilde{z}_{j_\beta}^0|^3}=0,\quad\forall\alpha,i_\alpha. \tag{A2}$$

Here we have introduced the relative masses $\mu_\alpha=m_\alpha/m_\sigma$, and the anisotropy of the trap frequencies $\kappa_\alpha=\omega_{\alpha,z}^2/\omega_{\sigma,z}^2$. In this expression, we write the positions in terms of a common unit of length $z_{i_\alpha}^0=l_\sigma\tilde{z}_{i_\alpha}^0$, where $l_\sigma=(e_0^2/m_\sigma\omega_{\sigma,z}^2)^{1/3}$. For linear Paul traps, these equilibrium positions lead to an inhomogeneous crystal, such that the ions in the center are more closely spaced than those at the boundaries [1]. By segmenting the electrodes, it is possible to introduce a quartic component in the axial trapping potential, such that the crystal becomes more homogeneous [2]. Moreover, with the advent of the so-called micro-fabricated surface traps, it is possible to design the distribution of radio-frequency electrodes, such that the ions are held in any desired lattice geometry above the trap surface [3]. Therefore, we will also investigate homogeneous linear ion crystal for quantum heat transport.

As customary, a Taylor expansion to second order in the small vibrations around these equilibrium position lead to a quadratic model, the so-called harmonic crystal [4]. In the particular case of the ion chain, the vibrations along each direction $r_{i_\alpha\nu}=r_{i_\alpha\nu}^0+\delta r_{i_\alpha\nu}$ get decoupled [1]. In particular, for the transversal direction $\nu=x$, after setting $\omega_{\alpha,x}=\omega_\alpha$ hereafter, the Hamiltonian becomes

$$H_x=\sum_{\alpha,i_\alpha}\left(\frac{p_{i_\alpha x}^2}{2m_\alpha}+\frac{m_\alpha}{2}\omega_\alpha^2\delta r_{i_\alpha x}^2\right)+\sum_{\alpha,\beta}\sum_{i_\alpha,j_\beta}\mathscr{V}_{i_\alpha j_\beta}\delta r_{i_\alpha x}\delta r_{j_\beta x}, \tag{A3}$$

where we have defined the following Coulomb couplings

$$\mathscr{V}_{i_\alpha j_\beta}=\frac{e_0^2}{2|z_{i_\alpha}^0-z_{j_\beta}^0|^3},\ i_\alpha\neq j_\beta,\quad \mathscr{V}_{i_\alpha i_\alpha}=-\sum_{\beta,j_\beta}\mathscr{V}_{i_\alpha j_\beta}. \tag{A4}$$

Table I. **Vibrational parameters for each ion species**

$\omega_\alpha/2\pi$	$\lvert z^0_{i_\alpha} - z^0_{(i+1)_\beta}\rvert$	$J_{i_\alpha(i+1)_\beta}/2\pi$	$\mu_\alpha = \frac{m_\alpha}{m_\sigma}$
1-10 MHz	1-10 μm	1-100 kHz	1-10

The coupling between the vibrations of distant ions can also be understood as the result of a dipole-dipole interaction $V_{\rm dd} \propto d_{i_\alpha} d_{j_\beta}/|z^0_{i_\alpha} - z^0_{j_\beta}|^3$ between the effective dipoles $d_{i_\alpha} = e\delta r_{i_\alpha x}$ induced by the vibrating charges [5]. By quantizing the vibrations via the creation-annihilation operators

$$p_{i_\alpha x} = \mathrm{i}\sqrt{\tfrac{m_\alpha \omega_\alpha}{2}}\left(a^\dagger_{i_\alpha} - a_{i_\alpha}\right), \quad \delta r_{i_\alpha x} = \sqrt{\tfrac{1}{2m_\alpha\omega_\alpha}}\left(a^\dagger_{i_\alpha} + a_{i_\alpha}\right), \tag{A5}$$

we get the announced quadratic model for lattice vibrons

$$H_x = \sum_{\alpha,i_\alpha} \omega_\alpha a^\dagger_{i_\alpha} a_{i_\alpha} + \frac{1}{2}\sum_{\alpha,\beta}\sum_{i_\alpha,j_\beta} J_{i_\alpha j_\beta}\left(a^\dagger_{i_\alpha} + a_{i_\alpha}\right)\left(a^\dagger_{j_\beta} + a_{j_\beta}\right), \tag{A6}$$

where we have defined the tunneling strengths

$$J_{i_\alpha j_\beta} = \frac{1}{\sqrt{m_\alpha\omega_\alpha m_\beta \omega_\beta}}\mathscr{V}_{i_\alpha j_\beta}. \tag{A7}$$

The final ingredient to obtain the desired tight-binding model (1) is to neglect the terms in Eq. (A6) that do not conserve the number of vibrons, which is justified when the trap frequencies are much stronger than the tunneling strengths [6], namely $J_{i_\alpha j_\beta} \ll \omega_\alpha + \omega_\beta$. Using a rotating wave approximation (RWA), the Hamiltonian (A6) can be expressed as the sum of the vibronic on-site energy term $H_{\rm vo}$, and the vibron tunneling $H_{\rm vt}$. This gives rise to the vibronic tight-binding model $H_{\rm tb} = H_{\rm vo} + H_{\rm vt}$ of Eq. (1) in the main text, namely

$$\begin{aligned} H_{\rm vo} &= \sum_{\alpha,i_\alpha} \omega_{i_\alpha} a^\dagger_{i_\alpha} a_{i_\alpha}, \quad \omega_{i_\alpha} = \omega_\alpha + J_{i_\alpha i_\alpha} \\ H_{\rm vt} &= \sum_{\alpha,\beta}\sum_{i_\alpha \neq j_\beta}\left(J_{i_\alpha j_\beta} a^\dagger_{i_\alpha} a_{j_\beta} + \text{H.c.}\right). \end{aligned} \tag{A8}$$

As demonstrated in recent experiments [5, 7, 8], this model allows for a controlled tunneling of vibrons between different ions, which can be used for quantum-information processing. We would like to note that for the longitudinal vibrations of the ions confined in linear Paul traps, it is not possible to neglect the terms that do not conserve the number of vibrons. In this respect, the analogy to electron transport via the tight-binding model is compromised, although the system would still allow for the study of quantum heat transport.

In order to show that the approximations leading to the vibronic tight-binding model are satisfied under realistic conditions, we perform a numerical comparison of the dynamics under Hamiltonians (A1) and (A8). The typical orders of magnitude for the vibronic parameters are summarized in Table I. Let us consider a particular example of a two-ion crystal with the species $\sigma = {}^{25}\mathrm{Mg}^+$, and $\tau = {}^{24}\mathrm{Mg}^+$. The trap frequencies are $(\omega_{\alpha x}, \omega_{\alpha y}, \omega_{\alpha z})/2\pi = (5, 5, 0.5)$ MHz, which lead to an inter-ion distance of $|z^0_{1_\tau} - z^0_{2_\sigma}| \approx 10\,\mu$m, and to a vibron tunneling strength of $J_{1_\tau 2_\sigma}/2\pi \approx 12$ kHz. We consider an initial pure state with a single vibronic excitation along the x-axis of the $\sigma = {}^{25}\mathrm{Mg}^+$ ion. As a consequence of the tunneling, this vibron should be periodically interchanged with the neighboring $\tau = {}^{24}\mathrm{Mg}^+$ ion. In Fig. 3, we observe the predicted periodic vibron tunneling. The filled circles and squares are the predictions of the approximate Hamiltonian (A8), whereas the solid lines correspond to the original Coulomb Hamiltonian (A1). To obtain the dynamics numerically, we truncate the vibron Hilbert space to $n_{\max} = 2$, and consider the three vibrational axis (i.e. 6 vibronic modes) with Coulomb non-linearities taken up to 8-th order (e.g. $a^8_{i_\alpha}$). This simulation shows that the approximations leading to the tight-binding model are very accurate for realistic parameters.

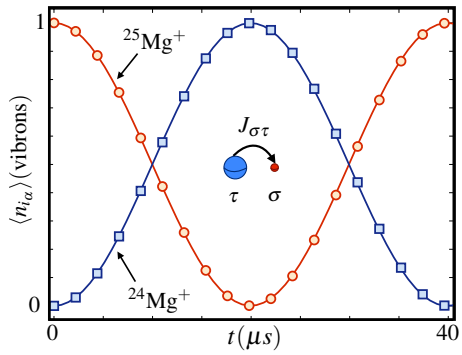

Figure 3. **Vibronic quantum dynamics:** Exchange of a vibrational quantum (i.e. vibron) between two distant $\sigma = {}^{25}\mathrm{Mg}^+$, and $\tau = {}^{24}\mathrm{Mg}^+$ ions confined by a linear Paul trap with an equilibrium distance of $10\,\mu$m. The solid lines represent the vibronic numbers given by the original Coulomb Hamiltonian (A1) (red: $\langle n_{1_\sigma}\rangle$ for ${}^{25}\mathrm{Mg}^+$, blue: $\langle n_{2_\tau}\rangle$ for ${}^{24}\mathrm{Mg}^+$), whereas the symbols stand for the vibronic numbers given the effective tight-binding model (A8) (red squares: $\langle n_{1_\sigma}\rangle$ for ${}^{25}\mathrm{Mg}^+$, blue circles: $\langle n_{2_\tau}\rangle$ for ${}^{24}\mathrm{Mg}^+$).

2. Atomic degrees of freedom

Once the vibronic Hamiltonian (A8) has been derived, let us turn our attention to the atomic degrees of freedom of the ion chain. The different ion species can be divided into two groups, depending on wether we want to exploit the coherent $\mathfrak{C}$ or incoherent $\mathfrak{I}$ (i.e. dissipative) dynamics of the ions. In particular, we select the ion species $\tau \in \mathfrak{I}$, and $\sigma, \kappa \in \mathfrak{C}$.

For the τ-ions, we select a dipole-allowed transition $|g_{\ell_\tau}\rangle \leftrightarrow |e_{\ell_\tau}\rangle$ [Fig. 4**(a)**], whereas for the $\{\sigma, \kappa\}$ ions, the dipole-allowed transitions from a two-dimensional ground-state manifold $\{|g_{i_{\alpha,1}}\rangle, |g_{i_\alpha,2}\rangle\} \leftrightarrow |e_{i_\alpha}\rangle$ define a so-called Λ-scheme [Fig. 4**(b)**]. We will now describe the atomic dynamics for any particular species. In the absence of any laser radiation, the master equation for the atomic density matrix, $\dot\rho = -\mathrm{i}[H_{\rm s}, \rho] + \mathscr{D}(\rho)$. This contains a Hamiltonian part $H_{\rm s} = H^\sigma_{\rm s} + H^\tau_{\rm s} + H^\kappa_{\rm s}$, where each ionic species $\alpha = \{\tau, \sigma, \kappa\}$

evolves under

$$H_{\rm s}^{\alpha}=\sum_{i_\alpha,n_\alpha}\varepsilon_{g_{\alpha,n_\alpha}}|g_{i_{\alpha,n_\alpha}}\rangle\langle g_{i_{\alpha,n_\alpha}}|+\sum_{i_\alpha}\varepsilon_{e_\alpha}|e_{i_\alpha}\rangle\langle e_{i_\alpha}|, \tag{A9}$$

and we have introduced the different atomic energies $\varepsilon_{(\cdot)}$, and the index $n_\tau=1$, $n_\sigma,n_\kappa\in\{1,2\}$ which depends on the dimension of the ground-state manifold. Due to the coupling with the electromagnetic environment, the dipole-allowed transitions are also characterized by a spontaneous decay rate Γ_α. Considering the recoil effects of the emitted photons [9], the dissipation is described by a super-operator $\mathscr{D}(\rho)=\sum_\alpha\mathscr{D}_\alpha(\rho)$, where we have introduced

$$\mathscr{D}_\alpha(\bullet)=\sum_{i_\alpha,n_\alpha}\int\mathrm{d}\xi_\alpha\Big(S^-_{i_\alpha,n_\alpha}\mathrm{e}^{-\mathrm{i}k_{n_\alpha}\mathbf{u}_k\cdot\mathbf{r}_{i_\alpha}}\bullet\,\mathrm{e}^{\mathrm{i}k_{n_\alpha}\mathbf{u}_k\cdot\mathbf{r}_{i_\alpha}}S^+_{i_\alpha,n_\alpha} -S^+_{i_\alpha,n_\alpha}S^-_{i_\alpha,n_\alpha}\bullet+\mathrm{H.c.}\Big). \tag{A10}$$

Here, we have defined the raising-lowering operators for each transition $S^+_{i_\alpha,n_\alpha}=|e_{i_\alpha}\rangle\langle g_{i_\alpha,n_\alpha}|=(S^-_{i_\alpha,n_\alpha})^\dagger$, and integrated (summed) over all different directions (polarizations) of the emitted photon $\int\mathrm{d}\xi_\alpha=\frac{3\Gamma_\alpha}{16\pi}\int_0^{4\pi}\mathrm{d}\Omega_{\mathbf{u}_k}\sum_{\boldsymbol{\varepsilon}}|\boldsymbol{\varepsilon}\cdot\mathbf{u}_{\alpha,n_\alpha}|^2$. In this expression, $k_{n_\alpha}\mathbf{u}_k$ is the wavevector of the emitted photon along the unit vector $\mathbf{u}_k$, whose modulus is determined by energy conservation $k_{n_\alpha}=\frac{1}{c}(\varepsilon_{e_\alpha}-\varepsilon_{g_{\alpha,n_\alpha}})$. Additionally, we have introduced the unit vectors of the atomic dipole operator $\mathbf{u}_{\alpha,n_\alpha}$, which depend on the angular-momentum rules for the dipole-allowed transition, and thus on the polarization of the emitted photon $q\in\{0,\pm1\}=\{\pi,\sigma^\pm\}$ [9]. If we assume that a quantization magnetic field is applied along the trap axis (i.e. z-axis), we have

$$\mathbf{u}_{\alpha,n_\alpha}=\mathbf{e}_z,\ \ q=0,\quad \mathbf{u}_{\alpha,n_\alpha}=\frac{1}{\sqrt{2}}(\mp\mathbf{e}_x-\mathrm{i}\mathbf{e}_y),\ \ q=\pm1. \tag{A11}$$

Let us note that the first term in the above dissipator contains the coupling of the atomic and vibrational degrees of freedom of the ions, which is a consequence of the recoil kicks associated to the photon-emission processes. This expression can be simplified further when the vibrations are much smaller than the wavelength of the emitted light, namely $\mathbf{r}_{i_\alpha}=\mathbf{r}^0_{i_\alpha}+\delta\mathbf{r}_{i_\alpha}$, such that $k_{n_\alpha}|\mathbf{u}_k\cdot\delta\mathbf{r}_{i_\alpha}|\ll1$ (i.e. Lamb-Dicke limit). We Taylor expand the dissipator (A10), and make use of the following integrals for dipole-allowed transitions

$$\begin{aligned}&\int\mathrm{d}\xi_\alpha 1=\tfrac{1}{2}\Gamma_\alpha,\qquad\int\mathrm{d}\xi_\alpha\mathbf{e}_\nu\cdot\mathbf{u}_k=0,\\&\int\mathrm{d}\xi_\alpha(\mathbf{e}_\nu\cdot\mathbf{u}_k)(\mathbf{e}_\mu\cdot\mathbf{u}_k)=\tfrac{1}{2}\Gamma_\alpha\alpha_{q\nu}\delta_{\nu,\mu},\end{aligned} \tag{A12}$$

where $\nu,\mu\in\{x,y,z\}$ account for the vibrational directions along the unit vectors $\mathbf{e}_\nu,\mathbf{e}_\mu$, $\delta_{\nu,\mu}$ is the Kronecker delta, and we have introduced the following constants

$$\alpha_{qx}=\alpha_{qy}=\frac{2+q^2}{5(1+q^2)},\quad \alpha_{qz}=\frac{1+3q^2}{5(1+q^2)}. \tag{A13}$$

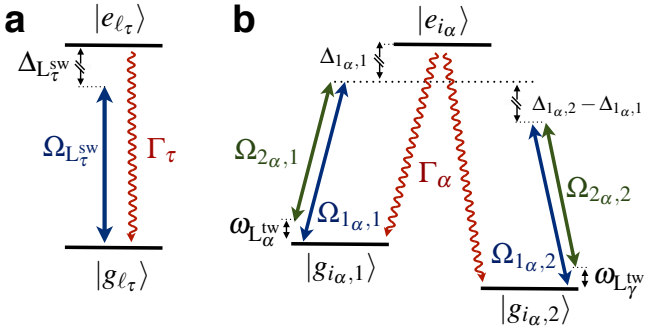

Figure 4. **Atomic level scheme for the different ions: (a)** Two-level scheme $\{|g_{\ell_\tau}\rangle,|e_{\ell_\tau}\rangle\}$ for a dipole-allowed transition with decay rate Γ_τ of the τ-ions, which is driven by a laser in a standing-wave configuration $\mathrm{L}^{\mathrm{sw}}_\tau$, such that the Rabi frequency is $\Omega_{\mathrm{L}^{\mathrm{sw}}_\tau}$. The standing wave is red-detuned $\Delta_{\mathrm{L}^{\mathrm{sw}}_\tau}<0$ from the atomic transition, such that we can use it for laser cooling. **(b)** Three-level Λ-scheme $\{|g_{i_{\alpha,1}}\rangle,|g_{i_\alpha,2}\rangle,|e_{i_\alpha}\rangle\}$ for a dipole-allowed transition with decay rate Γ_α of the $\alpha=\{\sigma,\kappa\}$-ions. We use a couple of laser beams in a traveling-wave configuration, such that their Rabi frequencies for each of the optical transitions are $\Omega_{l_\alpha,n_\alpha}$, where $n_\alpha=1,2$ stands for the two possible ground-states, and $l_\alpha=1_\alpha,2_\alpha$ stand for the two laser beams. In this case, the corresponding detunings $\Delta_{l_\alpha,n_\alpha}$ will be much larger than any other scale of the problem, such that we can preserve the coherence of the ground-state manifold, and use the two-photon transitions to manipulate the state of the ion in this ground-state manifold by tuning the effective laser frequency $\omega_{\mathrm{L}^{\mathrm{tw}}_\alpha}=\omega_{1_\alpha}-\omega_{2_\alpha}$ of the two beams.

Note that, in analogy with the Coulomb couplings (A3), the recoil events to second order (A12) do not couple the vibrations along different directions either. Therefore, we can focus on the transverse vibrations along the x-axis directly (A5).

Using these integrals, we can rewrite the dissipator (A10) as a sum of two terms $\mathscr{D}_\alpha(\rho)=\mathscr{D}^0_\alpha(\rho)+\mathscr{D}^1_\alpha(\rho)$, where

$$\mathscr{D}^0_\alpha(\bullet)=\sum_{i_\alpha n_\alpha}\frac{\Gamma_\alpha}{2}\big(S^-_{i_\alpha,n_\alpha}\bullet S^+_{i_\alpha,n_\alpha}-S^+_{i_\alpha,n_\alpha}S^-_{i_\alpha,n_\alpha}\bullet+\mathrm{H.c.}\big), \tag{A14}$$

describes the spontaneous emission of a collection of atoms with mutual distances much larger than the wavelength of the emitted light. In addition, the recoil effects are contained in

$$\begin{aligned}\mathscr{D}^1_\alpha(\bullet)=\sum_{i_\alpha n_\alpha}\tfrac{1}{2}\tilde{\Gamma}_\alpha S^-_{i_\alpha,n_\alpha}\big((a^\dagger_{i_\alpha}+a_{i_\alpha})\bullet(a^\dagger_{i_\alpha}+a_{i_\alpha})\\-(a^\dagger_{i_\alpha}+a_{i_\alpha})^2\bullet\big)S^+_{i_\alpha,n_\alpha}+\mathrm{H.c.},\end{aligned} \tag{A15}$$

where the strength of these terms $\tilde{\Gamma}_\alpha=\Gamma_\alpha\eta^2_{n_\alpha}\alpha_{qx}$ is smaller than the bare dissipation (A14) since $\eta_{n_\alpha}=k_{n_\alpha}/\sqrt{2m_\alpha\omega_\alpha}\ll1$. According to this expression, the photon recoil leads to dissipative events where the number of vibrons is modified.

Typical orders of magnitude of some of these parameters are listed in Table II. In order to be more precise, let us consider a particular mixed ion crystal with species $\sigma=^{25}\mathrm{Mg}^+$, $\kappa=^{9}\mathrm{Be}^+$, and $\tau=^{24}\mathrm{Mg}^+$. The internal states corresponding to the level structure in Fig. 4 can be expressed in terms of the hyperfine atomic levels $|nL_J,F,M\rangle$, where n is the principal quantum number, L,J are the orbital and total elec-

Table II. **Atomic and laser parameters for each ion species**

α	$\omega_0^\alpha/2\pi$	$\Gamma_\alpha/2\pi$	L_α	$\omega_{\mathrm{L}_\alpha}$	$\Omega_{\mathrm{L}_\alpha}$
τ	10^2-10^3THz	10-10^2MHz	1-photon	$\omega_{\mathrm{L}_\tau^{\mathrm{sw}}}=\omega_0^\tau-\frac{\Gamma_\tau}{2}$	1-10MHz
σ	1-10GHz	10^{-14}THz	2-photon	$\omega_{\mathrm{L}_\sigma^{\mathrm{tw}}}=0$	0.1-10kHz
κ	1-10GHz	10^{-14}THz	2-photon	$\omega_{\mathrm{L}_\kappa^{\mathrm{tw}}}\ll\omega_\alpha\ll\omega_0^\kappa$	0.1-10kHz

tronic angular momenta, and F,M are the total angular momentum and its Zeeman component along a quantizing magnetic field. The $\tau=^{24}\mathrm{Mg}^+$ ions have no nuclear spin, and thus no hyperfine structure. For the two levels in Fig. 4**(a)**, we choose $|e_{\ell_\tau}\rangle=|3P_{1/2}\rangle, |g_{\ell_\tau}\rangle=|2S_{1/2}\rangle$, such that the transition frequency is $\omega_0^\tau/2\pi=(\varepsilon_{e_\tau}-\varepsilon_{g_\tau})/2\pi\approx 10^3\,\mathrm{THz}$, and the natural linewidth $\Gamma_\tau/2\pi=41.4\,\mathrm{MHz}$. Conversely, the $\sigma=^{25}\mathrm{Mg}^+$ and $\kappa=^{9}\mathrm{Be}^+$ ions display a hyperfine structure, which allow us to select two states from the hyperfine ground-state manifold and a single excited state, in order to form the desired Λ-scheme of Fig. 4**(b)**. For $\sigma=^{25}\mathrm{Mg}^+$, we take $|g_{i_\sigma,1}\rangle=|3S_{1/2},2,2\rangle, |g_{i_\sigma,2}\rangle=|3S_{1/2},3,3\rangle$, and the excited state in the $|e_{i_\sigma}\rangle=|3P_{3/2}\rangle$ manifold. The corresponding transition frequency between the ground-states lies in the microwave regime $\omega_0^\sigma=(\varepsilon_{g_{\sigma,1}}-\varepsilon_{g_{\sigma,2}})/2\pi=1.8\,\mathrm{GHz}$, and there is a negligible decay rate (i.e. $\Gamma_\sigma/2\pi\approx 10^{-14}\,\mathrm{Hz}$). Therefore, all the spontaneous emission occurs via transitions to the excited state, which has a natural linewidth of $\Gamma_\sigma/2\pi=41.4\,\mathrm{MHz}$. Finally, for $\kappa=^{9}\mathrm{Be}^+$, the ground-states would be $|g_{i_\kappa,1}\rangle=|2S_{1/2},1,-1\rangle, |g_{i_\kappa,2}\rangle=|2S_{1/2},2,-2\rangle$ with a transition frequency $\omega_0^\kappa=(\varepsilon_{g_{\kappa,1}}-\varepsilon_{g_{\kappa,2}})/2\pi=1.25\,\mathrm{GHz}$, and also a negligible linewidth. In this case, the excited state is in the manifold $|e_{i_\kappa}\rangle=|2P_{1/2}\rangle$, such that $\Gamma_\kappa/2\pi=19.4\,\mathrm{MHz}$.

Once these realistic parameters have been introduced, we can test the validity of the effective dissipators in Eqs. (A14) and (A15). In Fig. 5, we compare the dynamics of $\tau=^{24}\mathrm{Mg}^+$ predicted by these effective terms to that given by the complete master equation (A10) including the photon recoil in all possible directions. To obtain the dynamics numerically, we truncate the vibron Hilbert space to $n_{\max}=2$ for each direction $\nu=x,y,z$ (i.e. three vibron modes), and consider all nonlinearities of the recoil jump operators in (A10) by discretizing the solid angle of the photon kicks in a mesh of 400 points. As follows from the displayed agreement, the description in terms of the dissipators (A14)-(A15) is very accurate. These equations are the starting point of the following sections.

3. Edge dissipation by Doppler cooling

We move onto the derivation of the effective dissipation (2) of the τ-vibrons. We will be interested in positioning these ions at the edges of the chain, such that they can act as reservoirs for quantum transport [Fig. 1**(a)**]. To control the dissipation of the edge vibrons, a laser beam $\mathrm{L}_\tau^{\mathrm{sw}}$ is tuned close to the resonance of the dipole-allowed transition. The master equation for the total density matrix ρ is

$$\dot\rho=-\mathrm{i}[H_{\mathrm{s}}+H_{\mathrm{tb}}+H_{\mathrm{L}_\tau^{\mathrm{sw}}},\rho]+\mathscr{D}_\tau(\rho)+\mathscr{D}_\sigma(\rho)+\mathscr{D}_\kappa(\rho), \tag{A16}$$

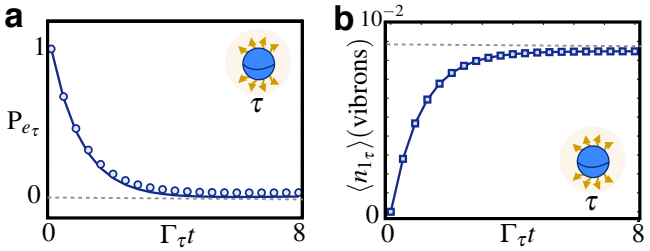

Figure 5. **Recoil dissipation for a dipole-allowed transition: (a)** Decay of the population of the excited state P_{e_τ} for $\tau=^{24}\mathrm{Mg}^+$ and an initial state $\rho_\tau(0)=|e_\tau\rangle\langle e_\tau|\otimes|0\rangle\langle 0|$, where $|0\rangle$ represents the vacuum of vibrons in all three directions of motion. The solid line represents P_{e_τ} according to the full dissipator (A10), while the circles represent the same population calculated from the effective description (A14) and (A15). **(b)** Dynamics of the mean number of vibrons $\langle n_{1_\tau}\rangle$ along the x-axis or $\tau=^{24}\mathrm{Mg}^+$ and the same initial state. Due to the recoil of the spontaneously emitted photons, the vibron number is slightly increased (i.e. recoil heating) until the excited state has completely decayed. The solid line represents $\langle n_{1_\tau}\rangle$ according to the full dissipator (A10), while the circles represent the same vibron number calculated from the effective description (A14) and (A15).

where the dissipators $\mathscr{D}_\alpha=\mathscr{D}_\alpha^0+\mathscr{D}_\alpha^1$ are given by Eqs. (A14) and (A15). Additionally, the laser-ion interaction is

$$H_{\mathrm{L}_\tau^{\mathrm{sw}}}=-\sum_{\ell_\tau}(\mathbf{d}_\tau S_{\ell_\tau}^+ +\mathbf{d}_\tau^* S_{\ell_\tau}^-)\cdot\mathbf{E}_{\mathrm{L}_\tau^{\mathrm{sw}}}(\mathbf{r}_{\ell_\tau},t), \tag{A17}$$

where we have introduced the laser electric field $\mathbf{E}_{\mathrm{L}_\tau^{\mathrm{sw}}}(\mathbf{r}_{\ell_\tau},t)$, and the atomic dipole $\mathbf{d}_\tau$. For reasons that will become clear later, we need cooling rates that are much stronger than the vibron tunnelings (A8). Therefore, the laser beam is arranged in a standing-wave configuration [10], $\mathbf{E}_{\mathrm{L}_\tau^{\mathrm{sw}}}(\mathbf{r}_{\ell_\tau},t)=\boldsymbol{\varepsilon}_\tau E_\tau\cos(\omega_{\mathrm{L}_\tau^{\mathrm{sw}}}t)\cos(\mathbf{k}_{\mathrm{L}_\tau}^{\mathrm{sw}}\cdot\mathbf{r}_{\ell_\tau})$, where $\boldsymbol{\varepsilon}_\tau, E_\tau, \omega_{\mathrm{L}_\tau^{\mathrm{sw}}}$ are the polarization, amplitude, and frequency of the laser, and $\mathbf{k}_{\mathrm{L}_\tau^{\mathrm{sw}}}$ is the laser wavevector directed along the x-axis (i.e. direction of the vibrons). Besides, we consider that the axis of the ion-chain lies at the node of the standing wave.

We introduce the Rabi frequency $\Omega_{\mathrm{L}_\tau^{\mathrm{sw}}}=-E_\tau\mathbf{d}_\tau\cdot\boldsymbol{\varepsilon}_\tau$, the Lamb-Dicke parameter $\eta_{\mathrm{L}_\tau^{\mathrm{sw}}}=k_{\mathrm{L}_\tau^{\mathrm{sw}}}/\sqrt{2m_\tau\omega_\tau}$, and the detuning $\Delta_{\mathrm{L}_\tau^{\mathrm{sw}}}=\omega_{\mathrm{L}_\tau^{\mathrm{sw}}}-(\varepsilon_{e_\tau}-\varepsilon_{g_\tau})$ [Fig. 4**(a)**]. When $|\Omega_{\mathrm{L}_\tau^{\mathrm{sw}}}|, |\Delta_{\mathrm{L}_\tau^{\mathrm{sw}}}|\ll\omega_0^\tau=(\varepsilon_{e_\tau}-\varepsilon_{g_\tau})$, and $\eta_{\mathrm{L}_\tau^{\mathrm{sw}}}\ll 1$, we can approximate the laser-ion coupling (A17) by the expression

$$H_{\mathrm{L}_\tau^{\mathrm{sw}}}=\sum_{\ell_\tau}F_{\ell_\tau}(a_{\ell_\tau}+a_{\ell_\tau}^\dagger),\quad F_{\ell_\tau}=-\tfrac{1}{2}\Omega_{\mathrm{L}_\tau^{\mathrm{sw}}}\eta_{\mathrm{L}_\tau^{\mathrm{sw}}}S_{\ell_\tau}^+\mathrm{e}^{-\mathrm{i}\omega_{\mathrm{L}_\tau^{\mathrm{sw}}}t}+\mathrm{H.c.} \tag{A18}$$

Since we are working at the node of the standing wave, let us note that the component of the laser-ion interaction that would drive the carrier is exactly cancelled. Therefore, the only fundamental constraint over the standing-wave Rabi frequency will be $|\Omega_{\mathrm{L}_\tau^{\mathrm{sw}}}|\ll\omega_0^\tau$, still allowing for high driving strengths.

To derive the effective dissipation of the τ-vibrons, which was introduced in Eq. (2) of the main text, the crucial point is to appreciate the clear separation of time-scales

$$|J_{i_\alpha j_\beta}|, |\tfrac{1}{2}\Omega_{\mathrm{L}_\tau^{\mathrm{sw}}}\eta_{\mathrm{L}_\tau^{\mathrm{sw}}}|, |\Gamma_\tau\eta_{\mathrm{L}_\tau^{\mathrm{sw}}}^2|\ll\Gamma_\tau, \tag{A19}$$

which implies that the spontaneous decay of the atomic states of the τ-ions is much faster than the dynamics introduced by

any other term. This allows us to partition the Liouvillian as follows $\tilde{\mathscr{L}} = \tilde{\mathscr{L}}_0 + \tilde{\mathscr{L}}_1$, where the two terms are

$$\begin{aligned}\tilde{\mathscr{L}}_0(\tilde{\rho}) &= \tilde{\mathscr{D}}^0_\tau(\tilde{\rho}),\\ \tilde{\mathscr{L}}_1(\tilde{\rho}) &= -\mathrm{i}[\tilde{H}_{\rm vt} + \tilde{H}_{\mathrm{L}^{\rm sw}_\tau}, \tilde{\rho}] + \tilde{\mathscr{D}}^1_\tau(\tilde{\rho}) + \tilde{\mathscr{D}}_\sigma(\tilde{\rho}) + \tilde{\mathscr{D}}_\kappa(\tilde{\rho}),\end{aligned} \tag{A20}$$

and where the "tildes" refer to the interaction picture with respect to $H_0 = H_{\rm s} + H_{\rm vo}$ in Eqs. (A8) and (A9). We can eliminate the fast degrees of freedom of the τ atomic states by projecting onto the steady-state of $\mathscr{L}_0(\mu^\tau_{\rm ss}) = 0$. This can be accomplished by projector-operator techniques [11], which lead to a second-order master equation

$$\dot{\tilde{\rho}} = \left\{ \mathscr{P}\tilde{\mathscr{L}}_1(t)\mathscr{P} + \int_0^\infty \mathrm{d}s\, \mathscr{P}\tilde{\mathscr{L}}_1(t)\mathscr{Q}\mathrm{e}^{\tilde{\mathscr{L}}_0 s}\mathscr{Q}\tilde{\mathscr{L}}_1(t-s)\mathscr{P} \right\}\tilde{\rho}, \tag{A21}$$

where $\mathscr{P}$, and $\mathscr{Q} = 1 - \mathscr{P}$ are the projectors of interest, which correspond to $\mathscr{P}_\tau\{\bullet\} = \mu^\tau_{\rm ss} \otimes \mathrm{Tr}_{\tau,\rm at}\{\bullet\}$ in this case. Since the ion chain lies at the node of the standing wave, the atomic steady state is $\mu^\tau_{\rm ss} = \otimes_{\ell_\tau} |g_{\ell_\tau}\rangle\langle g_{\ell_\tau}|$. After some algebra, Eq. (A21) leads to an effective master equation for the reduced density matrix after tracing over the atomic degrees of freedom of the τ-species $\mu = \mathrm{Tr}_{\tau,\rm at}\{\rho\}$. Back in the Schrödinger picture, this master equation reads as follows

$$\dot{\mu} = -\mathrm{i}[H^\sigma_{\rm s} + H^\kappa_{\rm s} + H_{\rm tb}, \mu] + \sum_{\ell_\tau} \mathscr{D}^{\ell_\tau}_{\rm v}(\mu) + \mathscr{D}_\sigma(\mu) + \mathscr{D}_\kappa(\mu). \tag{A22}$$

Here, we have introduced a dissipation super-operator that only acts on the vibrons of the ion chain, namely

$$\begin{aligned}\mathscr{D}^{\ell_\tau}_{\rm v}(\bullet) = \Lambda^+_{\ell_\tau}(a^\dagger_{\ell_\tau}\bullet a_{\ell_\tau} - a_{\ell_\tau}a^\dagger_{\ell_\tau}\bullet) +\\ + \Lambda^-_{\ell_\tau}(a_{\ell_\tau}\bullet a^\dagger_{\ell_\tau} - a^\dagger_{\ell_\tau}a_{\ell_\tau}\bullet) + \mathrm{H.c.}\end{aligned} \tag{A23}$$

As announced previously, the effective dissipation (A23) acts directly on the τ-vibrons. The heating-cooling coefficients can be expressed in terms of the power spectrum of the laser-induced couplings F_{ℓ_τ}, namely

$$S_{F_{\ell_\tau},F_{\ell_\tau}}(\omega) = \int_0^\infty \mathrm{d}t \langle \tilde{F}_{\ell_\tau}(t)\tilde{F}_{\ell_\tau}(0)\rangle_{\rm ss}\mathrm{e}^{\mathrm{i}\omega t}. \tag{A24}$$

In particular, the cooling depends on the power spectrum at positive frequencies $\Lambda^-_{\ell_\tau} = S_{F_{\ell_\tau},F_{\ell_\tau}}(+\omega_{\ell_\tau})$, while the heating is quantified by the noise spectrum at negative frequencies $\Lambda^+_{\ell_\tau} = S_{F_{\ell_\tau},F_{\ell_\tau}}(-\omega_{\ell_\tau})$. Such coefficients coincide with those of a single trapped ion [10], and it is the possibility of controlling experimentally the frequency asymmetry of the power spectrum which allows for an effective laser cooling of the vibrational modes, i.e. $S_{F_{\ell_\tau},F_{\ell_\tau}}(+\omega_{\ell_\tau}) > S_{F_{\ell_\tau},F_{\ell_\tau}}(-\omega_{\ell_\tau})$. By the quantum regression theorem [12], the coefficients can be expressed as follows

$$\Lambda^\pm_{\ell_\tau} = \frac{(\frac{1}{2}\Omega_{\mathrm{L}^{\rm sw}_\tau}\eta_{\mathrm{L}^{\rm sw}_\tau})^2}{\frac{1}{2}\Gamma_\tau + \mathrm{i}(-\Delta_{\mathrm{L}^{\rm sw}_\tau} \pm \omega_{\ell_\tau})}. \tag{A25}$$

Note that in the expression above (A23), we have neglected rapidly-rotating terms (e.g. $a^2_{\ell_\tau}$), an approximation that is valid when $\omega_{\ell_\tau} \gg |\Lambda^\pm_{\ell_\tau}| \approx (\Omega_{\mathrm{L}^{\rm sw}_\tau}\eta_{\mathrm{L}^{\rm sw}_\tau})^2/2\Gamma_\tau$. Finally, by using

$$\mathscr{D}[\Lambda, O_1, O_2](\bullet) = \Lambda(O_1\bullet O_2 - O_2O_1\bullet) + \mathrm{H.c.}, \tag{A26}$$

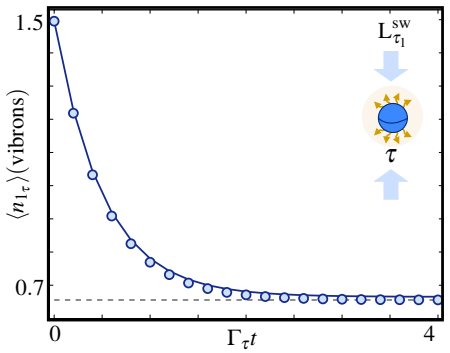

Figure 6. **Damping of the vibrons by laser cooling:** Decay of the average number of vibrons $\langle n_{1_\tau}\rangle$ for a single laser-cooled $\tau = {}^{24}\mathrm{Mg}^+$ ion. The solid line corresponds to the predictions of the original master equation (A27), whereas the circles are given by the effective dissipation (A23). We also display in a dashed straight line, the steady-state vibron number predicted by Eq. (A29).

the dissipator (A23) corresponds to Eq. (2) in the main text.

In Fig. 6, we compare the dynamics given by the effective edge dissipator (A23) with that given by the original master equation (A16) restricted to a single $\tau = {}^{24}\mathrm{Mg}^+$ ion, namely

$$\dot{\rho} = -\mathrm{i}[H^\tau_{\rm s} + H_{\rm vo} + H_{\mathrm{L}^{\rm sw}_\tau}, \rho] + \mathscr{D}_\tau(\rho). \tag{A27}$$

We consider an initial state $\rho_\tau(0) = |e_\tau\rangle\langle e_\tau| \otimes \rho^{\rm th}_\tau$, where $\rho^{\rm th}_\tau$ is a thermal state for the τ-vibrons with an average vibron number of $\bar{n}_{1_\tau} = 1.5$. In addition to the and atomic parameters for the $\tau = {}^{24}\mathrm{Mg}^+$ ions introduced above, we consider a trap frequency of $\omega_\tau/2\pi = 10\,\mathrm{MHz}$, and a standing-wave laser that is red-detuned $\Delta_{\mathrm{L}^{\rm sw}_\tau} = -\frac{1}{2}\Gamma_\tau$, such that its Rabi frequency is $\Omega_{\mathrm{L}^{\rm sw}_\tau} = 0.1|\Delta_{\mathrm{L}^{\rm sw}_\tau}|$. In the figure, the solid line corresponds to the average number of vibrons $\langle n_{1\tau}\rangle$ given by the original master equation (A27), whereas the circles correspond to the effective description of the edge dissipator (A23). In this case, we need to truncate the vibron Hilbert space to $n_{\rm max} = 15$ to account for the thermal effects accurately. As follows from the agreement shown, the effective description (A23) in terms of heating/cooling processes at the edges is very accurate.

Let us write down explicit expressions for the cooling rate $\gamma_{\ell_\tau} = \mathrm{Re}\{(\Lambda^-_{\ell_\tau})^* - \Lambda^+_{\ell_\tau}\}$, and the mean number of vibrons in the steady state $\bar{n}_{\ell_\tau} = \mathrm{Re}\{\Lambda^+_{\ell_\tau}\}/\gamma_{\ell_\tau}$, which read as follows

$$\gamma_{\ell_\tau} = \frac{\frac{1}{2}(\Omega_{\mathrm{L}^{\rm sw}_\tau}\eta_{\mathrm{L}^{\rm sw}_\tau})^2\Gamma_\tau\omega_{\ell_\tau}\left(-\Delta_{\mathrm{L}^{\rm sw}_\tau}\right)}{\left((\frac{1}{2}\Gamma_\tau)^2 + (\Delta_{\mathrm{L}^{\rm sw}_\tau} + \omega_{\ell_\tau})^2\right)\left((\frac{1}{2}\Gamma_\tau)^2 + (\Delta_{\mathrm{L}^{\rm sw}_\tau} - \omega_{\ell_\tau})^2\right)}, \tag{A28}$$

and

$$\bar{n}_{\ell_\tau} = \frac{(\frac{1}{2}\Gamma_\tau)^2 + (\Delta_{\mathrm{L}^{\rm sw}_\tau} + \omega_{\ell_\tau})^2}{4(-\Delta_{\mathrm{L}^{\rm sw}_\tau})\omega_{\ell_\tau}}. \tag{A29}$$

Note that the cooling rate (A28) changes sign depending on the laser detuning. In Fig. 7**(a)**, this rate is represented as a function of the detuning in the so-called Doppler-cooling regime $\Gamma_\tau \gg \omega_\tau$ of $\tau = {}^{24}\mathrm{Mg}^+$. For red detunings $\Delta_{\mathrm{L}^{\rm sw}_\tau} < 0$, we get an effective cooling of the τ-vibrons, whereas heating

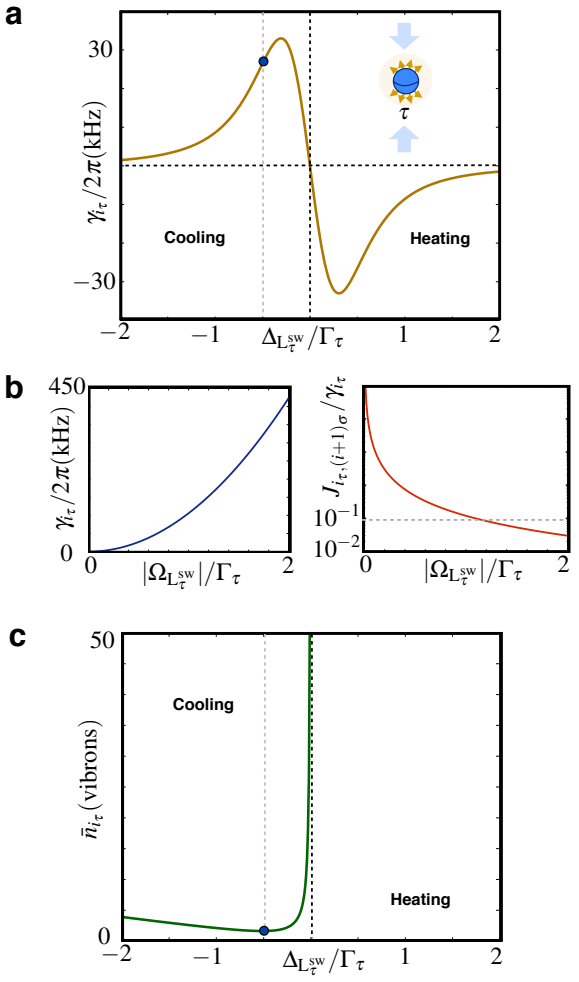

Figure 7. **Doppler cooling parameters: (a)** Effective laser cooling strength γ_{i_τ} for $\tau = {}^{24}\mathrm{Mg}^+$ (A28) as a function of the standing-wave detuning $\Delta_{\mathrm{L}_\tau^{\mathrm{sw}}}$ for a Rabi frequency $\Omega_{\mathrm{L}_\tau^{\mathrm{sw}}} = \frac{1}{2}\Gamma_\tau$. For red detunings, we obtain cooling rates that can be as high as tens of kHz. **(b)** (left panel) Quadratic increase of the cooling rate as a function of the Rabi frequency. (right panel) Ratio of the nearest-neighbor vibron tunneling and the effective cooling rate $J_{i_\tau,(i+1)_\sigma}/\gamma_{i_\tau}$ as a function of the standing-wave Rabi frequency. **(c)** Steady-state mean vibron number $\bar{n}_{\ell_\tau}$ (A29) as a function of the standing-wave detuning.

is obtained for blue detunings $\Delta_{\mathrm{L}_\tau^{\mathrm{sw}}} > 0$. Another important property is that the cooling rate (A28) increases quadratically with the laser Rabi frequency. In the left panel of Fig. 7**(b)**, we see how the red-detuning cooling rate increases with the Rabi frequency without saturation, which shall allow us to attain regimes where the cooling is much stronger than the vibron tunnelings $\gamma_{\ell_\tau} \gg |J_{i_\alpha j_\beta}|$, and the τ-ions act as vibronic reservoirs for the heat transport along the ion chain. In the right panel of Fig. 7**(b)**, we represent the ratio of the vibron tunneling and cooling rate as a function of the standing-wave strength. As announced previously, the cooling dominates over the tunneling for strong-enough standing waves. Finally, let us also note that the mean number of vibrons in the steady state (A29) is independent of the Rabi frequency. Therefore, increasing the laser power such that the desired regime $\gamma_{\ell_\tau} \gg |J_{i_\alpha j_\beta}|$ is attained, does not limit the tunability over the vibronic reservoirs (see Fig. 7**(c)**), a property that will be important to study the consequences of heat transport.

4. Tailoring the spin-vibron coupling

The final ingredient of our toolbox is the coherent spin-vibron coupling (3) for the ions $\alpha, i_\alpha \in \mathfrak{C}$. In particular, these ions will be positioned at the the bulk of the chain, such that the spin-vibron coupling can be used to control and measure the quantum heat transport [Fig. 1**(a)**]. In contrast to the engineered dissipation (A23), we use laser beams $\mathrm{L}_\alpha^{\mathrm{tw}}$ in a traveling-wave configuration that are far from the resonance of the corresponding dipole-allowed transitions [Fig. 4**(b)**]. In this section, we will use the indices $\alpha, \beta = \{\sigma, \kappa\}$ to refer only to the bulk ions. The corresponding laser-ion interactions $H_{\mathrm{L}_\alpha^{\mathrm{tw}}}$ are introduced in (A22) as follows

$$\dot{\mu} = -\mathrm{i}\big[\sum_\alpha (H_{\mathrm{s}}^\alpha + H_{\mathrm{L}_\alpha^{\mathrm{tw}}}) + H_{\mathrm{tb}}, \mu\big] + \sum_{\ell_\tau} \mathscr{D}_{\mathrm{v}}^{\ell_\tau}(\mu) + \sum_\alpha \mathscr{D}_\alpha(\mu), \tag{A30}$$

where the laser-ion Hamiltonians for the Λ-scheme are

$$H_{\mathrm{L}_\alpha^{\mathrm{tw}}} = -\sum_{i_\alpha, n_\alpha} \big(\mathbf{d}_{\alpha,n_\alpha} S^+_{i_\alpha,n_\alpha} + \mathbf{d}^*_{\alpha,n_\alpha} S^-_{i_\alpha,n_\alpha}\big) \cdot \mathbf{E}_{\mathrm{L}_\alpha^{\mathrm{tw}}}(\mathbf{r}_{i_\alpha}, t). \tag{A31}$$

Here, the electric field for each laser-beam arrangement is $\mathbf{E}_{\mathrm{L}_\alpha^{\mathrm{tw}}}(\mathbf{r}_{i_\alpha}, t) = \sum_{l_\alpha} \boldsymbol{\varepsilon}_{l_\alpha} E_{l_\alpha} \cos(\mathbf{k}_{l_\alpha} \cdot \mathbf{r}_{i_\alpha} - \omega_{l_\alpha} t)$, which consists of two $l_\alpha = 1_\alpha, 2_\alpha$ travelling waves with polarization, amplitude, and frequency $\boldsymbol{\varepsilon}_{l_\alpha}, E_{l_\alpha}, \omega_{l_\alpha}$, and a wavevector $\mathbf{k}_{l_\alpha}$.

To derive the spin-vibron couplings (3) from (A30), let us define the detunings and Rabi frequencies for each transition

$$\Delta_{l_\alpha n_\alpha} = \omega_{l_\alpha} - \big(\varepsilon_{e_\alpha} - \varepsilon_{g_{\alpha,n_\alpha}}\big), \quad \Omega_{l_\alpha n_\alpha} = -E_{l_\alpha} \mathbf{d}_{\alpha,n_\alpha} \cdot \boldsymbol{\varepsilon}_{l_\alpha}, \tag{A32}$$

as depicted in Fig. 4**(b)**. In the regime of weak excitations $|\Omega_{l_\alpha s_{i_\alpha}}| \ll \Delta_{l_\alpha s_{i_\alpha}}$, the auxiliary state is seldom populated, and we can obtain an effective description by projecting onto the atomic ground-state manifold. This is performed by using Eq. (A21), where the Liouvillian is now partitioned into

$$\begin{aligned} \tilde{\mathscr{L}}_0(\tilde{\mu}) &= \sum_\alpha \tilde{\mathscr{D}}_\alpha^0(\tilde{\mu}), \\ \tilde{\mathscr{L}}_1(\tilde{\mu}) &= -\mathrm{i}[\tilde{H}_{\mathrm{vt}} + \sum_\alpha \tilde{H}_{\mathrm{L}_\alpha^{\mathrm{tw}}}, \tilde{\mu}] + \sum_{\ell_\tau} \mathscr{D}_{\mathrm{v}}^{\ell_\tau}(\tilde{\mu}) + \sum_\alpha \tilde{\mathscr{D}}_\alpha^1(\tilde{\mu}), \end{aligned} \tag{A33}$$

and the "tildes" now refer to the interaction picture with respect to $H_0 = H_{\mathrm{s}}^\sigma + H_{\mathrm{s}}^\kappa + H_{\mathrm{vo}}$. In this case, the projection operator $\mathscr{P}_{\sigma\kappa} = \sum_{n_\sigma n_\kappa} |g_{\sigma,n_\sigma}, g_{\kappa,n_\kappa}\rangle\langle g_{\sigma,n_\sigma}, g_{\kappa,n_\kappa}|$ restricts the dynamics to the ground-state manifold. After some algebra, and making use of the adjoint master equation for atomic operators [12], equation (A21) leads to an effective master equation

$$\frac{\mathrm{d}\tilde{\mu}}{\mathrm{d}t} = -\mathrm{i}\big[\tilde{H}_{\mathrm{tb}}, \tilde{\mu}\big] + \sum_{\ell_\tau} \mathscr{D}_{\mathrm{v}}^{\ell_\tau}(\tilde{\mu}) + \Delta\tilde{\mathscr{L}}_\sigma(\tilde{\mu}) + \Delta\tilde{\mathscr{L}}_\kappa(\tilde{\mu}), \tag{A34}$$

where $\tilde{\mu}=(\mathscr{P}_{\sigma\kappa}\tilde{\mu})$ is the projected density matrix. The new super-operator in the Liouvillian can be expressed as follows

$$\Delta\tilde{\mathscr{L}}_{\alpha}(\bullet)=\sum_{i_\alpha}\sum_{l_\alpha,l'_\alpha}\sum_{n_\alpha,n'_\alpha}\mathscr{G}^{n_\alpha n'_\alpha}_{l_\alpha l'_\alpha}(\mathbf{r}_{i_\alpha},t)|g_{i_\alpha,n_\alpha}\rangle\langle g_{i_\alpha,n'_\alpha}|\bullet+\text{H.c.}, \tag{A35}$$

where we have introduced the following couplings

$$\mathscr{G}^{n_\alpha n'_\alpha}_{l_\alpha l'_\alpha}(\mathbf{r}_{i_\alpha},t)=\frac{-\Omega^*_{l_\alpha n_\alpha}\Omega_{l'_\alpha n'_\alpha}}{4(\Gamma_\alpha+\mathrm{i}\Delta_{l'_\alpha n'_\alpha})}\mathrm{e}^{-\mathrm{i}\left((\mathbf{k}_{l_\alpha}-\mathbf{k}_{l'_\alpha})\cdot\mathbf{r}_{i_\alpha}-(\Delta_{l_\alpha n_\alpha}-\Delta_{l'_\alpha n'_\alpha})t\right)}. \tag{A36}$$

Note that the form of these couplings (A36) tells us that the dynamics is due to two-photon processes that connect the ground-states via the excited state (see Fig. 4**(b)**). The real part of the coupling gives rise to an spontaneous decay due to the finite lifetime of the excited state, whereas its imaginary part leads to coherent dynamics within the ground-state manifold. As announced previously, in contrast to the engineered dissipation (A23), we use far-detuned laser beams $\Gamma_\alpha\ll|\Delta_{l_\alpha n_\alpha}|$. In this regime, the couplings become

$$\mathscr{G}^{n_\alpha n'_\alpha}_{l_\alpha l'_\alpha}(\mathbf{r}_{i_\alpha},t)\approx\mathrm{i}\frac{\Omega^*_{l_\alpha n_\alpha}\Omega_{l'_\alpha n'_\alpha}}{4\Delta_{l'_\alpha n'_\alpha}}\mathrm{e}^{-\mathrm{i}\left((\mathbf{k}_{l_\alpha}-\mathbf{k}_{l'_\alpha})\cdot\mathbf{r}_{i_\alpha}-(\Delta_{l_\alpha n_\alpha}-\Delta_{l'_\alpha n'_\alpha})t\right)}, \tag{A37}$$

such that the spontaneous decay is minimized, and the coherent Hamiltonian part prevails leading to

$$\Delta\tilde{\mathscr{L}}_{\alpha}(\tilde{\mu})=-\mathrm{i}[\Delta\tilde{H}_\alpha,\tilde{\mu}]. \tag{A38}$$

Let us remark that the effective decay rates within the ground-state manifold scale as $\Gamma_\alpha(|\Omega_{l_\alpha,n_\alpha}|/\Delta_{l_\alpha,n_\alpha})^2\ll\Gamma_\alpha$, and can be thus neglected for large-enough detunings. This is precisely the regime where $\Gamma_\tau\gg\Gamma_\sigma,\Gamma_\kappa$ considered in this work.

By tuning the two-photon frequencies $\omega_{\mathrm{L}^{\mathrm{tw}}_\alpha}=\omega_{1_\alpha}-\omega_{2_\alpha}$, such that $|\omega_{\mathrm{L}^{\mathrm{tw}}_\alpha}|\ll(\varepsilon_{g_{\alpha,1}}-\varepsilon_{g_{\alpha,2}})=\omega_0^\alpha$, the lasers do not provide enough energy to drive a two-photon Raman transition. Instead, they lead to the following two-beam Stark shift

$$\Delta\tilde{H}_\alpha=\sum_{n_\alpha}\sum_{l_\alpha,l'_\alpha}\mathrm{i}\mathscr{G}^{n_\alpha n_\alpha}_{l_\alpha l'_\alpha}(\mathbf{r}_{i_\alpha},t)|g_{i_\alpha,n_\alpha}\rangle\langle g_{i_\alpha,n_\alpha}|+\text{H.c.}. \tag{A39}$$

There are two kinds of terms in this expression $\Delta\tilde{H}_\alpha=\Delta\tilde{H}^\alpha_{\mathrm{ss}}+\Delta\tilde{H}^\alpha_{\mathrm{sv}}$. The two-photon processes whereby a photon is absorbed from and re-emitted into the same laser beam (i.e. $l_\alpha=l'_\alpha$) contribute with a standard ac-Stark shift

$$\Delta\tilde{H}^\alpha_{\mathrm{ss}}=\sum_{i_\alpha}\sum_{n_\alpha}\frac{1}{2}\Delta\varepsilon_{\alpha,n_\alpha}|g_{i_\alpha,n_\alpha}\rangle\langle g_{i_\alpha,n_\alpha}|,\ \ \Delta\varepsilon_{\alpha,n_\alpha}=\sum_{l_\alpha}\frac{-|\Omega_{l_\alpha n_\alpha}|^2}{2\Delta_{l_\alpha n_\alpha}}. \tag{A40}$$

Additionally, when the photon is absorbed from and re-emitted into different beams (i.e. $l_\alpha\neq l'_\alpha$), the corresponding Stark shift leads to a more interesting term that couples the internal and vibrational degrees of freedom

$$\Delta\tilde{H}^\alpha_{\mathrm{sv}}=\sum_{i_\alpha}\sum_{n_\alpha}\tfrac{1}{2}\Omega_{\mathrm{L}^{\mathrm{tw}}_\alpha,n_\alpha}\mathrm{e}^{-\mathrm{i}(\mathbf{k}_{\mathrm{L}^{\mathrm{tw}}_\alpha}\cdot\mathbf{r}_{i_\alpha}-\omega_{\mathrm{L}^{\mathrm{tw}}_\alpha}t)}|g_{i_\alpha,n_\alpha}\rangle\langle g_{i_\alpha,n_\alpha}|+\text{H.c.}, \tag{A41}$$

where we have introduced the crossed-beam Rabi frequencies

$$\Omega_{\mathrm{L}^{\mathrm{tw}}_\alpha,n_\alpha}=-\frac{\Omega^*_{1_\alpha n_\alpha}\Omega_{2_\alpha n_\alpha}}{2\Delta_{2_\alpha n_\alpha}}, \tag{A42}$$

and wavevectors $\mathbf{k}_{\mathrm{L}^{\mathrm{tw}}_\alpha}=\mathbf{k}_{1_\alpha}-\mathbf{k}_{2_\alpha}$, and used $\omega_0^\alpha\ll|\Delta_{l_\alpha n_\alpha}|$. This crossed-beam Stark shift (A41) can lead to a variety of spin-vibron couplings. We discuss now how to produce the desired spin-vibron couplings (3).

Let us introduce a notation where the two states in the ground-state manifold are referred to as spin states $|g_{i_\alpha,1}\rangle=|\uparrow_{i_\alpha}\rangle,|g_{i_\alpha,2}\rangle=|\downarrow_{i_\alpha}\rangle$. We substitute $\mathbf{r}_{i_\alpha}=\mathbf{r}^0_{i_\alpha,}+\delta\mathbf{r}_{i_\alpha}$ in Eq. (A41), such that the small vibrations are expressed in terms of the creation-annihilation operators (A5). By expanding in Taylor series of the Lamb-Dicke parameter

$$\eta_{\mathrm{L}^{\mathrm{tw}}_\alpha}=\frac{k_{\mathrm{L}^{\mathrm{tw}}_\alpha}}{\sqrt{2m_\alpha\omega_\alpha}}\ll1, \tag{A43}$$

and setting $|\Omega_{\mathrm{L}^{\mathrm{tw}}_\alpha}\eta_{\mathrm{L}^{\mathrm{tw}}_\alpha}|\ll\omega_\alpha$, we obtain

$$\Delta\tilde{H}^\alpha_{\mathrm{sv}}\approx\sum_{i_\alpha,s_{i_\alpha}}\tfrac{1}{2}\Omega_{\mathrm{L}_\alpha,s_{i_\alpha}}\left(1-\eta^2_{\mathrm{L}^{\mathrm{tw}}_\alpha}a^\dagger_{i_\alpha}a_{i_\alpha}\right)\mathrm{e}^{\mathrm{i}\omega_{\mathrm{L}^{\mathrm{tw}}_\alpha}t}|s_{i_\alpha}\rangle\langle s_{i_\alpha}|+\text{H.c.}, \tag{A44}$$

where $s_{i_\alpha}=\uparrow_{i_\alpha},\downarrow_{i_\alpha}$. The first term of this expression contributes with a periodic modulation of the Stark shift (A40)

$$\Delta\varepsilon_{\alpha,n_\alpha}\to\Delta\varepsilon_{\alpha,n_\alpha}+|\Omega_{\mathrm{L}^{\mathrm{tw}}_\alpha,n_\alpha}|\cos(\omega_{\mathrm{L}^{\mathrm{tw}}_\alpha}t-\phi_{\mathrm{L}^{\mathrm{tw}}_\alpha}), \tag{A45}$$

where we have introduced the phase of the Rabi frequencies $\Omega_{\mathrm{L}^{\mathrm{tw}}_\alpha,n_\alpha}=|\Omega_{\mathrm{L}^{\mathrm{tw}}_\alpha,n_\alpha}|\mathrm{e}^{-\mathrm{i}\phi_{\mathrm{L}^{\mathrm{tw}}_\alpha}}$. The second term leads to

$$H^\alpha_{\mathrm{sv}}(t)=-\sum_{i_\alpha}\sum_{s_{i_\alpha}}|\Omega_{\mathrm{L}^{\mathrm{tw}}_\alpha,s_{i_\alpha}}|\eta^2_{\mathrm{L}^{\mathrm{tw}}_\alpha}\cos(\omega_{\mathrm{L}^{\mathrm{tw}}_\alpha}t-\phi_{\mathrm{L}^{\mathrm{tw}}_\alpha})|s_{i_\alpha}\rangle\langle s_{i_\alpha}|a^\dagger_{i_\alpha}a_{i_\alpha}. \tag{A46}$$

We are now ready to derive the expression (3) used throughout this work. Let us make the following definitions

$$\Delta\omega_{s_{i_\alpha}}=-|\Omega_{\mathrm{L}^{\mathrm{tw}}_\alpha,s_{i_\alpha}}|\eta^2_{\mathrm{L}^{\mathrm{tw}}_\alpha},\quad\Delta\omega^\pm_\alpha=\Delta\omega_{\uparrow_{i_\alpha}}\pm\Delta\omega_{\downarrow_{i_\alpha}} \tag{A47}$$

together with the frequency and phase of the lasers

$$\nu_\alpha=\omega_{\mathrm{L}^{\mathrm{tw}}_\alpha},\quad\varphi_\alpha=\phi_{\mathrm{L}^{\mathrm{tw}}_\alpha}. \tag{A48}$$

Then, the crossed-beam Stark shift (A46) becomes exactly the desired spin-vibron coupling in Eq. (3) of the main text. Let us note that the above drivings in the spin-independent regime, $\Delta\omega^-_\alpha=0$, were used in [18] to mimic the effects of an external gauge field in the dynamics of the vibrons.

Let us now support numerically this derivation. Note that the dynamics of the Λ-system (A30) for a single $\sigma=$ $^{25}\mathrm{Mg}^+$ ion, which is given by

$$\dot{\mu}=-\mathrm{i}\left[H^\sigma_{\mathrm{s}}+H_{\mathrm{L}^{\mathrm{tw}}_\sigma}+H_{\mathrm{vo}},\mu\right]+\mathscr{D}_\sigma(\mu), \tag{A49}$$

covers a wide range of time dependences 1 GHz-10^3 THz. Since we apply two laser beams with different frequencies, it is not possible to find a suitable picture where the above Liouvillian becomes time-independent. As a consequence, the numerics with the $^{25}\mathrm{Mg}^+$ parameters require prohibitively large times. To avoid this numerical limitation, we shall work with dimensionless units, ensuring that the constraints for the derivation of Eq. (A39) are met. We set the atomic energies to $\varepsilon_{g_{\sigma,2}}=0,\varepsilon_{g_{\sigma,1}}=5,\varepsilon_{e_\sigma}=50$, and the laser frequencies to

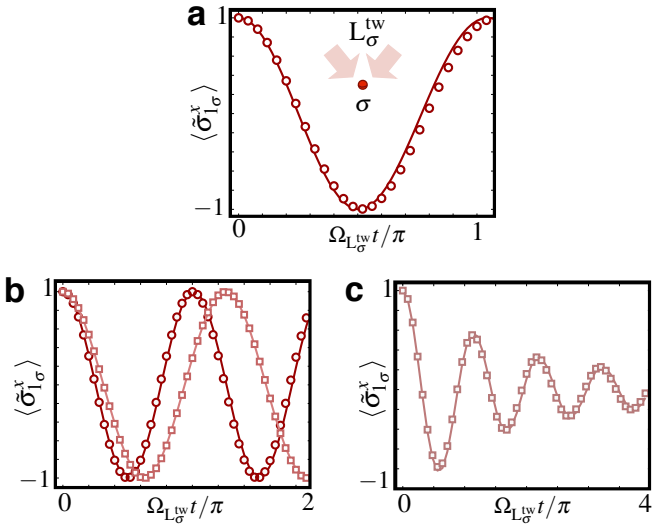

Figure 8. **Spin-vibron coupling: (a)** Dynamics of the spin coherence of a single ion initially prepared in the state $|\Psi_\sigma(0)\rangle = (|g_{\sigma,1}\rangle + |g_{\sigma,2}\rangle)/\sqrt{2}$ in the Λ-scheme [Fig. 4**(a)**] (see text for the particular parameters). The lasers are set according to $\mathbf{k}_{1_\sigma}, \mathbf{k}_{2_\sigma} \parallel \mathbf{e}_y$, such that there is no spin-vibron coupling, and thus the lasers only induce a periodic oscillation of the coherences. The oscillation of the coherences $\langle\tilde{\sigma}_1^x\rangle$ (solid line: dynamics given by the master equation (A49), whereas the circles correspond to the effective crossed-beam ac-Stark shift (A50)) confirms the analytical prediction. **(b, c)** Spin dynamics for the same state, but with the lasers fulfilling $(\mathbf{k}_{1_\sigma} - \mathbf{k}_{2_\sigma}) \parallel \mathbf{e}_x$, such that the effects of the spin-phonon coupling become appreciable. In **(b)**, we consider an initial vibrational Fock state with $\bar{n}_\sigma = 0$ (red solid line describes the coherences $\langle\tilde{\sigma}_1^x\rangle$ given by (A50); red circles correspond to (A44)), which coincide with the periodic oscillations of part **(a)**. We also display $\bar{n}_\sigma = 10$ (pink solid line describes the coherences $\langle\tilde{\sigma}_1^x\rangle$ given by (A50); pink squares correspond to (A44)), where one observes a shift of the oscillation period due to the vibronic state. In **(c)**, we consider an initial thermal state with $\bar{n}_\sigma = 10$ (pink solid line describes the coherences $\langle\tilde{\sigma}_1^x\rangle$ given by (A50); pink squares correspond to (A44)). In addition to the frequency shift, damping of the coherences is caused by the fluctuations of the number of vibrons associated to a thermal state.

$\omega_{1_\sigma} = 30$, and $\omega_{2_\sigma} = \omega_{1_\sigma} + 10^{-3}(\varepsilon_{g_{\sigma,1}} - \varepsilon_{g_{\sigma,2}})$, such that the condition $\omega_{L_\sigma^{tw}} = \omega_{1_\sigma} - \omega_{2_\sigma} \ll \omega_0^\sigma$ leading to Eq. (A39) is fulfilled. The Rabi frequencies are set to $\Omega_{1_\sigma,1} = -\Omega_{2_\sigma,1} = 0.01\varepsilon_{e_\sigma}$, and $\Omega_{1_\sigma,2} = \Omega_{2_\sigma,2} = 0.01\varepsilon_{e_\tau}$, such that the constraint $|\Omega_{l_\alpha s_{i_\alpha}}| \ll \Delta_{l_\alpha s_{i_\alpha}}$ is also fulfilled. The final, and more relevant part, is to set the decay rate consistent with the far-detuned constraint $\Gamma_\sigma \ll |\Delta_{l_\sigma n_\sigma}|$. We set $\Gamma_\sigma = 10^{-3}\Delta_{1_\sigma,1}$, which would correspond to detunings in the range 10-100 GHz for the $\sigma = {}^{25}Mg^+$ ion. Let us note that for these parameters, the standard ac-Stark shift (A40) is compensated, such that the dynamics should be given by the crossed-beam ac-Stark shift (A41). For our choice of Rabi frequencies, it becomes

$$\Delta\tilde{H}_{sv}^\sigma \approx \tfrac{1}{2}\Omega_{L_\sigma^{tw}}\sigma_{1_\sigma}^z e^{-i(\mathbf{k}_{L_\sigma^{tw}}\cdot\mathbf{r}_{i\sigma} - \omega_{L_\sigma^{tw}}t)} + \text{H.c.}, \tag{A50}$$

where $\Omega_{L_\sigma^{tw}} = 1.25\cdot 10^{-4}\varepsilon_{e_\sigma}$, $\sigma_{1_\sigma}^z = |\uparrow_{1_\sigma}\rangle\langle\uparrow_{1_\sigma}| - |\downarrow_{1_\sigma}\rangle\langle\downarrow_{1_\sigma}|$.

In order to show that this is correct, let us analyze the problem sequentially by first aligning the laser wavevectors $\mathbf{k}_{1_\sigma}, \mathbf{k}_{2_\sigma} \parallel \mathbf{e}_y$, such that there is no coupling to the vibrons under study (i.e. x-axis). Since Eq. (A50) corresponds to a σ^z periodic driving, it should induce a periodic oscillation in the coherences of the qubit. In Fig. 8**(a)**, we represent the spin coherences

$$\langle\tilde{\sigma}_{1_\sigma}^x(t)\rangle = \text{Tr}\{(\sigma_{1_\sigma}^+ e^{-i\omega_\sigma^0 t} + \sigma_{1_\sigma}^- e^{+i\omega_\sigma^0 t})\mu(t)\}, \tag{A51}$$

where $\sigma_{1_\sigma}^+ = |\uparrow_{1_\sigma}\rangle\langle\downarrow_{1_\sigma}| = (\sigma_{1_\sigma}^-)^\dagger$. The solid line corresponds to the complete Liouvillian (A49), whereas the circles are given by the crossed ac-Stark shift (A50). From the agreement displayed in this figure, we conclude that the "adiabatic elimination" of the excited state leading to Eq. (A50) is very accurate. This allows us to work directly in the ground-state manifold, where the numerical limitations disappear, and we can use again the real parameters for the the $\sigma = {}^{25}Mg^+$ ion.

Once this has been shown, let us align the laser wavevectors such that $\mathbf{k}_{1_\sigma} = -\mathbf{k}_{2_\sigma} \parallel \mathbf{e}_x$. In this case, the crossed-beam Stark shift (A50) introduces a coupling between the spin and vibrational degrees of freedom that will affect the coherences. We want to assess numerically the validity of the leading spin-vibron coupling derived in Eq. (A46). Hence, we consider a slowly oscillating $\omega_{L_\sigma^{tw}} = 10^{-3}\omega_\sigma$ laser arrangement with $\Omega_{L_\sigma^{tw}} = 0.1\omega_\sigma/(\eta_{L_\sigma^{tw}})$, where we recall that the transverse trap frequency for $\sigma = {}^{25}Mg^+$ ion is $\omega_\sigma/2\pi = 5$ MHz, and the Lamb-Dicke parameter is $\eta_{L_\sigma^{tw}} \approx 0.15$. We truncate the vibron Hilbert space to $n_{max} = 60$. In Fig. 8**(b)**, we represent the spin coherences. We consider two initial Fock states with $\bar{n}_\sigma \in \{0, 10\}$. First, we observe that the effective spin-vibron coupling (A46) is an accurate description. Second, we see that the period of the coherence oscillations depends on the number of vibrons, a feature that will be crucial to use this coupling as a measurement device. Finally, in Fig. 8**(c)**, we initialize the vibrons in a thermal state with $\bar{n}_\sigma = 10$. We observe that, for thermal states, the intrinsic fluctuations in the number of vibrons lead to a decoherence of the spin states. This feature will be crucial for heat transport measurements.

In this appendix of the supplemental material, we have presented a detailed derivation of Eqs. (A8), (A23), and (A46), which form our toolbox for quantum transport: the *driven dissipative spin-vibron model* (4). Moreover, all the different approximations have been supported by numerical analysis, which show that our analytical description is very accurate for realistic trapped-ion parameters. In the remaining part of this appendix, we will give details of the application of this toolbox for quantum heat transport. To ease notation, we write $\tilde{\mu} = (\mathscr{P}_{\sigma\kappa}\tilde{\mu}) \to \mu$ in Eq. (4), bearing in mind that the atomic levels of the τ-ions have been traced out, and we have projected onto the ground-state manifold of the $\{\sigma, \kappa\}$ bulk ions.

Appendix B: Thermalization: vibron number and current

The objective of this section is to present a detailed derivation, supported by numerical simulations, of the effective dissipation of the bulk vibrons (5), which forms the basis to understand the ballistic heat transport across an ion chain (6)-(7). Additionally, we describe how to introduce dephasing and disorder in the ion chain, and how they affect the transport.

1. Effective dissipation of the bulk vibrons

Let us derive the effective thermalization of the bulk vibrons (5) starting from the driven dissipative spin-vibron model (4). In Fig. 7, we showed that the Doppler cooling by a standing wave leads to cooling rates $\gamma_{\ell_\tau} = \mathrm{Re}\{(\Lambda^-_{\ell_\tau})^* - \Lambda^+_{\ell_\tau}\}$ that can be much stronger than the vibron tunnelings $2\gamma_{\ell_\tau} \gg J_{i_\alpha j_\beta}$. In this limit, there is again a separation of time-scales: the thermalization of the edge τ-vibrons is much faster than any other term in the Liouvillian (4). This allows for the partition of the Liouvillian into two terms

$$\begin{aligned}\tilde{\mathscr{L}}_0(\tilde{\mu}) &= \sum_{\ell_\tau} \tilde{\mathscr{D}}^{\ell_\tau}_{\mathrm{v}}(\tilde{\mu}),\\ \tilde{\mathscr{L}}_1(\tilde{\mu}) &= -\mathrm{i}[\tilde{H}_{\mathrm{vt}} + \tilde{H}^{\sigma}_{\mathrm{sv}}(t) + \tilde{H}^{\kappa}_{\mathrm{sv}}(t), \tilde{\mu}],\end{aligned} \tag{B1}$$

where the "tildes" refer to the interaction picture with respect to $H_0 = H^{\sigma}_{\mathrm{s}} + H^{\kappa}_{\mathrm{s}} + H_{\mathrm{vo}}$. Let us start by switching off the spin-vibron couplings. To integrate out the edge vibrons, we use the projection-operator techniques (A21) for a projector $\mathscr{P}_{\mathrm{edge}}\{\bullet\} = \mu^{\tau}_{\mathrm{ss}} \otimes \mathrm{Tr}_{\tau,\mathrm{vib}}\{\bullet\}$. Here, μ^{τ}_{ss} is the steady state of the laser-cooled τ-vibrons determined by the different laser cooling parameters applied to each edge of the chain $\mu^{\tau}_{\mathrm{ss}} = \mu^{\mathrm{th}}_{1_\tau} \otimes \mu^{\mathrm{th}}_{N_\tau}$. In particular, it corresponds the thermal states

$$\mu^{\mathrm{th}}_{\ell_\tau} = \sum_{n_{\ell_\tau}=0}^{\infty} (\bar{n}_{\ell_\tau})^{n_{\ell_\tau}} (1+\bar{n}_{\ell_\tau})^{-(1+n_{\ell_\tau})} |n_{\ell_\tau}\rangle\langle n_{\ell_\tau}|, \tag{B2}$$

with different mean vibron numbers $\bar{n}_{\ell_\tau} = \mathrm{Re}\{\Lambda^+_{\ell_\tau}\}/\gamma_{\ell_\tau}$. As discussed in the main text, as long as the laser-cooling is switched on, the edge ions remain in a vibrational thermal state that can be controlled by the laser parameters. These edge τ-ions act as a reservoir of vibrons for the remaining bulk of the ion chain. Our objective now is to derive the effective Liouvillian for the bulk ions.

After some algebraic manipulations, and making use of the quantum regression theorem, we obtain the two-time correlation functions of the vibrons

$$\begin{aligned}\langle a^{\dagger}_{\ell_\tau}(s) a_{\ell'_\tau}(0)\rangle_{\mathrm{ss}} &= \delta_{\ell_\tau,\ell'_\tau}\bar{n}_{\ell_\tau} \mathrm{e}^{-(\gamma_{\ell_\tau} - \mathrm{i}\delta_{\ell_\tau})s},\\ \langle a_{\ell_\tau}(s) a^{\dagger}_{\ell'_\tau}(0)\rangle_{\mathrm{ss}} &= \delta_{\ell_\tau,\ell'_\tau}(\bar{n}_{\ell_\tau}+1) \mathrm{e}^{-(\gamma_{\ell_\tau} - \mathrm{i}\delta_{\ell_\tau})s},\end{aligned} \tag{B3}$$

where we have introduced $\gamma_{\ell_\tau} = \mathrm{Re}\{(\Lambda^-_{\ell_\tau})^* - \Lambda^+_{\ell_\tau}\} > 0$, $\delta_{\ell_\tau} = -\mathrm{Im}\{(\Lambda^-_{\ell_\tau})^* - \Lambda^+_{\ell_\tau}\} > 0$, and $\delta_{\ell_\tau,\ell'_\tau}$ is the Kronecker delta. Using these expression, together with the projection-operator formula (A21), we arrive at a master equation that only involves the degrees of freedom of the bulk ions

$$\dot{\mu}_{\mathrm{bulk}} = -\mathrm{i}\big[\sum_{\alpha} H^{\alpha}_{\mathrm{s}} + H^{\mathrm{bulk}}_{\mathrm{tb}}, \mu_{\mathrm{bulk}}\big] + \Delta\mathscr{L}(\mu_{\mathrm{bulk}}), \tag{B4}$$

where $\mu_{\mathrm{bulk}} = \mathrm{Tr}_{\tau,\mathrm{vib}}\{\mu\}$, and $H^{\mathrm{bulk}}_{\mathrm{tb}}$ is the vibron tight-binding model restricted to the bulk ion species $\alpha,\beta \in \{\sigma,\kappa\}$. In the expression above, we have introduced the super-operator

$$\begin{aligned}\Delta\mathscr{L}(\bullet) = \sum_{\alpha,\beta}\sum_{i_\alpha,j_\beta,\ell_\tau} \Upsilon^{\ell_\tau}_{i_\alpha j_\beta}\Big\{&(\bar{n}_{\ell_\tau}+1)(a_{j_\beta}\bullet a^{\dagger}_{i_\alpha} - a^{\dagger}_{i_\alpha}a_{j_\beta}\bullet)\\ &+\bar{n}_{\ell_\tau}(a^{\dagger}_{i_\alpha}\bullet a_{j_\beta} - a_{j_\beta}a^{\dagger}_{i_\alpha}\bullet)\Big\} + \mathrm{H.c.},\end{aligned} \tag{B5}$$

which is expressed in terms of the couplings

$$\Upsilon^{\ell_\tau}_{i_\alpha j_\beta} = \frac{J_{i_\alpha \ell_\tau} J_{\ell_\tau j_\beta}}{\gamma_{\ell_\tau} - \mathrm{i}((\omega_{i_\alpha} - \delta_{\ell_\tau}) - \omega_{\ell_\tau})}. \tag{B6}$$

The imaginary part of the Υ-coefficients can be rewritten as a Hamiltonian term, which leads to a renormalization of the vibron tunnelings and the on-site energies

$$\tilde{J}_{i_\alpha j_\beta} = J_{i_\alpha j_\beta} + \sum_{\ell_\tau} \mathrm{Im}\{\Upsilon^{\ell_\tau}_{i_\alpha j_\beta}\}, \quad \tilde{\omega}_{i_\alpha} = \omega_\alpha + \tilde{J}_{i_\alpha i_\alpha}. \tag{B7}$$

This leads to the renormalized tight-binding model

$$H_{\mathrm{rtb}} = \sum_{\alpha,i_\alpha} \tilde{\omega}_{i_\alpha} a^{\dagger}_{i_\alpha} a_{i_\alpha} + \sum_{\alpha,\beta}\sum_{i_\alpha \neq j_\beta} \tilde{J}_{i_\alpha j_\beta} a^{\dagger}_{i_\alpha} a_{j_\beta}, \tag{B8}$$

introduced in Eq. (5) of the main text. In addition, the real part of the Υ-coefficients leads to a dissipative super-operator

$$\begin{aligned}\mathscr{D}_{\mathrm{bulk}}(\bullet) = \sum_{\alpha,\beta}\sum_{i_\alpha j_\beta}\Big\{&\tilde{\Lambda}^+_{i_\alpha j_\beta}\big(a^{\dagger}_{j_\beta}\bullet a_{i_\alpha} - a_{i_\alpha}a^{\dagger}_{j_\beta}\bullet\big)\\ &+\tilde{\Lambda}^-_{i_\alpha j_\beta}\big(a_{j_\beta}\bullet a^{\dagger}_{i_\alpha} - a^{\dagger}_{i_\alpha}a_{j_\beta}\bullet\big)\Big\} + \mathrm{H.c.},\end{aligned} \tag{B9}$$

where the dissipation rates are the following

$$\tilde{\Lambda}^+_{i_\alpha j_\beta} = \sum_{\ell_\tau} \mathrm{Re}\{\Upsilon^{\ell_\tau}_{i_\alpha j_\beta}\}\bar{n}_{\ell_\tau}, \quad \tilde{\Lambda}^-_{i_\alpha j_\beta} = \sum_{\ell_\tau} \mathrm{Re}\{\Upsilon^{\ell_\tau}_{i_\alpha j_\beta}\}(\bar{n}_{\ell_\tau}+1). \tag{B10}$$

Using the super-operator (B52), the above dissipator can be written as the bulk dissipator below Eq. (5) of the main text.

2. Mesoscopic transport in ion chains

The objective of this section is to provide numerical evidence supporting Eq. (5) for the effective thermalization of the bulk vibrons. Additionally, we will also check the accuracy of the predictions derived thereof, namely Eqs. (6) and (7) for the vibronic number and current through the ion chain

$$\langle n_{i_\alpha}\rangle_{\mathrm{ss}} = \frac{\Gamma_{\mathrm{L}}\bar{n}_{\mathrm{L}} + \Gamma_{\mathrm{R}}\bar{n}_{\mathrm{R}}}{\Gamma_{\mathrm{L}} + \Gamma_{\mathrm{R}}}, \quad \langle I^{\mathrm{vib}}_{i_\alpha \to}\rangle_{\mathrm{ss}} = \frac{\Gamma_{\mathrm{L}}\Gamma_{\mathrm{R}}}{\Gamma_{\mathrm{L}} + \Gamma_{\mathrm{R}}}(\bar{n}_{\mathrm{L}} - \bar{n}_{\mathrm{R}}). \tag{B11}$$

Following the philosophy of "*one*, *two*, *many*", we first consider the smallest setup, a single-ion channel that will play the role of a thermal quantum dot (TQD). This will allow us to test the validity of Eq. (5), and the predicted number of bulk vibrons in the steady state. Then, we will move to a two-ion channel that will act as a double thermal quantum dot (DTQD). This will allow us to test the validity of the predicted current of bulk vibrons. Finally, we will explore the mesoscopic limit of a thermal quantum wire (TQW) formed by a longer ion chain, or a TQD connected to two thermal leads, where the leads are formed by a large number of ions.

In order to test these predictions, we compare the dynamics given by the bulk master equation (5), with that given

by the master equation where dissipation only occurs at the edges (4). Since both Liouvillians are quadratic in creation-annihilation operators, it is possible to obtain a closed system of $(N-2)^2$ or N^2 differential equations for the two-point correlators $C_{i_\alpha j_\beta} = \langle a^\dagger_{i_\alpha} a_{j_\beta}\rangle$, respectively. Both theories can be recast in a matrix differential equation

$$\frac{\mathrm{d}C}{\mathrm{d}t} = \mathrm{i}[\mathbb{J}, C] - (\mathbb{W}C + C\mathbb{W}^*) + \mathbb{K}, \tag{B12}$$

where the matrices $\mathbb{J}, \mathbb{W}, \mathbb{K}$ depend on the particular master equation, Eq. (4) or Eq. (5). In particular, for the edge dissipation (4), we get the following matrices

$$\begin{aligned}
\mathbb{J}^{\mathrm{edge}}_{i_\alpha j_\beta} &= \omega_\alpha \delta_{i_\alpha j_\beta} + J_{i_\alpha j_\beta},\\
\mathbb{W}^{\mathrm{edge}}_{i_\alpha j_\beta} &= ((\Lambda^-_{\ell_\tau})^* - \Lambda^+_{\ell_\tau})\delta_{i_\alpha,\ell_\tau}\delta_{j_\beta,\ell_\tau}, \qquad \alpha,\beta \in \{\sigma,\kappa,\tau\}\\
\mathbb{K}^{\mathrm{edge}}_{i_\alpha j_\beta} &= 2\mathrm{Re}\{\Lambda^+_{\ell_\tau}\}\delta_{i_\alpha \ell_\tau}\delta_{j_\beta,\ell_\tau},
\end{aligned} \tag{B13}$$

whereas for the effective bulk dissipation (5), we get

$$\begin{aligned}
\mathbb{J}^{\mathrm{bulk}}_{i_\alpha j_\beta} &= \omega_\alpha \delta_{i_\alpha j_\beta} + \tilde{J}_{i_\alpha j_\beta},\\
\mathbb{W}^{\mathrm{bulk}}_{i_\alpha j_\beta} &= (\tilde{\Lambda}^-_{i_\alpha j_\beta})^* - \tilde{\Lambda}^+_{i_\alpha j_\beta}, \qquad \alpha,\beta \in \{\sigma,\kappa\}\\
\mathbb{K}^{\mathrm{bulk}}_{i_\alpha j_\beta} &= 2\mathrm{Re}\{\tilde{\Lambda}^+_{i_\alpha j_\beta}\}.
\end{aligned} \tag{B14}$$

The possibility of expressing the dissipative dynamics as a closed set of differential equations (B12) allows us to circumvent the numerical limitations, which would arise due to the large truncation of the vibron Hilbert space required for some of the simulations of the dissipative vibron model.

a. *Thermal Quantum dot: vibron number*

Let us consider the minimal scenario: the *thermal quantum dot*. In this case, the chain is composed of three ions

$$\tau - \sigma - \tau, \tag{B15}$$

such that the heat transport takes place along the minimal channel, namely a single-ion connecting the two τ-reservoirs. According to Eq. (5), the bulk vibrons evolve under

$$\dot{\mu}_{\mathrm{bulk}} = -\mathrm{i}[(\omega_\sigma + \tilde{J}_{2_\sigma 2_\sigma})a^\dagger_{2_\sigma} a_{2_\sigma}, \mu_{\mathrm{bulk}}] + \mathscr{D}_{2_\sigma 2_\sigma}(\mu_{\mathrm{bulk}}), \tag{B16}$$

where the dissipator contains the heating and cooling terms

$$\begin{aligned}
\mathscr{D}_{2_\sigma 2_\sigma}(\bullet) =& \tilde{\Lambda}^+_{2_\sigma 2_\sigma}\left(a^\dagger_{2_\sigma}\bullet a_{2_\sigma} - a_{2_\sigma}a^\dagger_{2_\sigma}\bullet\right) +\\
&+\tilde{\Lambda}^-_{2_\sigma 2_\sigma}\left(a_{2_\sigma}\bullet a^\dagger_{2_\sigma} - a^\dagger_{2_\sigma}a_{2_\sigma}\bullet\right) + \mathrm{H.c.}.
\end{aligned} \tag{B17}$$

Such a single-oscillator master equation can be solved exactly, and yields a non-equilibrium steady-state mean vibron number of $\bar{n}_{2_\sigma} = \mathrm{Re}\{\tilde{\Lambda}^+_{2_\sigma 2_\sigma}\}/\mathrm{Re}\{\tilde{\Lambda}^-_{2_\sigma 2_\sigma} - \tilde{\Lambda}^+_{2_\sigma 2_\sigma}\}$. According to Eq. (B10), this mean vibron number is the following

$$\bar{n}_{2_\sigma} = \frac{\Gamma_{\mathrm{L}}\bar{n}_{\mathrm{L}} + \Gamma_{\mathrm{R}}\bar{n}_{\mathrm{R}}}{\Gamma_{\mathrm{L}} + \Gamma_{\mathrm{R}}}, \tag{B18}$$

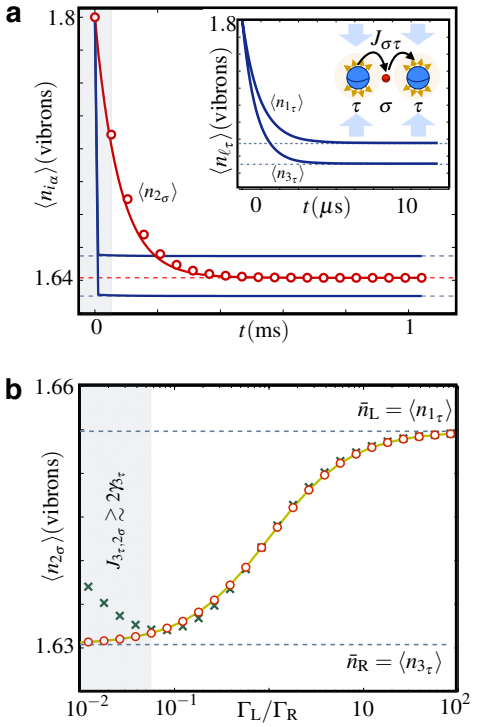

Figure 9. **Thermalization of a thermal quantum dot: (a)** Dynamics of the vibronic numbers $\langle n_{i_\alpha}\rangle$ for a ^{24}Mg$^+$-^{25}Mg$^+$-^{24}Mg$^+$ ion chain (see the text for the particular parameters). The solid lines represent the numerical solution of Eqs. (B12)-(B13), showing that the edge ions thermalize much faster (see also the inset for $\langle n_{1_\tau}\rangle$, $\langle n_{3_\tau}\rangle$). For the bulk ion, the numerical solution for the vibron number $\langle n_{2_\sigma}\rangle$ given by Eqs. (B12)-(B14) is displayed with red circles, and shows a good agreement with the previous dynamics. **(b)** Steady state number of bulk vibrons $\langle n_{2_\sigma}\rangle$ as a function of the reservoir couplings $\Gamma_{\mathrm{L}}/\Gamma_{\mathrm{R}}$. The solid yellow line corresponds to the prediction (B18), the green crosses are obtained from the numerical integration of Eqs. (B12) and (B13), and the red circles correspond to the numerical solution of the effective dynamics in Eqs. (B12) and (B14). The grey area marks the region where the constraint $2\gamma_{\ell_\tau} \gg J_{i_\alpha j_\beta}$ is not fulfilled any longer, and thus deviations from the theory appear.

where we have introduced the mean vibron numbers $\bar{n}_{\mathrm{L}} = \bar{n}_{1_\tau}, \bar{n}_{\mathrm{R}} = \bar{n}_{3_\tau}$ for the left and right reservoirs. Here, we have also used the couplings $\Gamma_{\mathrm{L}} = \Gamma^{1_\tau}_{2_\sigma,2_\sigma}$ and $\Gamma_{\mathrm{R}} = \Gamma^{3_\tau}_{2_\sigma,2_\sigma}$, which were introduced below Eq. (5) in the main text, namely

$$\Gamma^{\ell_\tau}_{2_\sigma,2_\sigma} = 2\pi J_{2_\sigma,\ell_\tau}\rho_{\ell_\tau}(\omega_{2_\sigma})J_{\ell_\tau,2_\sigma}, \tag{B19}$$

where $\rho_{\ell_\tau}(\varepsilon)$ is the Lorentzian density of states for the laser-cooled ions. Let us note that, considering the symmetry of the vibron tunnelings $J_{2_\sigma 1_\tau} = J_{2_\sigma 3_\tau}$, we find that the steady-state vibron number of the TQD does not depend on the Coulomb couplings, and thus on its distance to the reservoir.

Let us now consider the realistic parameters for a τ-σ-τ chain, where $\tau =^{24}$Mg$^+$ and $\sigma =^{25}$Mg$^+$. In addition to the parameters introduced in previous sections, we consider the detunings $\Delta_{1_\tau} = -0.6\Gamma_\tau$, $\Delta_{3_\tau} = -0.5\Gamma_\tau$, and the Rabi frequencies $\Omega_{\mathrm{L}^{\mathrm{sw}}_{1_\tau}} = \Omega_{\mathrm{L}^{\mathrm{sw}}_{3_\tau}} = \Gamma_\tau$ for the laser cooling of the τ-

ions, where we recall that $\Gamma_\tau/2\pi = 41.4\,\mathrm{MHz}$. With these parameters, the effective cooling rates (A28) of the τ-ions would be $\gamma_{1_\tau}/2\pi \approx 86\,\mathrm{kHz}$, and $\gamma_{3_\tau}/2\pi \approx 106\,\mathrm{kHz}$. Additionally, the mean number of vibrons for each reservoir (A29) would be $\bar{n}_{1_\tau} = 1.65$, and $\bar{n}_{3_\tau} = 1.63$. The trap frequencies are $(\omega_{\alpha x}, \omega_{\alpha y}, \omega_{\alpha z})/2\pi = (5, 5, 0.5)\,\mathrm{MHz}$, which lead to an inter-ion distance of $|z^0_{1_\tau} - z^0_{2_\sigma}| = |z^0_{3_\tau} - z^0_{2_\sigma}| \approx 9\,\mu\mathrm{m}$, and to a vibron tunneling strength of $J_{1_\tau 2_\sigma}/2\pi = J_{3_\tau 2_\sigma}/2\pi \approx 30\,\mathrm{kHz}$. With these parameters, the constraint $2\gamma_{\ell_\tau} \gg J_{i_\alpha j_\beta}$ is fulfilled, and we expect that the τ-ions thermalize very fast and act as an effective reservoir for the bulk σ-ion.

In Fig. 9**(a)**, we confirm this behavior numerically. The blue solid lines represent the vibron number of the edge τ-ions, namely $\langle n_{1_\tau}\rangle, \langle n_{3_\tau}\rangle$, obtained by integrating Eqs. (B12)-(B13). As displayed in the figure, the edge vibrons thermalize on a μs-scale (see also the inset). The red solid line stands for the bulk vibron number $\langle n_{2_\sigma}\rangle$, which reaches the steady state on a longer millisecond-scale. The red circles represent the numerical solution of the effective bulk dissipation from Eqs. (B12)-(B14), whereas the red solid line corresponds to Eqs. (B12)-(B13). The agreement of these results shows that the effective bulk Liouvillian (B4) is a good description of the problem. Moreover, the red dashed line represents our prediction for the stationary bulk vibrons (B18), which also displays a good agreement with the numerical results. Finally, the blue dashed lines represent the laser-cooling vibron numbers $\bar{n}_{1_\tau}, \bar{n}_{3_\tau}$, which perfectly match the edge steady state. This shows that the τ-ions behave as a perfect vibronic reservoir, whose properties are not modified by the bulk ion chain.

In Fig. 9**(b)**, we display the dependence of the steady-state number of bulk vibrons $\langle n_{2_\sigma}\rangle$ as a function of the laser-cooling parameters at the edges of the chain. We keep the same parameters as above, but let one of the laser-cooling Rabi frequencies vary in the range $\Omega_{\mathrm{L}^{\mathrm{sw}}_{3_\tau}} \in [0.1\Gamma_\tau, 10\Gamma_\tau]$, while the other one is fixed $\Omega_{\mathrm{L}^{\mathrm{sw}}_{1_\tau}} = \Gamma_\tau$. This does not modify the reservoir vibron number, but only the bulk-reservoir couplings to the $\Gamma_\mathrm{L}, \Gamma_\mathrm{R}$. In the figure, we again observe a regime with a very good agreement of the theoretical prediction (B18) and the numerics from Eqs. (B12)-(B13) or Eqs. (B12)-(B14). It is also very instructive to analyze the shaded region, where deviations from the theory start arising. In this region, the condition $2\gamma_{\ell_\tau} \gg J_{i_\alpha j_\beta}$ is no longer fulfilled, and one cannot treat the edge ions as an effective reservoir any more. This is the underlying reason for the displayed differences.

b. *Double thermal quantum dot: vibron current*

Let us now move into the double thermal quantum dot, which is formed by a two-oscillator channel connected to the two laser-cooled reservoirs

$$\tau - \sigma - \sigma - \tau, \tag{B20}$$

where $\tau = {}^{24}\mathrm{Mg}^+$ and $\sigma = {}^{25}\mathrm{Mg}^+$. In this case, we choose the detunings $\Delta_{1_\tau} = -0.8\Gamma_\tau$, $\Delta_{4_\tau} = -0.6\Gamma_\tau$, and the Rabi frequencies $\Omega_{\mathrm{L}^{\mathrm{sw}}_{1_\tau}} = 1.4\Gamma_\tau$, $\Omega_{\mathrm{L}^{\mathrm{sw}}_{4_\tau}} = \Gamma_\tau$ for the laser cooling. The trap frequencies are set to $(\omega_{\alpha x}, \omega_{\alpha y}, \omega_{\alpha z})/2\pi = (5, 5, 0.2)\,\mathrm{MHz}$. We consider an initial thermal state, where the two σ-ions have a different vibronic number $\bar{n}_{2_\sigma}(0) = 2.4$, and $\bar{n}_{3_\sigma}(0) = 1$. Accordingly, we expect to observe a periodic exchange of vibrons between the bulk ions, which is additionally damped due to their contact with the reservoirs.

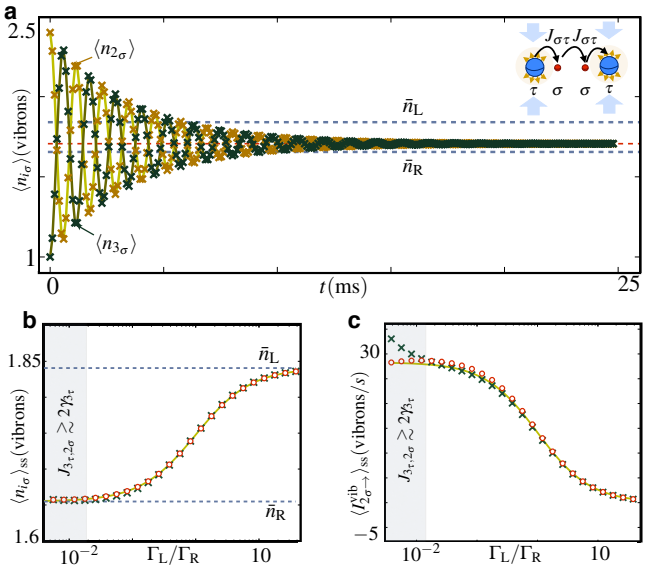

Figure 10. **Vibron number and current in a double thermal quantum dot: (a)** Thermalization dynamics for the number of bulk vibrons $\langle n_{2_\sigma}\rangle, \langle n_{3_\sigma}\rangle$ (see the text for the particular parameters). The solid lines correspond to the numerical solution of Eqs. (B12)-(B13), and the symbols to the numerical solution of Eqs. (B12)-(B14). The grey dashed lines represent the reservoir mean vibron numbers $\bar{n}_\mathrm{L}, \bar{n}_\mathrm{R}$, while the red dashed line stands for the theoretical prediction for the bulk vibron number (B11). **(b)** Steady-state bulk vibron number $\langle n_{2_\sigma}\rangle = \langle n_{3_\sigma}\rangle$ as a function of the system-reservoir effective couplings $\Gamma_\mathrm{L}, \Gamma_\mathrm{R}$. The green crosses represent the numerical solution of Eqs. (B12)-(B13), the red circles that of Eqs. (B12)-(B14), and the yellow solid line corresponds to the theoretical prediction in Eq. (B11). **(c)** Same as above, but displaying the steady-state vibron currents $\langle I^{\mathrm{vib}}_{2_\sigma\to}\rangle_{\mathrm{ss}}$ according to Eqs. (B12)-(B13) (crosses), Eqs. (B12)-(B14) (circles), and the prediction (B11) (solid line).

In Fig. 10**(a)**, we show the thermalization dynamics of such a two-oscillator channel. The solid lines correspond to the numerical solution of Eqs. (B12)-(B13) ($\langle n_{2_\sigma}\rangle$ yellow, and $\langle n_{3_\sigma}\rangle$ green), whereas the symbols stand for the numerical solution of Eqs. (B12)-(B14) ($\langle n_{2_\sigma}\rangle$ yellow crosses, and $\langle n_{3_\sigma}\rangle$ green crosses). The clear agreement supports once more the validity of our analytical derivations. More importantly, we also observe how both vibronic numbers tend to the same equilibrium value given by Eq. (B11) (red dashed line).

Let us now address the validity of the predictions (B11). In order to calculate the vibron current, let us note that the current operator can be defined through a continuity equation $\mathrm{d}n_{i_\alpha}/\mathrm{d}t = I^{\mathrm{vib}}_{\to i_\alpha} - I^{\mathrm{vib}}_{\to i_\alpha}$. By applying this to the tight-binding

Hamiltonian (A8), we get

$$I^{\rm vib}_{\to i_\alpha} = -{\rm i}\sum_\beta \sum_{j_\beta > i_\alpha} J^*_{j_\beta i_\alpha} a^\dagger_{i_\alpha} a_{j_\beta} + {\rm H.c.},$$
$$I^{\rm vib}_{i_\alpha \to} = -{\rm i}\sum_\beta \sum_{j_\beta > i_\alpha} J_{i_\alpha j_\beta} a^\dagger_{j_\beta} a_{i_\sigma} + {\rm H.c.}, \tag{B21}$$

where we have used $J_{i_\alpha j_\beta} = J_{j_\beta i_\alpha}$. In the particular case of Eq. (A8), the tunnelings are real. However, we keep the above expression general since it will be useful in other sections below. In Figs. 10**(b)**-**(c)**, we let one of the Rabi frequencies vary in the range $\Omega_{{\rm L}^{\rm sw}_{4_\tau}} \in [0.1\Gamma_\tau, 10\Gamma_\tau]$, which allows us to modify the ratio $\Gamma_{\rm L}/\Gamma_{\rm R}$. As shown in these figures, when the constraint $2\gamma_{\ell_\tau} \gg J_{i_\alpha j_\beta}$ is fulfilled, there is an excellent agreement of both numerical solutions based on Eqs. (B12)-(B13) (green crosses), or Eqs. (B12)-(B14) (red circles), and the theoretical predictions (B11) (yellow lines). As expected, we can thus conclude that Fourier's law is violated in the TDQD.

c. *Thermal quantum wire: assessing Fourier's law*

Let us now consider a mesoscopic TQW with $N = 20$ ions, which would have a length of $L \approx 0.21\,$mm for the trap frequencies $(\omega_{\alpha x}, \omega_{\alpha y}, \omega_{\alpha z})/2\pi = (5, 5, 0.1)\,$MHz. The configuration of ions species is

$$\tau - \sigma - \cdots - \sigma - \cdots - \sigma - \tau, \tag{B22}$$

where $\tau = {}^{24}{\rm Mg}^+$ and $\sigma = {}^{25}{\rm Mg}^+$, and we choose the detunings $\Delta_{1_\tau} = -0.8\Gamma_\tau$, $\Delta_{N_\tau} = -0.6\Gamma_\tau$. We shall use this setup to test the validity of Fourier's law of thermal conduction. As discussed in the main text, this law predicts the onset of a linear gradient in the number of carriers between the reservoirs

$$\langle n_{i_\alpha}\rangle_{\rm FL} = \bar{n}_{\rm L} + \frac{(\bar{n}_{\rm R} - \bar{n}_{\rm L})}{N} i_\alpha. \tag{B23}$$

In Fig. 11, we represent the number of vibrons in the steady state of the TWQ when the laser-cooling Rabi frequencies are set to $\Omega_{{\rm L}^{\rm sw}_{1_\tau}} = \Omega_{{\rm L}^{\rm sw}_{10_\tau}} = 1.4\Gamma_\tau$. The yellow bars represent the number of bulk vibrons $\langle n_{i_\sigma}\rangle_{\rm ss}$ obtained numerically from the steady-state solution of Eqs. (B12)-(B13), whereas the green bars stand for the numerical solution of Eqs. (B12)-(B14). These numerical simulations confirm the theoretical prediction (B11) to a good degree of accuracy. It is also clear from this figure that the number of vibrons does not display a linear gradient, as predicted by Fourier's law, but is rather homogeneous along the whole ion chain.

As mentioned in the main text, the violation of Fourier's law is not a surprise, since this law applies to diffusive processes, whereas our vibron transport is ballistic. Let us now explore two possible mechanisms to introduce diffusive dynamics in the problem.

i) Noise-induced pure dephasing.– A possible mechanism to introduce diffusion in the transport of heat is to consider an engineered noise leading to dephasing in the vibron tunneling. This can be accomplished by injecting a noisy signal in the trap electrodes [13], leading to fluctuating trap frequencies that modify the on-site energies of the tight-binding Hamiltonian

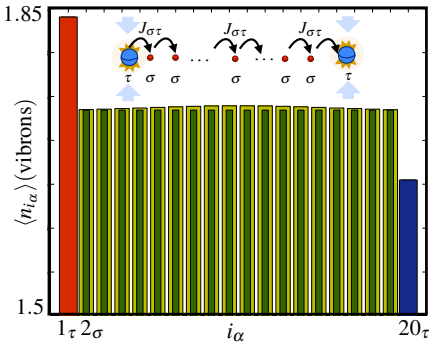

Figure 11. **Violation of Fourier's law:** Steady-state number of vibrons $\langle n_{i_\alpha}\rangle$ along the ion chain (see the text for the particular parameters). The bulk of the TQW displays a homogeneous number of vibrons, in clear contrast to the prediction of Fourier's law. The yellow (green) bars correspond to the numerical solution of Eqs. (B12)-(B13) (Eqs. (B12)-(B14)).

$$H_{\rm vo} \to H_{\rm vo} + \delta H_{\rm vo}(t) = \sum_{i_\alpha} (\omega_{i_\alpha} + \delta\omega_{i_\alpha}(t)) a^\dagger_{i_\alpha} a_{i_\alpha}. \tag{B24}$$

Here, we have considered that $\delta\omega_{i_\alpha}(t)$ is a zero-mean random Markov process that is stationary and Gaussian. Such process, usually known as the Ornstein-Uhlenbeck process [14], is typically characterized by a diffusion constant c, and a correlation time $\tau_{\rm c}$, which we assume to be much shorter than the time-scales of interest $t \gg \tau_{\rm c}$. Moreover, we introduce a correlation length $\xi_{\rm c}$ in order to model the extent of the noisy signal on the trap electrodes. The power spectrum of this noise is defined as

$$S_{\delta\omega_{i_\alpha},\delta\omega_{j_\beta}}(\omega) = {\rm Re}\left\{\int_0^\infty {\rm d}t\, \overline{\delta\omega_{i_\alpha}(t)\delta\omega_{j_\beta}(0)}\, {\rm e}^{+{\rm i}\omega t}\right\}, \tag{B25}$$

where the "bar" refers to the statistical average over the random process. In particular, the above three constants determine completely the noise spectrum

$$S_{\delta\omega_{i_\alpha},\delta\omega_{j_\beta}}(\omega) = \frac{\Gamma_{\rm d}}{1 + (\omega\tau_{\rm c})^2} {\rm e}^{-\frac{|z^0_{i_\alpha} - z^0_{j_\beta}|}{\xi_{\rm c}}}, \tag{B26}$$

where we have introduced the equilibrium positions of the ions given by Eq. (A2), and the rate $\Gamma_{\rm d} = c\tau_{\rm c}^2/2$.

By using a Born-Markov approximation to study the effects of the fluctuating trap frequencies, the master equation for the TQW becomes

$$\dot{\mu} = \mathscr{L}_{\rm ddsv}(\mu) - \int_0^\infty {\rm d}t' \overline{[\delta H_{\rm vo}(t), [\delta H_{\rm vo}(t - t'), \mu]]}. \tag{B27}$$

Using the above noise spectrum, the Liouvillian of the TQW gets the additional contribution of a pure-dephasing superoperator $\mathscr{L}_{\rm ddsv} \to \mathscr{L}_{\rm ddsv} + \mathscr{D}_{\rm d}$, where

$$\mathscr{D}_{\rm d}(\bullet) = \sum_{\alpha,\beta} \sum_{i_\alpha, j_\beta} S_{\delta\omega_{i_\alpha},\delta\omega_{j_\beta}}(0)(n_{i_\alpha} \bullet n_{j_\beta} - n_{j_\beta} n_{i_\alpha} \bullet) + {\rm H.c.}, \tag{B28}$$

such that the dephasing rate only depends on the zero-frequency component of noise spectrum. We also observe that ξ_c controls the collective effects in the dephasing dynamics of the TQW: when $\xi_c \to 0$, we obtain a purely local dephasing that introduces phase-breaking processes in the vibron transport, whereas for $\xi_c \to \infty$, the noise is purely global, such that the tunneling dynamics is not affected, and remains in the purely ballistic regime.

This collective dephasing modifies the system of differential equations (B12) for the two-point vibron correlators $C_{i_\alpha,j_\beta} = \langle a^\dagger_{i_\alpha} a_{j_\beta}\rangle$, which becomes

$$\frac{\mathrm{d}C}{\mathrm{d}t} = \mathrm{i}[\mathbb{J},C] - (\mathbb{W}C + C\mathbb{W}^*) - \mathbb{D}C + \mathbb{K}, \tag{B29}$$

where we have introduced the following matrix

$$\mathbb{D} = \sum_{\alpha,\beta}\sum_{i_\alpha,j_\beta} 2\Gamma_\mathrm{d}\left(1 - \mathrm{e}^{-|z^0_{i_\alpha} - z^0_{j_\beta}|/\xi_c}\right)|i_\alpha\rangle\langle j_\beta|, \tag{B30}$$

where $\{|i_\alpha\rangle\}_{i_\alpha=1}^N$ form an orthogonal basis of the N-dimensional subspace of the two-point correlators.

In Fig. 12, we compute the steady state solution of the above system of differential equations (B29). We consider the same experimental parameters as previously, and set the dephasing rate to $\Gamma_\mathrm{d} = 10\gamma_{N_\tau}$. As can be observed in Fig. 12**(a)**, in the limit of large correlation lengths $\xi_c \sim |\tilde{z}_{1_\tau} - \tilde{z}_{N_\tau}|$, the vibrons display the same homogeneous distribution that violates Fourier's law (i.e. ballistic regime). As the correlation length is decreased, a linear gradient starts to develop at the bulk of the chain (diffusive regime). It is interesting that we have a single parameter to control the ballistic-diffusive crossover. However, note that edge effects mask the linear gradient.

We have found that these edge effects are particularly strong for a linear Paul trap, since the equilibrium positions in Eq. (A2) lead to an inhomogeneous crystal. By modifying the dc trapping potentials, or by considering micro-fabricated ion traps, it is possible to obtain an homogeneous ion crystal. In Fig. 12**(b)**, we study numerically the distribution of vibrons in this regime, as the correlation length is decreased. Our results show that edge effects are less pronounced in this case, and a perfect linear gradient, as predicted by Fourier's law, develops along the whole chain.

ii) Spin-assisted random disorder.– In order to introduce another diffusive mechanism for the transport of vibrons, we apply a spin-vibron coupling (3). By controlling the laser intensities, polarizations and detunings, we further impose that $\Delta\omega^+_\sigma = 0$, which leads to a static spin-vibron coupling

$$H^\sigma_\mathrm{sv} = \sum_{i_\sigma} \tfrac{1}{2}\Delta\omega^-_\sigma n_{i_\sigma}\sigma^z_{i_\sigma}, \tag{B31}$$

whose strength $\Delta\omega^-_\sigma$ can be controlled at will, and made strong enough. The idea to mimic the effects of diagonal disorder is to use the spin degrees of freedom as a gadget to build a Liouvillian with random on-site energies. Here, the randomness is inherited from the quantum superposition principle in the spin degrees of freedom [15, 16].

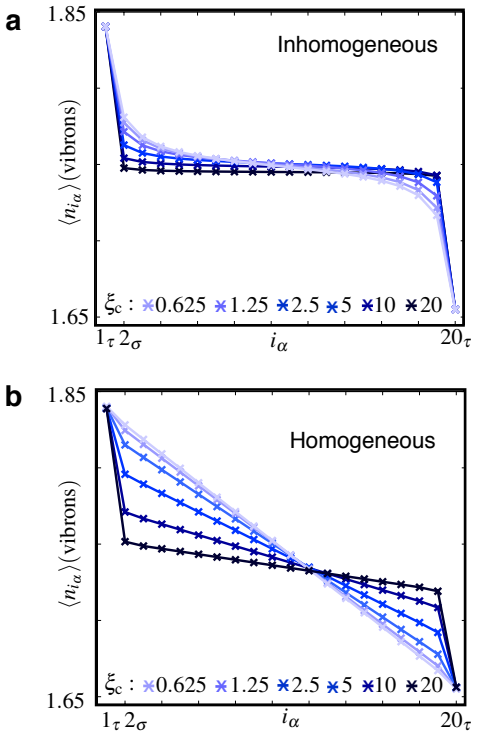

Figure 12. **The dephasing route to Fourier's law: (a)** Steady-state number of vibrons $\langle n_{i_\alpha}\rangle$ for an inhomogeneous ion chain in a linear Paul trap. As the correlation length of the dephasing noise ξ_c decreases (in units of the nearest-neighbor spacing at the center of the chain), keeping $\Gamma_\mathrm{d} = 10\gamma_{N_\tau}$, we observe a inhomogeneous distribution of vibrons across the chain. Far away from the edges and close to the bulk of the chain, the distribution displays a linear gradient. **(b)** Steady-state number of vibrons $\langle n_{i_\alpha}\rangle$ for an homogeneous chain in micro-fabricated ion trap array. As ξ_c decreases and $\Gamma_\mathrm{d} = 10\gamma_{N_\tau}$ is fixed, we observe a perfect linear gradient across the chain. Therefore, edge effects are less pronounced in this homogeneous scenario.

Let us consider an initial pure state for the σ-spins of the TQW, namely $\mu_\mathrm{spin}(0) = |\Psi_0\rangle\langle\Psi_0|$. Without loss of generality, it can be expressed as $|\Psi_0\rangle = \sum_{\{s_{i_\sigma}\}} c_{\{s_{i_\sigma}\}}|\{s_{i_\sigma}\}\rangle$, where $\{s_{i_\sigma}\} = \{s_{2_\sigma}, s_{3_\sigma}, \cdots, s_{N-1_\sigma}\}$ is a particular spin configuration for the bulk σ-ions $s_{i_\sigma} \in \{\uparrow_{i_\sigma}, \downarrow_{i_\sigma}\}$. The reduced density matrix of the vibrons evolves in time according to

$$\mu_\mathrm{vib}(t) = \mathrm{Tr}_\mathrm{spin}\{\mathrm{e}^{\mathscr{L}_\mathrm{ddsv}(\{\sigma^z_{i_\sigma}\})t}\mu_\mathrm{spin}(0)\otimes\mu_\mathrm{vib}(0)\}, \tag{B32}$$

where we have rewritten the spin-vibron Liouvillian (4) making explicit reference to its dependence on the spin operators $\mathscr{L}_\mathrm{ddsv}(\{\sigma^z_{i_\sigma}\}) = \mathscr{L}_\mathrm{ddsv}(\{\sigma^z_{2_\sigma}, \sigma^z_{3_\sigma}, \cdots, \sigma^z_{N-1_\sigma}\})$. From this expression, the reduced density matrix evolves as

$$\mu_\mathrm{vib}(t) = \sum_{\{s_{i_\sigma}\}} p_{\{s_{i_\sigma}\}}\mathrm{e}^{\mathscr{L}_\mathrm{ddsv}(\{s_{i_\sigma}\})t}\mu_\mathrm{vib}(0), \tag{B33}$$

which can be interpreted as an statistical average of the time-evolution under a stochastic Liouvillian. In particular, the Liouvillian $\mathscr{L}_\mathrm{ddsv}(\{s_{i_\sigma}\})$ depends on the binary variables $\{s_{i_\sigma}\}$, which inherit their randomness from the quantum parallelism

of the initial spin state. In fact, the associated probability distribution for the binary random variable is $p_{\{s_{i\sigma}\}} = |c_{\{s_{i\sigma}\}}|^2$. Therefore, we can formally write $\mu_{\rm vib}(t) = \overline{\mu_{\rm vib}(t)}$, where the "bar" refers to a statistical average over a random Liouvillian

$$\mathscr{L}_{\rm ddsv} \to \mathscr{L}_{\rm sdtb}(\mu_{\rm vib}) = -{\rm i}[H_{\rm stb}, \mu_{\rm vib}] + \sum_{\ell_\tau} \mathscr{D}_{\rm v}^{\ell_\tau}(\mu_{\rm vib}). \quad \text{(B34)}$$

Here, $\mathscr{D}_{\rm v}^{\ell_\tau}$ is the dissipator acting on the edge vibrons (2), whereas the stochastic tight-binding Hamiltonian is

$$H_{\rm stb} = \sum_{\alpha,i_\alpha} \varepsilon_{i_\alpha} a_{i_\alpha}^\dagger a_{i_\alpha} + \sum_{\alpha,\beta} \sum_{i_\alpha \neq j_\beta} \left(J_{i_\alpha j_\beta} a_{i_\alpha}^\dagger a_{j_\beta} + {\rm H.c.} \right).$$

Here, the on-site energies of the bulk σ-ions are binary random variables sampling $\varepsilon_{i_\sigma} \in \{\omega_{i_\sigma} - \frac{1}{2}\Delta\omega_\sigma^-, \omega_{i_\sigma} + \frac{1}{2}\Delta\omega_\sigma^-\}$. In particular, if we consider the initial spin state $|\Psi_0\rangle = \otimes_{i_\sigma}(|\uparrow_{i_\sigma}\rangle + |\downarrow_{i_\sigma}\rangle)/\sqrt{2}$, this diagonal disorder has a flat probability distribution $p(\varepsilon_{i_\sigma}) = \frac{1}{2}$. Let us note that exactly the same formalism would apply to the effective Liouvillian for the bulk vibrons. In this case, however, the collective dissipation rates would also become stochastic variables.

In order to study the steady state for the vibrons thermalizing under this disordered Liouvillian (B34), we can solve the system of differential equations for the two-point correlators (B12) for each realization of the diagonal disorder

$$\frac{{\rm d}C_{\{\varepsilon_{i\sigma}\}}}{{\rm d}t} = {\rm i}[\mathbb{J}, C_{\{\varepsilon_{i_\sigma}\}}] - (\mathbb{W} C_{\{\varepsilon_{i_\sigma}\}} + C_{\{\varepsilon_{i_\sigma}\}} \mathbb{W}^*) + \mathbb{K}. \quad \text{(B35)}$$

Then, we should average over the random variable according to the probability distribution $p(\varepsilon_{i_\sigma}) = \frac{1}{2}$. Due to the disorder, one of the matrices becomes stochastic

$$\mathbb{J}^{\rm edge}_{i_\alpha j_\beta}(\{\varepsilon_{k_\sigma}\}) = \varepsilon_{i_\alpha}\delta_{i_\alpha j_\beta} + J_{i_\alpha j_\beta}. \quad \text{(B36)}$$

After performing the statistical average $\overline{C}(t)$, we can reconstruct the vibron density of the disordered TQW.

We consider the same setup as in Fig. 11 for the ordered TQW, namely a $N = 20$ ion chain. Moreover, we use the same parameters introduced there. For the spin-induced disorder, we set $\Delta\omega_\sigma^- = 10\gamma_{N_\tau}$, which corresponds to a strong spin-vibron coupling. In Fig. 13, we represent the distribution of vibrons along the TQW in the steady-state. In this case, the predictions for both a homogeneous ion crystal (i.e. microtrap array), and an inhomogeneous one (i.e. linear Paul trap) coincide. As a consequence of the disorder-induced diffusion, the vibron layout is no longer homogeneous, but rather displays a linear gradient far way from the edges of the chain.

Before closing this section, let us also comment on another interesting perspective for the TQW, namely the possibility of realizing *noise-assisted quantum heat transport*. As demonstrated in [17], the efficiency of transport in quantum networks including linear chains with disorder may be sometimes increased by the presence of local dephasing noise. In order to test this prediction in our current scenario, let us note first that the presence of disorder (B34) will partially inhibit the heat transport. By switching on the local dephasing (B28), the interference leading to Anderson localization, or transport bottlenecks due to energy mismatches between neighboring sites, can be overcome thanks to the presence of noise, thus assisting the transport of heat. This can be probed by the current measurement described in a section below.

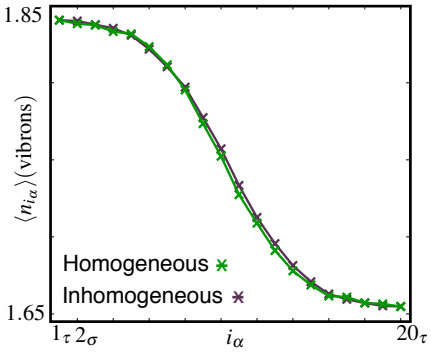

Figure 13. **The disorder route to Fourier's law:** Steady-state number of vibrons $\langle n_{i_\alpha} \rangle$ for an inhomogeneous ion chain in a linear Paul trap (purple crosses), and a homogeneous ion chain in a microtrap array (green crosses). We observe an inhomogeneous distribution of vibrons across the chain. Far away from the edges, and close to the bulk of the chain, the distribution displays a linear gradient.

d. *Effective thermal leads and single-spin heat switch*

Let us now consider a mesoscopic ion chain with N ions. The configuration of ions species is

$$\tau - \sigma - \cdots - \sigma - \kappa - \sigma - \cdots - \sigma - \tau, \quad \text{(B37)}$$

where $\tau = {}^{24}{\rm Mg}^+$, $\sigma = {}^{25}{\rm Mg}^+$, and $\kappa = {}^{9}{\rm Be}^+$. The κ-ion plays the role of the thermal quantum dot (TQD), the τ-ions act effective vibronic reservoirs, and the left/right chain of σ-ions acts as leads that connects the TQD to the reservoirs. We will start by discussing the conditions under which the σ-ions can be interpreted as effective thermal leads. Then we will discuss how to control the tunneling of vibrons across the κ-ion, which can be exploited to build a single-spin heat switch.

i) Effective thermal leads.– In order to devise the leads, we apply a strong and static spin-vibron coupling (3) to the σ-spins (see Eq. (B31)), namely

$$H_{\rm sv} = \sum_{i_\sigma} \tfrac{1}{2}\Delta\omega_\sigma^- n_{i_\sigma} \sigma_{i_\sigma}^z, \quad \text{(B38)}$$

In this case, we consider the strong-driving regime

$$\tilde{J}_{i_\alpha j_\beta}, \tilde{\Lambda}^{\pm}_{i_\alpha j_\beta} \ll |\Delta\omega_\sigma^-| \ll \delta_{l_\tau}, \gamma_{l_\tau}, \quad \text{(B39)}$$

and the following initial state for the spins of the leads

$$|\psi_0\rangle = |\downarrow_\sigma \cdots \downarrow_\sigma\rangle |\phi_{p_\kappa}\rangle |\uparrow_\sigma \cdots \uparrow_\sigma\rangle, \quad \text{(B40)}$$

where $|\phi_\kappa\rangle$ is an arbitrary spin state of the κ-ion acting as the TQD. In this regime, the spin-vibron coupling (B31) provides a large and static shift of the vibron on-site energies

$$\omega_{i_\sigma} \to \tilde{\omega}_{i_\sigma} = \omega_{i_\sigma} - \tfrac{1}{2}\Delta\omega_\sigma^- \theta(p_\kappa - i_\sigma) + \tfrac{1}{2}\Delta\omega_\sigma^- \theta(i_\sigma - p_\kappa), \quad \text{(B41)}$$

where we have introduced the Heaviside step function $\theta(x) = 1$, if $x > 0$. Due to these shifts, the effective thermalization of the bulk ions described in Sec. B 1 must be re-addressed. Assuming that the separation of time-scales is valid, whereby the laser-cooled τ-ions reach the steady state much faster than any other process in the problem, we can derive a similar master equation (B4) for the bulk ions

$$\dot{\mu}_{\rm bulk} = -\mathrm{i}\big[\sum_{\alpha} H_{\rm s}^{\alpha} + H_{\rm tb}^{\rm bulk}, \mu_{\rm bulk}\big] + \Delta\mathscr{L}(\mu_{\rm bulk}), \tag{B42}$$

where $\alpha = \{\sigma, \kappa\}$ are the bulk species. In this expression, the tight-binding model for the bulk vibrons must be modified to account for the on-site energy shifts (B41), and reads as follows $H_{\rm tb}^{\rm bulk} = H_{\rm vo}^{\rm bulk} + H_{\rm vt}^{\rm bulk}$, where

$$H_{\rm vo}^{\rm bulk} = \sum_{\alpha, i_\alpha} \tilde{\omega}_{i_\alpha} a_{i_\alpha}^\dagger a_{i_\alpha}, \;\; H_{\rm vt}^{\rm bulk} = \sum_{\alpha,\beta} \sum_{i_\alpha \neq j_\beta} J_{i_\alpha j_\beta} a_{i_\alpha}^\dagger a_{j_\beta} + \text{H.c.}. \tag{B43}$$

Additionally, the second-order processes where vibrons tunnel between the edge and bulk lead to a similar super-operator

$$\Delta\mathscr{L}(\bullet) = \sum_{\alpha,\beta} \sum_{i_\alpha, j_\beta, \ell_\tau} \tilde{\Upsilon}_{i_\alpha j_\beta}^{\ell_\tau} \Big\{ (\bar{n}_{\ell_\tau} + 1)(a_{j_\beta} \bullet a_{i_\alpha}^\dagger - a_{i_\alpha}^\dagger a_{j_\beta} \bullet) + \bar{n}_{\ell_\tau}(a_{i_\alpha}^\dagger \bullet a_{j_\beta} - a_{j_\beta} a_{i_\alpha}^\dagger \bullet) \Big\} + \text{H.c.}, \tag{B44}$$

where the υ-couplings (B6) are modified due to the shifts

$$\Upsilon_{i_\alpha j_\beta}^{\ell_\tau} \to \tilde{\Upsilon}_{i_\alpha j_\beta}^{\ell_\tau} = \frac{J_{i_\alpha \ell_\tau} J_{\ell_\tau j_\beta}}{\gamma_{\ell_\tau} - \mathrm{i}((\tilde{\omega}_{i_\alpha} - \delta_{\ell_\tau}) - \omega_{\ell_\tau})}. \tag{B45}$$

By assuming that all the ion species have the same trap frequencies, and that the conditions (B39) are fulfilled, one can check that $\tilde{\Upsilon}_{i_\alpha j_\beta}^{\ell_\tau} \approx \Upsilon_{i_\alpha j_\beta}^{\ell_\tau}$. If we now move to the interaction picture with respect to $H_0 = H_{\rm s}^{\sigma} + H_{\rm s}^{\kappa} + H_{\rm vo}^{\rm bulk}$, we obtain

$$\dot{\tilde{\mu}}_{\rm bulk} = -\mathrm{i}\big[\tilde{H}_{\rm vt}^{\rm bulk}(t), \tilde{\mu}_{\rm bulk}\big] + \Delta\tilde{\mathscr{L}}(\tilde{\mu}_{\rm bulk}), \tag{B46}$$

where we have introduced the vibron tunneling Hamiltonian

$$\tilde{H}_{\rm vt}^{\rm bulk}(t) = \sum_{\alpha,\beta} \sum_{i_\alpha \neq j_\beta} J_{i_\alpha, j_\beta} a_{i_\alpha}^\dagger a_{j_\beta} \mathrm{e}^{\mathrm{i}(\tilde{\omega}_{i_\alpha} - \tilde{\omega}_{j_\beta})t} + \text{H.c.}, \tag{B47}$$

and the super-operator for the virtual edge-bulk tunneling

$$\Delta\tilde{\mathscr{L}}(\bullet) = \sum_{\alpha,\beta} \sum_{i_\alpha, j_\beta, \ell_\tau} \Upsilon_{i_\alpha j_\beta}^{\ell_\tau} \Big\{ \bar{n}_{\ell_\tau}(a_{i_\alpha}^\dagger \bullet a_{j_\beta} - a_{j_\beta} a_{i_\alpha}^\dagger \bullet) \mathrm{e}^{\mathrm{i}(\tilde{\omega}_{i_\alpha} - \tilde{\omega}_{j_\beta})t} + (\bar{n}_{\ell_\tau} + 1)(a_{j_\beta} \bullet a_{i_\alpha}^\dagger - a_{i_\alpha}^\dagger a_{j_\beta} \bullet) \mathrm{e}^{\mathrm{i}(\tilde{\omega}_{i_\alpha} - \tilde{\omega}_{j_\beta})t} \Big\} + \text{H.c.}. \tag{B48}$$

Note that, when the conditions (B39) are satisfied, we get $|J_{i_\alpha, j_\beta}|, |\Upsilon_{i_\alpha j_\beta}^{\ell_\tau}| \ll |\tilde{\omega}_{i_\alpha} - \tilde{\omega}_{j_\beta}|$ for the ions that belong to different halves of the chain. Therefore, a rotating wave approximation allows us to neglect all the tunneling processes that lead to the thermalization between the two halves of the ion chain. This observation allows use to rewrite the partition the master equation (B46) into three terms

$$\dot{\tilde{\mu}}_{\rm bulk} = \mathscr{L}_{\rm L}(\tilde{\mu}_{\rm bulk}) + \mathscr{L}_{\rm L\kappa R}(\tilde{\mu}_{\rm bulk}) + \mathscr{L}_{\rm R}(\tilde{\mu}_{\rm bulk}). \tag{B49}$$

Here, we have introduced the Liouvillian for each of the leads $\mathscr{L}_{\rm L/R}(\bullet) = -\mathrm{i}[H_{\rm L/R}, \bullet] + \mathscr{D}_{\rm L/R}(\bullet)$, where

$$\begin{aligned} H_{\rm L} &= \sum_{i_\sigma, j_\sigma < p_\kappa} \tilde{J}_{i_\sigma, j_\sigma} a_{i_\sigma}^\dagger a_{j_\sigma} \mathrm{e}^{+\mathrm{i}(\tilde{\omega}_{i_\sigma} - \tilde{\omega}_{j_\sigma})t} + \text{H.c.}, \\ H_{\rm R} &= \sum_{i_\sigma, j_\sigma > p_\kappa} \tilde{J}_{i_\sigma, j_\sigma} a_{i_\sigma}^\dagger a_{j_\sigma} \mathrm{e}^{+\mathrm{i}(\tilde{\omega}_{i_\sigma} - \tilde{\omega}_{j_\sigma})t} + \text{H.c.}, \end{aligned} \tag{B50}$$

where we have used the renormalized tunnelings of Eq. (B7). Additionally, the dissipators are

$$\begin{aligned} \mathscr{D}_{\rm L} &= \sum_{i_\sigma, j_\sigma < p_\kappa} \mathscr{D}[\tilde{\Lambda}_{i_\sigma, j_\sigma}^{+}, a_{i_\sigma}^\dagger(t), a_{j_\sigma}(t)] + \mathscr{D}[\tilde{\Lambda}_{i_\sigma, j_\sigma}^{-}, a_{i_\sigma}(t), a_{j_\sigma}^\dagger(t)], \\ \mathscr{D}_{\rm R} &= \sum_{i_\sigma, j_\sigma > p_\kappa} \mathscr{D}[\tilde{\Lambda}_{i_\sigma, j_\sigma}^{+}, a_{i_\sigma}^\dagger(t), a_{j_\sigma}(t)] + \mathscr{D}[\tilde{\Lambda}_{i_\sigma, j_\sigma}^{-}, a_{i_\sigma}(t), a_{j_\sigma}^\dagger(t)], \end{aligned} \tag{B51}$$

where we have used the dissipative couplings in Eq. (B10), the interaction picture operators $a_{i_\sigma}(t) = a_{i_\sigma} \mathrm{e}^{-\mathrm{i}\tilde{\omega}_{i_\sigma} t}$, and the generic super-operator

$$\mathscr{D}[\Lambda, O_1, O_2](\bullet) = \Lambda(O_1 \bullet O_2 - O_2 O_1 \bullet) + \text{H.c.}. \tag{B52}$$

The final part is the coupling of the leads to the TQD, which reads

$$\mathscr{L}_{\rm L\kappa R}(\bullet) = -\mathrm{i}\big[H_{\rm L\kappa R}(t), \bullet\big] + \mathscr{D}_{\kappa}(\bullet), \tag{B53}$$

where we have introduced the Hamiltonian

$$H_{\rm L\kappa R}(t) = \sum_{i_\sigma \neq p_\kappa} 2\tilde{J}_{i_\sigma, p_\kappa} a_{i_\sigma}^\dagger a_{p_\kappa} \mathrm{e}^{+\mathrm{i}(\tilde{\omega}_{i_\sigma} - \tilde{\omega}_{\ell_\kappa})t} + \text{H.c.}, \tag{B54}$$

and the dissipator due to the long-range tunneling between the reservoir and the TQD

$$\mathscr{D}_{\kappa} = \mathscr{D}[\tilde{\Lambda}_{p_\kappa, p_\kappa}^{+}, a_{p_\kappa}^\dagger, a_{p_\kappa}] + \mathscr{D}[\tilde{\Lambda}_{p_\kappa, p_\kappa}^{-}, a_{p_\kappa}, a_{p_\kappa}^\dagger], \tag{B55}$$

From the master equation (B49), we thus expect that the left/right half or the chain thermalizes individually with the left/right reservoir, such that the vibron number in the steady state is

$$\langle n_{i_\sigma} \rangle_{\rm ss} \approx \bar{n}_{\rm L}\theta(p_\kappa - i_\sigma) + \bar{n}_{\rm R}\theta(i_\sigma - p_\kappa). \tag{B56}$$

Thus, the two chains of σ-ions serve as a thermal lead to connect the reservoirs to the thermal quantum dot (i.e. the κ-ion), and modify the local density of states seen by the TQD.

In order to support this theoretical prediction, we integrate numerically the system of differential equations for the two-point correlators $C_{i_\alpha j_\beta} = \langle a_{i_\alpha}^\dagger a_{j_\beta} \rangle$, namely

$$\frac{\mathrm{d}C}{\mathrm{d}t} = \mathrm{i}[\tilde{\mathbb{J}}^{\rm edge}, C] - (\mathbb{W}^{\rm edge} C + C(\mathbb{W}^{\rm edge})^*) + \mathbb{K}^{\rm edge}, \tag{B57}$$

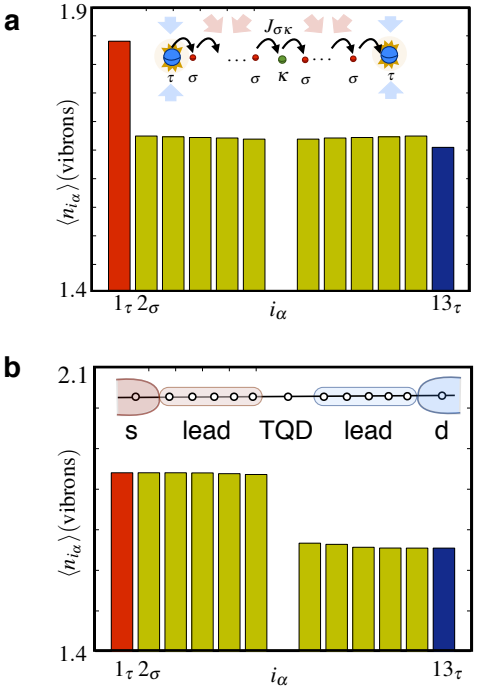

Figure 14. **Thermal leads: (a)** Steady-state number of vibrons $\langle n_{i_\alpha}\rangle$ along the ion chain in the absence of the static spin-vibron coupling $\Delta\omega_\sigma^- = 0$ (see the text for the remaining parameters). The bulk of the chain yields a homogeneous number of vibrons. The bars (yellow, red, and blue) correspond to the numerical solution of Eqs. (B57)-(B58). **(b)** Same as above but setting a strong spin-vibron coupling $\Delta\omega_\sigma^- = 200 J_{1_\tau 2_\sigma}$. This turns the homogeneous number of vibrons into a step-like function

where the matrices $\mathbb{W}^{\rm edge}, \mathbb{K}^{\rm edge}$ have been defined in Eqs. (B13). Due to the on-site energy shifts, we have to modify the $\mathbb{J}$ matrices as follows

$$\tilde{\mathbb{J}}^{\rm edge}_{i_\alpha j_\beta} = \tilde{\omega}_{i_\alpha}\delta_{i_\alpha j_\beta} + J_{i_\alpha j_\beta}, \qquad \alpha,\beta \in \{\sigma,\kappa,\tau\}, \tag{B58}$$

In Fig. 14, we represent the mean value of vibrons in the steady state of a $N = 13$ ion chain, where we recall that the chosen species are $\tau = {}^{24}{\rm Mg}^+$, $\sigma = {}^{25}{\rm Mg}^+$, and $\kappa = {}^{9}{\rm Be}^+$. We consider the following trap frequencies $(\omega_{\alpha x}, \omega_{\alpha y}, \omega_{\alpha z})/2\pi = (5, 5, 0.1)\,{\rm MHz}$, and the laser-cooling parameters $\Delta_{1_\tau} = -0.8\Gamma_\tau$, $\Delta_{13_\tau} = -0.6\Gamma_\tau$, and $\Omega_{{\rm L}^{\rm sw}_{1_\tau}} = \Omega_{{\rm L}^{\rm sw}_{13_\tau}} = 2.4\Gamma_\tau$, such that we expect each reservoir to thermalize to $\bar{n}_{1_\tau} = 1.84$, and $\bar{n}_{13_\tau} = 1.65$. In Fig. 14**(a)**, we represent our results in the absence of the on-site energy shifts $\Delta\omega_\sigma^- = 0$. In analogy to the TQW [Fig. 11**(a)**], we recover the expected homogeneous mean number of vibrons along the whole bulk. In Fig. 14**(b)**, we study the consequences of switching a very strong spin-vibron coupling $\Delta\omega_\sigma^- = 200 J_{1_\tau 2_\sigma}$. In this case, the left half of the chain thermalizes to the left reservoir $\langle n_{i_\sigma}\rangle_{\rm ss} \approx \bar{n}_{\rm L}$ for $i_\sigma < 7_\kappa$, whereas the right half thermalizes to $\langle n_{i_\sigma}\rangle_{\rm ss} \approx \bar{n}_{\rm R}$ for $i_\sigma > 7_\kappa$. We can thus conclude that the prediction for the behavior of the leads (B56) describes considerably well the actual steady state of the mixed ion chain.

Let us also note that, according to the coupling of the leads to the TQD described by $\mathscr{L}_{{\rm L}\kappa{\rm R}}$ in Eq. (B53), the tunneling of vibrons across the TQD also becomes rapidly rotating in the regime of strong couplings $\Delta\omega_\sigma^- = 200 J_{1_\tau 2_\sigma}$, such that the current through the TQD is inhibited. In fact, we find numerically that the vibron current through the κ-ion is $\langle I^{\rm vib}_{p_\kappa\to}\rangle_{\rm ss} \approx 1.6\cdot 10^{-4}{\rm vibrons}/s$. This must be contrasted to the case of $\Delta\omega_\sigma^- = 0$, where $\langle I^{\rm vib}_{p_\kappa\to}\rangle_{\rm ss} \approx 15{\rm vibrons}/s$. For experimental time-scales, we can consider that the strong drivings $\Delta\omega_\sigma^-$ suppress completely the vibron current through the TQD. Hence, only the long-range tunnelings to the reservoirs influence the thermalization of the TQD $\mathscr{L}_{{\rm L}\kappa{\rm R}} \approx \mathscr{D}_\kappa$.

ii) Single-spin heat switch.– We now describe a mechanism to switch on the vibron current across the TQD. We make use of the last ingredient in our toolbox (4), a periodic spin-vibron coupling (3) applied to the κ-ions

$$H^\kappa_{\rm sv}(t) = \tfrac{1}{2}(\Delta\omega_\kappa^+ + \Delta\omega_\kappa^-\sigma^z_{p_\kappa})\cos(\nu_\kappa t - \varphi_\kappa)n_{p_\kappa}. \tag{B59}$$

According to Sec. A 4, and the explicit relations in Eqs. (A47)-(A48), we can achieve such a spin-vibron coupling by using a pair of laser beams with different frequencies $\omega_{1_\kappa} \neq \omega_{2_\kappa}$, such that the frequency of the spin-vibron coupling (3) $\nu_\kappa = \omega_{{\rm L}^{\rm tw}_\kappa} = \omega_{1_\kappa} - \omega_{2_\kappa}$. Moreover, by adjusting the laser intensities, detunings, polarizations, and phases, we impose

$$\nu_\kappa = \tfrac{1}{2}\Delta\omega_\sigma^-, \;\; \varphi_\kappa = 0, \;\; \Delta\omega_\kappa^- = r\Delta\omega_\kappa^+. \tag{B60}$$

The idea is to use this periodic modulation to bridge the gradient of on-site energies between the two halves of the chain, assisting in this way the tunneling through the TQD. In the spin-independent case, the tunneling of vibrons can mimic a synthetic external gauge field [18]. In the current context, we exploit the spin-dependent drivings, such that depending on the parameter r, we can build a single-spin heat switch.

Let us supplement the Liouvillian in Eq. (B53) with the periodic spin-vibron coupling

$$H_{{\rm L}\kappa{\rm R}}(t) \to \tilde{H}_{{\rm L}\kappa{\rm R}}(t) = H_{{\rm L}\kappa{\rm R}}(t) + H^\kappa_{\rm sv}(t). \tag{B61}$$

In order to understand its effects, we move into another interaction picture with respect to the periodic driving $a_{p_\kappa} \to U_{\rm sv} a_{p_\kappa} U_{\rm sv}^\dagger$, where $U_{\rm sv} = \exp\{{\rm i}\int_0^t {\rm d}t' H^\kappa_{\rm sv}(t')\}$. This leads to

$$a_{p_\kappa} \to a_{p_\kappa} {\rm e}^{-{\rm i}\zeta_\kappa(1+r\sigma^z_{p_\kappa})\sin(\nu_\kappa t)}, \quad \zeta_\kappa = \frac{\Delta\omega_\kappa^+}{2\nu_\kappa}, \tag{B62}$$

which can be inserted in the the tunneling of vibrons between the TQD and the leads (B54). By using the Jacobi-Anger expansion for the first-kind Bessel functions $\mathfrak{J}_n(z)$, namely

$${\rm e}^{{\rm i}z\sin\theta} = \sum_{n\in\mathbb{Z}} \mathfrak{J}_n(z){\rm e}^{{\rm i}n\theta}, \tag{B63}$$

together with the constraints (B60), it is possible to derive an effective Hamiltonian for the coupling of the leads to the TQD

$$\begin{aligned} H^{\rm PAT}_{{\rm L}\kappa{\rm R}} \approx & -\sum_{i_\sigma < p_\kappa} 2\tilde{J}_{i_\sigma p_\kappa}\mathfrak{J}_1\big(\zeta_\kappa(1+r\sigma^z_{p_\kappa})\big)a^\dagger_{i_\sigma}a_{p_\kappa} \\ & + \sum_{i_\sigma > p_\kappa} 2\tilde{J}_{i_\sigma p_\kappa}\mathfrak{J}_1\big(\zeta_\kappa(1+r\sigma^z_{p_\kappa})\big)a^\dagger_{i_\sigma}a_{p_\kappa} + {\rm H.c.}, \end{aligned} \tag{B64}$$

where we have considered that all species have the same trap frequencies, and we have also used a rotating wave approximation for $\tilde{J}_{i_\sigma p_\kappa} \ll \frac{1}{2}|\Delta\omega_\sigma^-|$. As announced previously, the expression above (B64) shows that for the resonance condition $\nu_\kappa = \frac{1}{2}\Delta\omega_\sigma^-$, the periodic spin-vibron coupling is capable of assisting the tunneling of vibrons across the TQD. Moreover, the spin-dependence of the effective tunneling strengths via $\mathfrak{J}_1\big(\zeta_\kappa(1+r\sigma^z_{p_\kappa})\big)$ can be exploited to build the aforementioned single-spin heat switch. By setting $r=1$, we obtain $\mathfrak{J}_1\big(\zeta_\kappa(1+\sigma^z_{p_\kappa})\big) = \mathfrak{J}_1(2\zeta_\kappa)|{\uparrow_\kappa}\rangle\langle{\uparrow_\kappa}|$, which means that tunneling is only allowed if the κ-ion is in the spin-up state. Therefore, by controlling the κ-spin using microwave or laser radiation (i.e. π pulses), it is possible to switch on/off the heat current.

In order to check these predictions numerically, we consider a simplified setup, namely a $\sigma-\kappa-\sigma$ junction mimicking the connection of the thermal leads to the TQD. Rather than studying the steady state, we will concentrate on the coherent dynamics to show that the tunneling can be switched on/off by controlling the spin state of the the κ-ion. Let us define the parameters for this setup. We consider the usual trap frequencies $(\omega_{\alpha x},\omega_{\alpha y},\omega_{\alpha z})/2\pi = (5,5,0.1)\,\mathrm{MHz}$, which determine the equilibrium positions, and thus the tight-binding Hamiltonian for the vibrons $H_{\rm tb}$. The static spin-vibron coupling is

$$H^\sigma_{\rm sv} = \sum_{i_\sigma=1_\sigma,3_\sigma} \tfrac{1}{2}(\Delta\omega^+_\sigma + \Delta\omega^-_\sigma\sigma^z_{i_\sigma})n_{i_\sigma}, \qquad \text{(B65)}$$

where $\Delta\omega^+_\sigma = -2(J_{2_\kappa 2_\kappa} - J_{1_\sigma 1_\sigma})$ and $\Delta\omega^-_\sigma = 10^3 J_{1_\sigma 2_\kappa}$. This provides an energy gradient that inhibits the tunneling across the TQD. The periodic spin-vibron coupling of the κ-ion $H^\kappa_{\rm sv}(t)$ is given by Eqs. (B59) and (B60), where we set $r=1$. All these ingredients contribute to the dynamics given by $H(t) = H^\sigma_{\rm sv} + H^\kappa_{\rm sv}(t) + H_{\rm tb}$, which is solved numerically and compared to the theoretical predictions from $H^{\rm PAT}_{\rm L\kappa R}$ (B64).

We consider the initial state $\rho(0) = \rho_{1_\sigma}\otimes\rho_{2_\kappa}\otimes\rho_{3_\sigma}$, where $\rho_{i_\alpha} = |n_{i_\alpha}\rangle\langle n_{i_\alpha}|\otimes|s_{i_\alpha}\rangle\langle s_{i_\alpha}|$ is determined by the vibrational Fock states $n_{1_\sigma}=1$, $n_{2_\kappa}=0$, $n_{3_\sigma}=0$, and the spin states $s_{i_\alpha}\in\{{\uparrow_{i_\alpha}},{\downarrow_{i_\alpha}}\}$. We want to understand how the dynamics of such an initial state for $s_{1_\sigma}={\downarrow_{1_\sigma}}$, $s_{3_\sigma}={\uparrow_{1_\sigma}}$, is modified by changing $s_{2_\kappa}\in\{{\uparrow_{2_\kappa}},{\downarrow_{2_\kappa}}\}$. In Fig. 15**(a)**, we set $s_{2_\kappa}={\uparrow_{2_\kappa}}$, and observe how the vibron initially at the leftmost σ-ion tunnels through the TQD until it reaches the rightmost σ-ion. The solid lines correspond to the numerical solution of the full Hamiltonian $H(t)$, while the open symbols are the predictions given by $H^{\rm PAT}_{\rm L\kappa R}$. The agreement between both results supports the validity of our derivation. Therefore, we expect that by interspersing π pulses that invert the κ-spin $|{\uparrow_{2_\kappa}}\rangle \leftrightarrow |{\downarrow_{2_\kappa}}\rangle$, we can switch on/off the vibron current. In Fig. 15**(b)**, we show that two consecutive π pulses allow us to switch off the vibron current momentarily, which thus confirms our prediction.

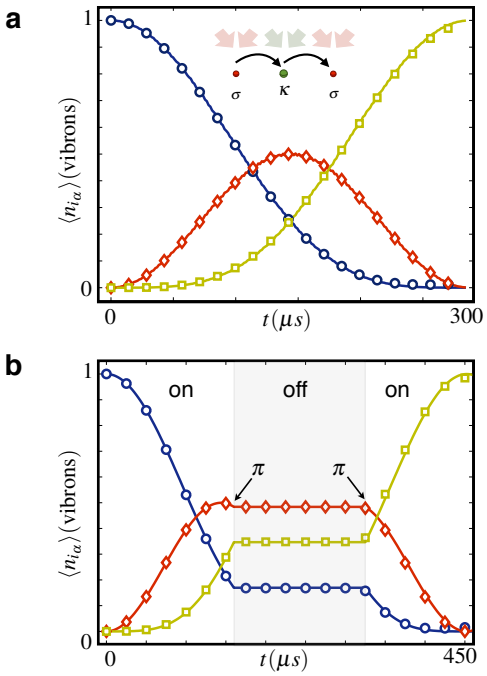

Figure 15. **Single-spin heat switch: (a)** Mean number of vibrons $\langle n_{i_\alpha}\rangle$ as a function of time in the regime of photon-assisted tunneling $s_{2_\kappa}={\uparrow_{2_\kappa}}$ (see the text for the remaining parameters). The solid lines ($\langle n_{1_\sigma}\rangle$ blue, $\langle n_{2_\kappa}\rangle$ red, $\langle n_{3_\sigma}\rangle$ yellow) represent the exact solution of $H(t)$, while the open symbols ($\langle n_{1_\sigma}\rangle$ circles, $\langle n_{2_\kappa}\rangle$ diamonds, $\langle n_{3_\sigma}\rangle$ squares) correspond to the effective photon-assisted-tunneling Hamiltonian $H^{\rm PAT}_{\rm L\kappa R}$. **(b)** Mean number of vibrons $\langle n_{i_\alpha}\rangle$ (same as in **(a)**) as a function of time, where the κ-spin undergoes two consecutive π-pulses that switch off/on the current. Note that the π-pulses are synchronized with the period of the spin-vibron coupling $H^\kappa_{\rm sv}(t)$.

Appendix C: Spin-based measurements for heat transport

The objective of this section is to present a detailed derivation, supported by numerical simulations, of the Ramsey probes for measuring arbitrary vibronic observables (8). Then we particularize to the measurements of the vibron number and the heat current.

1. Ramsey-type measurement of vibronic observables

Let us start from the bulk spin-vibron model in Eq. (5), and consider a generic spin-vibron coupling for the κ-spins

$$H^{\rm bulk}_{\rm sv}(t) \to \tilde{H}^O_{\rm sv} = \sum_{i_\kappa} \tfrac{1}{2}\lambda_O O_{i_\kappa}\sigma^z_{i_\kappa}, \qquad \text{(C1)}$$

where the "tildes" refer to the interaction picture with respect to the spin and on-site vibron Hamiltonians $H_0 = H^\sigma_{\rm s} + H^\kappa_{\rm s} + H_{\rm rvo}$. Here, we have introduced an arbitrary vibronic operator $O_{i_\kappa} = O_{i_\kappa}(\{a_{j_\kappa}, a^\dagger_{j_\kappa}\})$, and the spin-vibron coupling λ_0. In the sections bellow, we will specify to measurements of the vibron numbers $O_{i_\kappa} = n_{i_\kappa}$, and vibron currents $O_{i_\kappa} = I^{\rm vib}_{i_\kappa\to}$.

Since we want to probe the steady state of the bulk ion chain, the above spin-vibron coupling should disturb minimally the dynamics of the vibrons. Therefore, we impose

$$|\lambda_O| \ll \tilde{J}_{i_\alpha j_\beta}, \tilde{\Lambda}^\pm_{i_\alpha j_\beta}. \qquad \text{(C2)}$$

This allows us to partition the bulk dissipative spin-vibron model (5) into two terms

$$\begin{aligned}\tilde{\mathscr{L}}_0(\tilde{\mu}_{\rm bulk}) &= -{\rm i}[\tilde{H}_{\rm rvt},\tilde{\mu}_{\rm bulk}]+\tilde{\mathscr{D}}_{\rm bulk}(\tilde{\mu}_{\rm bulk}),\\ \tilde{\mathscr{L}}_1(\tilde{\mu}_{\rm bulk}) &= -{\rm i}[\tilde{H}^O_{\rm sv},\tilde{\mu}_{\rm bulk}],\end{aligned} \tag{C3}$$

where $\tilde{H}_{\rm rvt}$ is tunneling part of the renormalized tight-binding model (5). The idea now is to project onto the steady-state of the bulk ions, which is given by $\mathscr{L}_0(\mu^{\rm ss}_{\rm bulk})=0$. We use again the projection-operator techniques in Eq. (A21), where the projector is now $\mathscr{P}_{\rm bulk}\{\bullet\}=\mu^{\rm ss}_{\rm bulk}\otimes{\rm Tr}_{\sigma,{\rm spin}}\{{\rm Tr}_{\rm vib}\{\{\bullet\}\}$. This allows us to obtain an effective master equation for the κ-spins, which reads as follows

$$\frac{{\rm d}\tilde{\mu}^{\rm spin}_{\kappa}}{{\rm d}t}=\mathscr{L}_{\rm Ramsey}(\tilde{\mu}^{\rm spin}_{\kappa})=-{\rm i}[H_{\rm R},\tilde{\mu}^{\rm spin}_{\kappa}]+\mathscr{D}_{\rm R}(\tilde{\mu}^{\rm spin}_{\kappa}). \tag{C4}$$

Here, we have introduced a Hamiltonian that is responsible for the coherent part of the probe

$$H_{\rm R}=\sum_{i_\kappa}\tfrac{1}{2}\lambda_0\langle O_{i_\kappa}\rangle_{\rm ss}\sigma^z_{i_\kappa}. \tag{C5}$$

This term maps the information about the mean value of the vibronic operator O_{i_κ} in the steady-state of the bulk ions onto the phase evolution of the spins. The vibronic fluctuations will be coded into the incoherent part of the probe

$$\mathscr{D}_{\rm R}(\bullet)=\sum_{i_\kappa,j_\kappa}\tfrac{1}{4}\lambda_0^2 S_{O_{i_\kappa}O_{j_\kappa}}(0)(\sigma^z_{i_\kappa}\bullet\sigma^z_{j_\kappa}-\sigma^z_{j_\kappa}\sigma^z_{i_\kappa}\bullet)+{\rm H.c.}. \tag{C6}$$

Here, we have introduced the spectral function of the correlator between two vibronic observables

$$S_{O_{i_\kappa}O_{j_\kappa}}(\omega)=\int_0^\infty {\rm d}t\langle\tilde{O}_{i_\kappa}(t)\tilde{O}_{j_\kappa}(0)\rangle_{\rm ss}{\rm e}^{+{\rm i}\omega t}, \tag{C7}$$

where the operators $\tilde{O}_{i_\kappa}=O_{i_\kappa}-\langle O_{i_\kappa}\rangle_{\rm ss}$ quantify the fluctuations from the steady-state values, and we use

$$\langle\tilde{O}_{i_\kappa}(t)\tilde{O}_{j_\kappa}(0)\rangle_{\rm ss}={\rm Tr}\{\tilde{O}_{i_\kappa}{\rm e}^{\tilde{\mathscr{L}}_0 t}\tilde{O}_{j_\kappa}\mu^{\rm ss}_{\rm bulk}\}. \tag{C8}$$

Therefore, the zero-frequency component of the above spectral function (C7) determines the dephasing dynamics (C6) of the spins forming our probe due to the vibron fluctuations around the steady-state. Thus, by measuring the spin dephasing, we will acquire information about the quantum noise of the vibronic observable being probed.

We now describe in detail how the mean value and the fluctuations of the vibronic operator O_{i_κ} can be measured in analogy to a Ramsey interferometer [Fig. 16**(a)-(b)**]. Let us analyze the case where the probe is made of a single κ-ion, which is initialized by a $\pi/2$-pulse in the spin state $\mu^{\rm spin}_{i_\kappa}(0)=|+_{i_\kappa}\rangle\langle+_{i_\kappa}|$, where $|+_{i_\kappa}\rangle=(|\uparrow_{i_\kappa}\rangle+|\downarrow_{i_\kappa}\rangle)/\sqrt{2}$. Then, the bulk ions evolve under the Liouvillian $\mathscr{L}_0$ (C3), such that their vibrons reach the steady state, while the κ-spins evolve according to $\mathscr{L}_{\rm Ramsey}$ (C4), acquiring thus information about the vibron observable O_{i_κ}. In order to recover this information, we perform another $\pi/2$-pulse, and measure the probability of observing the κ-ion in the spin-down state $P_{\downarrow_{i_\kappa}}$.

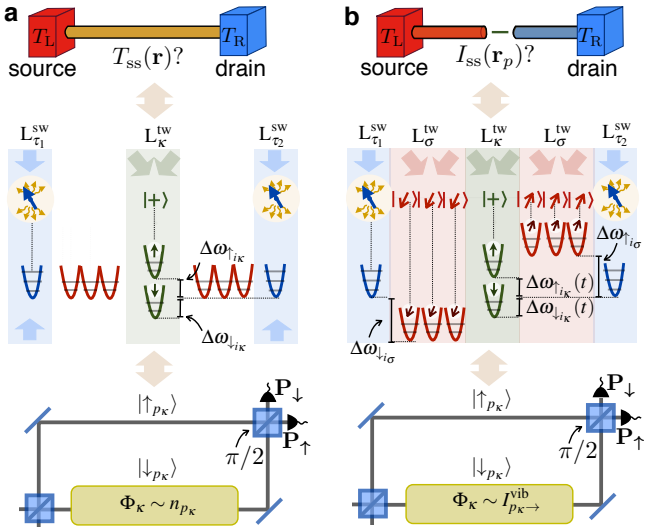

Figure 16. **Spin-based measurements for heat transport: (a)** (upper panel) We consider a situation analogous to a thermal quantum wire (TQW) (i.e. a bar connected to two heat reservoirs with different temperatures), and try to find a probe of the temperature along the TQW. (mid panel) In the trapped-ion scheme [Fig. 1], we switch on the lasers $\mathrm{L}^{\rm tw}_\kappa$ for the κ-species leading to a static and weak spin-vibron coupling (3). If the κ-spins are initialized in a linear superposition $|+_{i_\kappa}\rangle=(|\uparrow_{i_\kappa}\rangle+|\downarrow_{i_\kappa}\rangle)/\sqrt{2}$, the spin dynamics resembles a Ramsey interferometer capable of capturing the information about the mean vibron number and its fluctuations (lower panel). **(b)** (upper panel) We consider a situation analogous to a thermal quantum dot (TQD) connected to two thermal leads in equilibrium with two reservoirs held at different temperatures. We want to find a probe of the heat current flowing through the TQD. (mid pannel) In addition to the static spin-vibron coupling of the σ-ions of (**a**), the lasers $\mathrm{L}^{\rm tw}_\kappa$ should induce now a periodic and weak spin-vibron coupling (3). In this case the driving is responsible for assisting the tunneling, but also for mapping the information about the vibron current to the spin coherences in a Ramsey-type interferometer (lower pannel).

The second pulse, and the projective measurement, are equivalent to the measurement of the spin coherences $\langle\tilde{\sigma}^x_{i_\kappa}(t)\rangle$, where $\tilde{\sigma}^x_{i_\kappa}=|\uparrow_{i_\kappa}\rangle\langle\downarrow_{i_\kappa}|{\rm e}^{-{\rm i}\omega_0^\sigma t}+|\downarrow_{i_\kappa}\rangle\langle\uparrow_{i_\kappa}|{\rm e}^{+{\rm i}\omega_0^\sigma t}$. According to Eq. (C4), the κ-spin coherences evolve as follows

$$\langle\tilde{\sigma}^x_{i_\kappa}(t)\rangle=\cos(\lambda_O\langle O_{i_\kappa}\rangle_{\rm ss}t){\rm e}^{-\lambda_O^2{\rm Re}\{S_{O_{i_\kappa}O_{i_\kappa}}(0)\}t}. \tag{C9}$$

Therefore, by measuring the spin populations as a function of time, we expect to get damped oscillations, the period of which gives us information about the mean number of vibrons, while their damping is proportional to the vibron-number fluctuations in the steady-state. Let us note that the spin-population measurements can be performed through the state-dependent fluorescence of the trapped ion, a technique routinely used in many laboratories that allow for accuracies reaching 100% for detection times in the millisecond range [19]. Let us remark that, since we are interested in steady-state properties of the vibrons, this measurement scheme is not sensitive to the time-resolution of the spin-state readout. Hence, this does not pose any limitation to the target accuracies reaching 100%.

. Let us finally note that, according to Eq. (C7), if the probe consists of several κ-ions, we will also have access to the two-point correlations of distant ions.

2. Particular applications: vibron number and current

a. *Measurement of the vibron number*

In order to tailor the coupling (C1) to probe the vibron number (i.e. $O_{i_\kappa} = n_{i_\kappa}$), we must resort to a weak and static spin-vibron coupling (3). According to Eq. (B31), we can achieve such a spin-vibron coupling by using a pair of laser beams with equal frequencies, leading to

$$H_{\rm sv}^{\kappa} = \sum_{i_\kappa} \tfrac{1}{2}\Delta\omega_\kappa^- n_{i_\kappa}\sigma_{i_\kappa}^z,, \tag{C10}$$

where we recall that the Rabi frequency and the Lamb-Dicke parameter, defined by Eqs. (A42)-(A43), can be fully controlled experimentally. In light of the notation used in Eq. (C1), we identify $O_{i_\kappa} = n_{i_\kappa}$ [Fig. 16(**a**)], and $\lambda_0 = \Delta\omega_\kappa^-$, which can be tuned to fulfill the required probe condition (C2). If we restrict to a single probing ion labeled by p_κ, according to Eqs. (C4), the coherences evolve as follows

$$\langle\tilde{\sigma}_{p_\kappa}^x(t)\rangle = \cos(\Delta\omega_\kappa^-\langle n_{p_\kappa}\rangle_{\rm ss}t)\mathrm{e}^{-(\Delta\omega_\kappa^-)^2{\rm Re}\{S_{n_{p_\kappa}n_{p_\kappa}}(0)\}t}, \tag{C11}$$

which coincides with the description in the main text, and allows us to extract the quasi-particle mean number and fluctuations. We remark that for more than one probing ion, the dissipative dynamics would also gives us information about the vibronic correlations between distant ions.

In order to support our derivations, let us analyze numerically the Ramsey measurement for the TQW. Due to the introduction of the κ-spins, the dynamics of the system is no longer quadratic as in Sec. (B 2), which forbids finding a closed system of differential equations for the vibronic two-point correlators. Therefore, we have to obtain numerically the time evolution of the complete density matrix $\mu_{\rm bulk}(t)$ given by Eq. (C3), and then calculate the observable $\langle\tilde{\sigma}_{i_\kappa}^x(t)\rangle$. Due to the computational cost of this problem, let us simplify maximally the setup where the Ramsey measurement can be developed by considering a thermal quantum dot (TQD) once more. However, in contrast to Sec. B 2 a, we will consider the arrangement $\tau-\kappa-\tau$, where $\tau = {}^{24}{\rm Mg}^+$ and $\kappa = {}^{9}{\rm Be}^+$. We consider the same parameters introduced in previous sections, but set the detunings $\Delta_{1_\tau} = -0.6\Gamma_\tau$, $\Delta_{3_\tau} = -0.5\Gamma_\tau$, and the Rabi frequencies $\Omega_{{\rm L}_{1_\tau}^{\rm sw}} = \Omega_{{\rm L}_{3_\tau}^{\rm sw}} = \Gamma_\tau$ for the laser cooling of the τ-ions, where we recall that $\Gamma_\tau/2\pi = 41.4\,$MHz. With these parameters, the effective cooling rates (A28) of the τ-ions would be $\gamma_{1_\tau}/2\pi \approx 86\,$kHz, and $\gamma_{3_\tau}/2\pi \approx 106\,$kHz. Additionally, the mean number of vibrons for each reservoir (A29) would be $\bar{n}_{1_\tau} = 1.65$, and $\bar{n}_{3_\tau} = 1.63$. The trap frequencies are $(\omega_{\alpha x},\omega_{\alpha y},\omega_{\alpha z})/2\pi = (5,5,0.25)\,$MHz, which lead to a vibron tunneling strength of $J_{1_\tau 2_\kappa}/2\pi = J_{3_\tau 2_\kappa}/2\pi \approx 35\,$kHz. With these parameters, we expect that the τ-ions thermalize very fast and act as an effective reservoir for the bulk κ-ion.

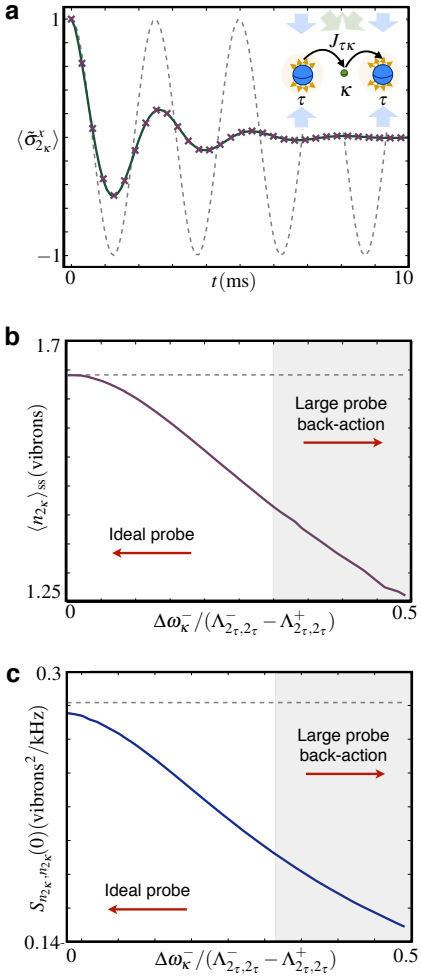

Figure 17. **Ramsey-type measurement of the vibron number: (a)** Dynamics for the coherence of the probe spin $\langle\tilde{\sigma}_{2_\kappa}^x(t)\rangle$ in a Ramsey-type measurement. The grey dashed line would represent the periodic oscillations in Eq. (C22) that would be obtained in a noiseless scenario. However, due to the quantum noise $S_{n_{i_\kappa}n_{i_\kappa}}(0)$, such oscillations get damped as shown by the numerical solution (green solid line). The crosses correspond to a numerical fit $\langle\tilde{\sigma}_{2_\kappa}^x(t)\rangle = \cos(at)\exp\{-bt\}$, with fitting parameters a,b, which allow us to recover the mean value and fluctuations of the number of vibrons in the steady state via Eq. (C22). **(b)** Mean value of the vibron number obtained from the numerical fit $\langle n_{2_\kappa}\rangle_{\rm ss} = a/\Delta\omega_\kappa^-$ (solid line) as a function of the probing strength. The dashed line represents the theoretical prediction (C14). As expected, for $\Delta\omega_\kappa^- \to 0$, the probe does not disturb the properties of the bulk vibrons, and we recover the predicted mean number of vibrons (C14) (dashed line). **(c)** Quantum noise of the vibron number obtained from the numerical fit $\langle S_{n_{2_\kappa}n_{2_\kappa}}(0)\rangle_{\rm ss} = b/(\Delta\omega_\kappa^-)^2$ (solid line) as a function of the probing strength. For $\Delta\omega_\kappa^- \to 0$, the probe does not disturb the properties of the bulk vibrons, and we recover the prediction (C14) (dashed line).

According to Eq. (5), the κ-ion evolves under $\dot{\mu}_{\rm bulk} = \mathscr{L}_{2_\sigma 2_\sigma}(\dot{\mu}_{\rm bulk})$, where

$$\mathscr{L}_{2_\sigma 2_\sigma}(\bullet) = -{\rm i}\left[(\omega_\kappa + \tilde{J}_{2_\kappa 2_\kappa} + \frac{\Delta\omega_\kappa^-}{2}\sigma_{2_\kappa}^z)a_{2_\kappa}^\dagger a_{2_\kappa},\bullet\right] + \mathscr{D}_{2_\kappa 2_\kappa}(\bullet), \tag{C12}$$

where the dissipator contains the heating and cooling terms

$$\begin{aligned}\mathscr{D}_{\rm bulk}(\bullet) =&\tilde{\Lambda}^{+}_{2_\kappa 2_\kappa}\big(a^{\dagger}_{2_\kappa}\bullet a_{2_\kappa}-a_{2_\kappa}a^{\dagger}_{2_\kappa}\bullet\big)+\\&+\tilde{\Lambda}^{-}_{2_\kappa 2_\kappa}\big(a_{2_\kappa}\bullet a^{\dagger}_{2_\kappa}-a^{\dagger}_{2_\kappa}a_{2_\kappa}\bullet\big)+\text{H.c.}.\end{aligned}\tag{C13}$$

Let us note that, in this case, the mean number of vibrons and the noise fluctuations in the steady state can be calculated exactly by means of the quantum regression theorem

$$\bar{n}_{2_\kappa}=\frac{\Gamma_{\rm L}\bar{n}_{\rm L}+\Gamma_{\rm R}\bar{n}_{\rm R}}{\Gamma_{\rm L}+\Gamma_{\rm R}},\quad S_{n_{2_\kappa},n_{2_\kappa}}(0)=\frac{\bar{n}^2_{2_\kappa}+\bar{n}_{2_\kappa}}{2(\tilde{\Lambda}^{-}_{2_\kappa 2_\kappa}-\tilde{\Lambda}^{+}_{2_\kappa 2_\kappa})}.\tag{C14}$$

Therefore, this particular TQD offers a neat playground to test the proposed measurement scheme.

We now solve numerically the master equation (C12) considering the above realistic parameters, and compute the dynamics of the coherences $\langle\tilde{\sigma}^{x}_{2_\kappa}(t)\rangle$. In Fig. 17**(a)**, we represent the numerical results for these coherences (solid line), and perform a numerical fit (crosses) to the expected behavior in Eq. (C22), which allows us to infer the mean value and the quantum noise of the vibron number $\langle n_{2_\kappa}\rangle_{\rm ss}$, $S_{n_{2_\kappa}n_{2_\kappa}}(0)$. In Figs. 17**(b)-(c)**, we represent the results obtained from this numerical fit as a function of the probing strength $\Delta\omega^{-}_{\kappa}$. When the probe is too strong, there is an important back-action on the bulk vibrons, and the values obtained from the fit depart from the theoretical prediction (C14). Conversely, for $\Delta\omega^{-}_{\kappa}\to 0$, the probe disturbs minimally the system, and one attains an acceptable agreement with the theoretical predictions (C14). It is important to emphasize that, although $\Delta\omega^{-}_{\kappa}\to 0$, the time required for the Ramsey measurement is fixed to $t=10\,$ms, which is a reasonable regime considering typical decoherence times in trapped-ion experiments. Hence, the limit $\Delta\omega^{-}_{\kappa}\to 0$ does not require to maintain the spin coherences for prohibitively large experimental times.

b. *Measurement of the vibron current*

We now address a possible way of designing the coupling (C1) to probe the vibron current (i.e. $O_{i_\kappa}=I^{\rm vib}_{i_\kappa\to}$). In particular, we analyze the current through a TQD connected to the reservoirs by a couple of leads [Fig. 16**(b)**]. Let us recall that this setup is described by the Liouvillian in Eq. (B49), where the reservoirs correspond to the laser-cooled τ-ions, the leads to the σ-chains, and the TQD to the κ-ion. As discussed below Eq. (B49), the current through the TQD can be suppressed by means of a strong energy off-set between the two halves of the chain. Then, a periodic spin-vibron coupling (B59) serves as gadget to switch on the current, such that the tunneling strengths depend on the particular spin state of the κ-ion (see Eq. (B64)).

In this section, we will make use of this spin-dependence to build a Ramsey probe for the vibron current. However, in order to design design the Ramsey-type coupling (C1) such that $O_{i_\kappa}=I^{\rm vib}_{i_\kappa\to}$, we need to modify the spin-vibron couplings. In particular, we exploit a bi-chromatic spin-vibron coupling

$$H^{\kappa}_{\rm sv}(t)=\sum_{n=1,2}\tfrac{1}{2}(\Delta\omega^{+}_{\kappa,n}+\Delta\omega^{-}_{\kappa,n}\sigma^{z}_{p_\kappa})\cos(\nu_{\kappa,n}t-\varphi_{\kappa,n})n_{p_\kappa}.\tag{C15}$$

Moreover, by adjusting the laser intensities, detunings, polarizations, and phases, we impose

$$\begin{aligned}&\nu_{\kappa,1}=\tfrac{1}{2}\Delta\omega^{-}_{\sigma},\ \ \varphi_{\kappa,1}=\tfrac{\pi}{2},\ \ \Delta\omega^{-}_{\kappa,1}=0,\ \ \zeta_{\kappa,1}=\tfrac{\Delta\omega^{+}_{\kappa,1}}{2\nu_{\kappa,1}}=\pi,\\&\nu_{\kappa,2}=\tfrac{1}{2}\Delta\omega^{-}_{\sigma},\ \ \varphi_{\kappa,2}=0,\ \ \Delta\omega^{+}_{\kappa,2}=0,\ \ \zeta_{\kappa,2}=\tfrac{\Delta\omega^{-}_{\kappa,2}}{2\nu_{\kappa,2}}\ll 1,\end{aligned}\tag{C16}$$

where we recall that $\Delta\omega^{-}_{\sigma}$ is the energy off-set between the two halves of the chain (i.e. the leads).

In analogy to the derivation of Eq. (B64), to understand the effects of the bi-chromatic spin-vibron coupling (C15), we move into an interaction picture with respect to the driving

$$a_{p_\kappa}\to a_{p_\kappa}=-a_{p_\kappa}\mathrm{e}^{-\mathrm{i}\zeta_{\kappa,1}\sin(\nu_{\kappa,1}t-\pi/2)}\mathrm{e}^{-\mathrm{i}\zeta_{\kappa,2}\sigma^{z}_{p_\kappa}\sin(\nu_{\kappa,2}t)}.\tag{C17}$$

By using the Jacobi-Anger expansion again, together with the constraints (C16), it is possible to derive an effective Hamiltonian for the coupling of the leads to the TQD

$$\begin{aligned}H_{\rm L\kappa R}\approx&\sum_{i_\sigma<p_\kappa,m\in\mathbb{Z}}-2\tilde{J}_{i_\sigma p_\kappa}\mathfrak{J}_{-1-m}(\pi)\mathfrak{J}_m(\zeta_{\kappa,2}\sigma^{z}_{p_\kappa})(\mathrm{i})^{-1-m}a^{\dagger}_{i_\sigma}a_{p_\kappa}\\&+\sum_{i_\sigma>p_\kappa,m\in\mathbb{Z}}-2\tilde{J}_{i_\sigma p_\kappa}\mathfrak{J}_{1-m}(\pi)\mathfrak{J}_m(\zeta_{\kappa,2}\sigma^{z}_{p_\kappa})(\mathrm{i})^{1-m}a^{\dagger}_{i_\sigma}a_{p_\kappa}\\&+\text{H.c.},\end{aligned}\tag{C18}$$

where we have used a rotating wave approximation for $\tilde{J}_{i_\sigma p_\kappa}\ll\frac{1}{2}|\Delta\omega^{-}_{\sigma}|$. As announced previously, the expression above shows that for the resonance conditions $\nu_{\kappa,1}=\nu_{\kappa,2}=\frac{1}{2}\Delta\omega^{-}_{\sigma}$, the bi-chromatic spin-vibron coupling is capable of assisting the tunneling of vibrons across the TQD.

We will now exploit the spin-dependence of the effective tunneling strengths via the Bessel function $\mathfrak{J}_m(\zeta_{\kappa,2}\sigma^{z}_{p_\kappa})$ to build a Ramsey probe of the vibron current. In particular, taking into account that $\zeta_{\kappa,2}\ll 1$, we can rewrite $H_{\rm L\kappa R}=H^{\rm PAT}_{\rm L\kappa R}+H^{I}_{\rm sv}$, where we have introduced the Hamiltonian

$$H^{\rm PAT}_{\rm L\kappa R}=\sum_{i_\sigma}(\tilde{J}^{\rm PAT}_{i_\sigma,p_\kappa}a^{\dagger}_{i_\sigma}a_{p_\kappa}+\text{H.c.}),\quad \tilde{J}^{\rm PAT}_{i_\sigma,p_\kappa}=-\mathrm{i}2\tilde{J}_{i_\sigma p_\kappa}\mathfrak{J}_1(\pi),\tag{C19}$$

This term describes a spin-independent tunneling of vibrons across the TQD, which will be responsible for setting a vibron current. The important feature of the assisted-tunneling strength is that it has become purely imaginary, which becomes relevant in the definition of the current operators (B21). This turns out to be crucial to devise the Ramsey probe, since the remaining terms in the Hamiltonian can be written as

$$H^{I}_{\rm sv}=\tfrac{1}{4}\tilde{\lambda}_I(I^{\rm vib}_{p_\kappa\to}+I^{\rm vib}_{\to p_\kappa})\sigma^{z}_{p_\kappa},\tag{C20}$$

where we have introduced the dimensionless coupling

$$\tilde{\lambda}_I=\zeta_{\kappa,2}\frac{2(\mathfrak{J}_0(\pi)+\mathfrak{J}_2(\pi))}{\mathfrak{J}_1(\pi)}.\tag{C21}$$

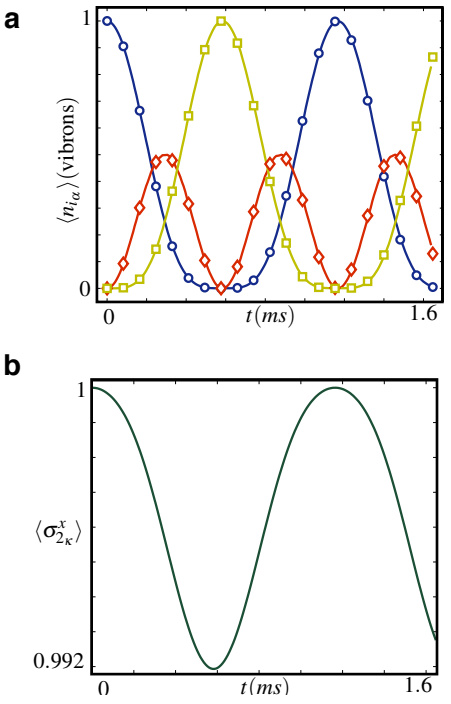

Figure 18. **Effective tunneling for the current Ramsey measurements: (a)** Mean number of vibrons $\langle n_{i_\alpha}\rangle$ as a function of time in the regime of photon-assisted tunneling $s_{2_\kappa} = \uparrow_{2_\kappa}$ (see the text for the remaining parameters). The solid lines ($\langle n_{1_\sigma}\rangle$ blue, $\langle n_{2_\kappa}\rangle$ red, $\langle n_{3_\sigma}\rangle$ yellow) represent the exact solution of $H(t)$, while the open symbols ($\langle n_{1_\sigma}\rangle$ circles, $\langle n_{2_\kappa}\rangle$ diamonds, $\langle n_{3_\sigma}\rangle$ squares) correspond to the effective photon-assisted-tunneling Hamiltonian $H_{\mathrm{L}\kappa\mathrm{R}} = H^{\mathrm{Pat}}_{\mathrm{L}\kappa\mathrm{R}} + H^{I}_{\mathrm{sv}}$. **(b)** Time evolution of the spin coherence of the probe κ-ion, $\langle\sigma^x_{2_\kappa}(t)\rangle$, for an initial spin state $|\Psi_{2_\kappa}(0)\rangle = |+_{2_\kappa}\rangle$. Due to the effective spin-current coupling (C20), the the coherences display periodic oscillations that depend on the periodicity of the assisted tunneling of vibrons between the ions.

Remarkably enough, we can make the coupling of the Ramsey probe arbitrarily small by simply letting $\zeta_{\kappa,2} \to 0$. In this limit, we have an ideal Ramsey probe of the vibronic current. According to Eqs. (C4), the κ-spin coherences evolve as

$$\langle\tilde{\sigma}^x_{p_\kappa}(t)\rangle = \cos(\tilde{\lambda}_I\langle I^{\mathrm{vib}}_{\to p_\kappa}\rangle_{\mathrm{ss}}t)\mathrm{e}^{-\tilde{\lambda}_I^2\mathrm{Re}\{S_{I_{p_\kappa}I_{p_\kappa}}(0)\}t}, \qquad \text{(C22)}$$

where we have made use of the fact that $\langle I^{\mathrm{vib}}_{\to p_\kappa}\rangle_{\mathrm{ss}} = \langle I^{\mathrm{vib}}_{p_\kappa\to}\rangle_{\mathrm{ss}}$ in the steady state. We have also defined the zero-frequency intensity noise

$$S_{I_{p_\kappa}I_{p_\kappa}}(0) = \int_0^\infty \mathrm{d}t\langle\tilde{I}_{p_\kappa}(t)\tilde{I}_{p_\kappa}(0)\rangle_{\mathrm{ss}}, \qquad \text{(C23)}$$

where we have introduced the current fluctuations through

$$\tilde{I}_{p_\kappa} = \tfrac{1}{2}(I^{\mathrm{vib}}_{\to p_\kappa} + I^{\mathrm{vib}}_{p_\kappa\to}) - \langle I^{\mathrm{vib}}_{p_\kappa\to}\rangle_{\mathrm{ss}}. \qquad \text{(C24)}$$

Let us note that, in order to give supporting numerical evidence of this prediction, the minimal setup to explore would be a $\tau-\sigma-\kappa-\sigma-\tau$ chain. In analogy to the single-spin switch, computing the dynamics of the spin coherences in this case becomes a non-linear problem that exceeds our numerical capabilities. Therefore, we cannot obtain the analogue of Fig. 17 for the current operator. Instead, we will content ourselves with showing that the effective Hamiltonians in Eqs. (C19)-(C20) describe the dynamics of a $\sigma-\kappa-\sigma$ setup faithfully. This has been shown in Fig. 18.

[1] D. F. V. James, Appl. Phys. B **66,** 181 (1998).
[2] G.-D. Lin, S.-L. Zhu, R. Islam, K. Kim, M.-S. Chang, S. Korenblit, C. Monroe, and L.-M. Duan, Europhys. Lett. **86,** 60004 (2009).
[3] R. Schmied, J. H. Wesenberg, and D. Leibfried, Phys. Rev. Lett. 102, 233002 (2009).
[4] R. P. Feynman, Statistical Mechanics: A Set Of Lectures (Benjamin/Cummings Publishing, Massachusetts, 1972).
[5] M. Harlander, et *al.*, Nature **471,** 200 (2011).
[6] D. Porras and J.I. Cirac, Phys. Rev. Lett. **93,** 263602 (2004).
[7] K. R. Brown, et *al.*, Nature **471,** 196 (2011).
[8] S. Haze, et *al.*, Phys. Rev A **85,** 031401(R) (2012).
[9] J. Dalibard and C. Cohen-Tannoudji, J. Phys. B: At. Mol. Phys. **18,** 166 (1985); Y. Castin, H. Wallis, and J. Dalibard, J. Opt. Soc. Am. B. **6,** 2046 (1989).
[10] J. I. Cirac, R. Blatt, P. Zoller, and W. D. Phillips, Phys. Rev. A **46,** 2668 (1992).
[11] S. Chaturvedi and F. Shibata, Zeit. Physik B, **35,** 297 (1979).
[12] H. P. Breuer and F. Petruccione, The theory of open quantum systems, (Oxford University Press, Oxford, 2003).
[13] C. J. Myatt, B. E. King, Q. A. Turchette, C. A. Sackett, D. Kielpinski, W. M. Itano, C. Monroe, and D. J. Wineland, Nature **403,** 269 (2000).
[14] D. T. Gillespie, Am. J. Phys. **64,** 3 (1996).
[15] B. Paredes, F. Verstraete, and J.I. Cirac, Phys. Rev. Lett. **95,**140501 (2005).
[16] A. Bermudez, M. A. Martin-Delgado, and D. Porras, New J. Phys. **12,** 123016 (2010).
[17] M.B. Plenio and S.F. Huelga, New J. Phys. **10,** 113019 (2008).
[18] A. Bermudez, T. Schaetz, and D. Porras, Phys. Rev. Lett. **107,** 150501 (2011); *ibid.* New J. Phys. **14,** 053049 (2012).
[19] H. Haeffner, C. F. Roos, and R. Blatt, Phys. Rep. **469,** 155 (2008).